UC San Diego
UC San Diego Electronic Theses and Dissertations

Title

Bacterial surface-particle interactions: organic colloidal particle attachment and aggregation on cells

Permalink

Author

Patel, Nirav Rajesh

Publication Date

2022

Peer reviewed|Thesis/dissertation

UNIVERSITY OF CALIFORNIA SAN DIEGO

Bacterial surface-particle interactions: organic colloidal particle attachment and aggregation on cells

A dissertation submitted in partial satisfaction of the requirements for the degree Doctor of Philosophy

in

Bioengineering

by

Nirav Rajesh Patel

Committee in charge:

Professor Ratnesh Lal, Chair
Professor Farooq Azam, Co-Chair
Professor Douglas H. Bartlett
Professor Adam J. Engler
Professor Simpson Joseph

2022

The dissertation of Nirav Rajesh Patel is approved, and it is acceptable in quality and form for publication on microfilm and electronically.

University of California San Diego

2022

TABLE OF CONTENTS

LIST OF FIGURES

LIST OF TABLES

ACKNOWLEDGEMENTS

vii

Diego Cellular & Molecular Medicine Electron Microscopy Facility for help in preparing negative-stain samples for TEM imaging and help in TEM operating and image acquisition.

Chapter 2, in full, is a reprint of the material as it appears in Patel, N., Yamada, Y., and Azam, F. (2021). Bacterial Nanotubes as Intercellular Linkages in Marine Assemblages. Frontiers in Marine Science. The dissertation author was the primary investigator and author of this paper.

Chapter 3, in part, has been submitted for publication of the material as it may appear in Patel, N., Guillemette, R., and Azam, F. (2022). Bacterial surface interactions with organic colloidal particles: nanoscale hotspots of organic matter in the ocean. The dissertation author was the primary investigator and author of this paper.

Chapter 4, in part, is currently being prepared for submission for publication of the material in Patel, N., Lal, R., and Azam, F. (2022). AFM curvature radius analysis for detection and enumeration of surface-attached particles on marine bacteria. The dissertation author was the primary investigator and author of this material.

2012   Bachelor of Science, University of California San Diego

2015   Master of Science, University of California San Diego

2015-2019   Research Assistant, University of California San Diego

2022   Doctor of Philosophy, University of California San Diego

PUBLICATIONS

Patel, N., Yamada, Y., and Azam, F. (2021). Bacterial Nanotubes as Intercellular Linkages in Marine Assemblages. Frontiers in Marine Science, (8).

Patel, N., Ramachandran, S., Azimov, R., Kagan, B. L., & Lal, R. (2015). Ion channel formation by tau protein: implications for Alzheimer's disease and tauopathies. Biochemistry, 54(50), 7320-7325.

ABSTRACT OF THE DISSERTATION

Bacterial surface-particle interactions: organic colloidal particle attachment and
aggregation on cells

by

Nirav Rajesh Patel

Doctor of Philosophy in Bioengineering

University of California San Diego, 2022

Professor Ratnesh Lal, Chair
Professor Farooq Azam, Co-Chair

Marine bacterial influence on colloidal dissolved organic matter is a major driver
in the biogeochemical cycling of carbon through the marine microbial loop. Interactions of
individual bacteria with ambient colloids can affect nutrient availability and acquisition
strategies, reshaping their immediate microenvironment. Direct observation of marine
bacteria using atomic force microscopy (AFM) and complementary microscopies can yield
insight and empirical evidence regarding mechanisms and effects of interactions of
individual bacteria with colloidal particles from dissolved organic matter. The discovery
of bacterial nanotubes in marine bacteria is reported with descriptive physical properties.

Nanotube structures in *Pseudoalteromonas* sp. TW7 cells and *Alteromonas* sp. ALTSIO cell were determined to range between 200–600 nm in length and 50–160 nm in width. Individual connections were observed as hollow structures connecting bacterial cytoplasmic spaces. Particle aggregates, ranging 40–200 nm in width, were localized on marine bacteria surfaces, varying in size and quantity in a cell population, from interactions with *E. coli* ribosomes as model colloids. TW7 cells were observed with altered surface corrugation features and surface pits that can influence surface interaction with individual colloids. Corrugation features were determined to be 50–100 nm in size, and 20 nm deep. Hollow surface pits were measured to be 50–300 nm in width, and 10–50 nm in depth. A method using curvature radius analysis is proposed for analyzing AFM time-lapse image data of ALTSIO exposed to *E. coli* ribosomes to quantify particle attachment rates and coverage of cells. From observations, bacteria presented an average increase of 6.0 attached ribosomes when exposed to ribosome-amended seawater medium (approximate concentration of 8×10^{11} particles mL^{-1}). In conclusion, bacterial nanotubes, surface particle clusters and surface pits are various cell features in bacterial interactions with organic colloid particles that are indicative of underlying mechanisms of bacterial transformation of dissolved organic matter throughout the global ocean.

Chapter 1 Introduction

1.1 Marine organic matter

1.1.1 The global ocean

The global ocean covers approximately 70% of the Earth's surface and has a significant impact on the humans and human activity. Roughly half of the daily oxygen production necessary for the sustenance of aerobic lifeforms on the planet occurs at the surface waters of the oceans from the activity of marine phytoplankton and cyanobacteria. The marine ecosystem contains a plethora of lifeforms with extensive biodiversity that surpasses their terrestrial counterparts. The expansive air-sea interface at the ocean's surface is a significant factor in climate patterns due to its responsiveness to atmospheric conditions, e.g., temperature and carbon dioxide levels. As such, the ocean is the largest sink of carbon dioxide, responsive to atmospheric and anthropogenic sources of carbon dioxide, with an estimated 38,000 Pg (10^{15} g) of carbon accumulated (Houghton, 2007). Perturbations to the carbon cycling between atmosphere and ocean and within the ocean can have significant biogeochemical effects and influence on the marine ecology over a range of spatial and temporal scales.

1.1.2 Carbon cycling

The internal and vertical transport and accumulation of carbon in the ocean occurs by four mechanisms or "pumps". One mechanism is the solubility pump where atmospheric carbon dioxide is solubilized into seawater and then mixed and transported by current activity. Due to carbon dioxide by more soluble in colder waters compared to warmer waters,

the interplay between oceanic currents and temperature fluctuations contribute to in-gassing into and out-gassing from surface waters of carbon dioxide (Hansell and Carlson, 2014). Another mechanism is the carbonate pump in which a fraction of dissolved carbon dioxide is converted to carbonate (CO_3^{2-}) compounds and subsequently precipitated by calcium ions as calcium carbonate. The sinking of calcium carbonate precipitates deposits the carbon, enabling it to avoid dissolution and forming a carbon reservoir in the ocean (Hansell and Carlson, 2014).

In addition to these two physico-chemical pumps, the organic carbon pump is a biologically mediated cycle that contributes to the cycling of carbon in the ocean. Carbon dioxide is fixed into particulate and dissolved organic carbon from the photosynthetic activity of primary producers in the surface waters. The fixed carbon is essentially integrated into the sugars, proteins, and other components of the organic matter in phytoplankton biomass. A fraction of this organic carbon sinks vertically through the divisions of the water column. This sinking movement physically transports the organic carbon to the ocean sediment, resulting in the vertical stratification of dissolved organic carbon throughout the water column to the ocean depths (Hansell and Carlson, 2014). Another biological pump is the microbial carbon pump, wherein marine microorganisms process carbon in the organic material produced by primary producers and influence the partitioning of organic matter and the available dissolved organic matter (DOM) pool. The microbial activity processes the available DOM in the surface waters and incorporates a fraction into microbial biomass, which in turn flows through the marine food web, with the remained respired as carbon dioxide (Hansell and Carlson, 2014).
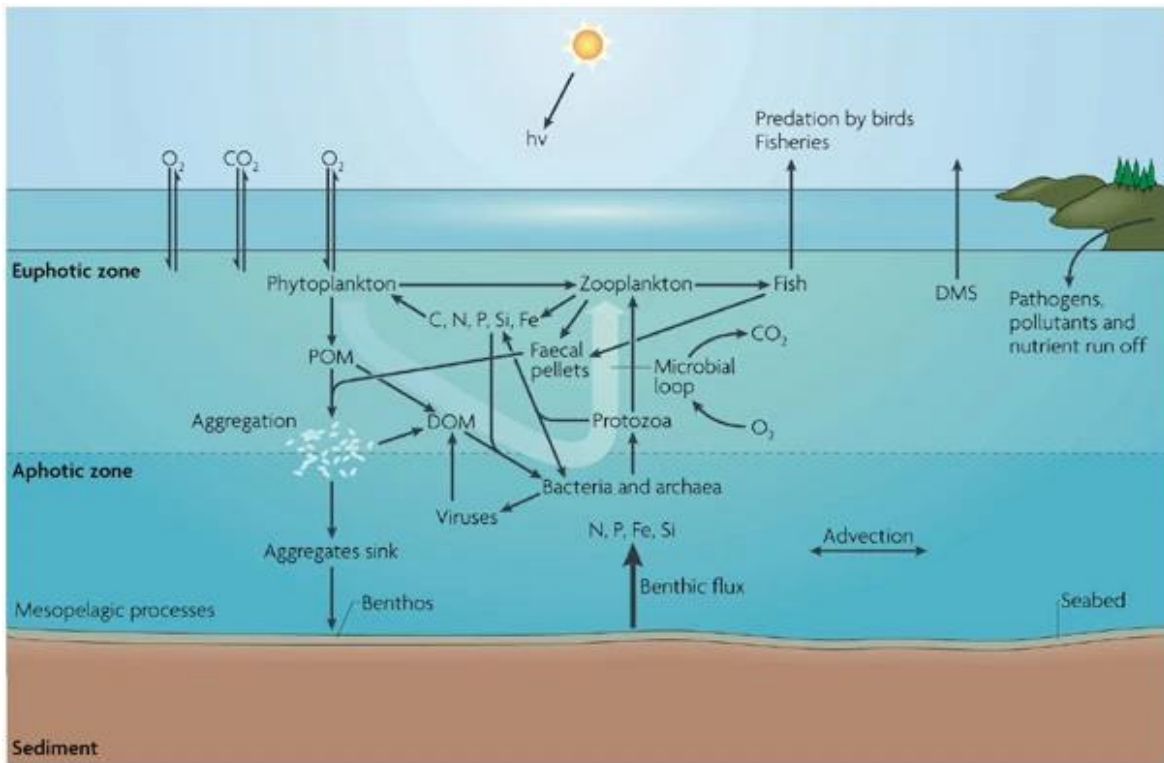
Figure 1.1: The marine food web. Schematic of microbial carbon pump in relation to the marine food web and carbon cycling from influences of biological and physiochemical process. Figure from (Azam and Malfatti, 2007).

With an estimated 1×10^{29} bacterial cells in the ocean, the cumulative microbial activity is a significant influence on the availability of organic carbon and its and transport within the surface waters, and of the sequestration of organic carbon within the ocean (Flemming and Wuertz, 2019). The total accumulated amount of dissolved inorganic carbon in the oceans is estimated to be around 38,000 Gt (Houghton, 2007). Compared to this vast pool, the size of the dissolved organic carbon pool is ~662 ± 32 Pg, making the ocean one of the largest reservoirs of bioreactive organic carbon on the planet (Hansell and Carlson, 2014). The aggregate of microorganism activity and respiration enacted upon this vast pool of organic carbon can have significant effects on its biogeochemical cycles. Understanding the mechanisms and effects of microbial activity on the pool of organic carbon is of significant interest for evaluating the ecological effects and responses to climate change and increased atmospheric carbon dioxide levels on the changes in the carbon biogeochemical cycling and sequestration of organic carbon within the ocean. Annually, 15 to 25 Pg of dissolved organic matter is added to seawater by various means (e.g. microbial activity, atmospheric, fluvial or groundwater transport) (Burdige, 2007;Jurado et al., 2008;Bauer and Bianchi, 2011;Hansell, 2013). In relation to the global carbon budget, there is a net uptake of an estimated 1.9 Pg C per year of anthropogenic carbon through the air-sea exchange into a pool of approximately 118 Pg of anthropogenic carbon sequestered within the ocean (Mikaloff Fletcher et al., 2006;Gruber et al., 2009).

1.1.3 Organic matter

Particulate and dissolved organic matter are differentiated by filtration, typically using a glass fiber filter with a nominal pore size of 0.7 µm, where particulate organic matter (POM) is operationally defined as the fraction that is retained upon the filter and dissolved organic matter (DOM) as the fraction that passes through it (Hansell and Carlson, 2014). This operational definition of DOM includes a medley of bacteria-sized particles, marine viral particles, colloidal organic matter and truly dissolved molecules (Hansell and Carlson, 2014). An estimated 50 Pg C is annually fixed by phytoplankton, from which a substantial amount is released as dissolved organic carbon (DOC) directly into seawater (Chavez et al., 2010). DOC is also released by various biological processes and activities, such as viral lysis, sloppy feeding by grazers, egestion by protists and metazoan, and external hydrolysis in POC degradation (Jiao et al., 2010). There is an estimated 10^{12}–10^{15} unique molecules in the accumulated oceanic DOC pool, contributing to an extensive diversity to the molecular species in the chemical environment surrounding individual microorganisms (Hansell and Carlson, 2014).
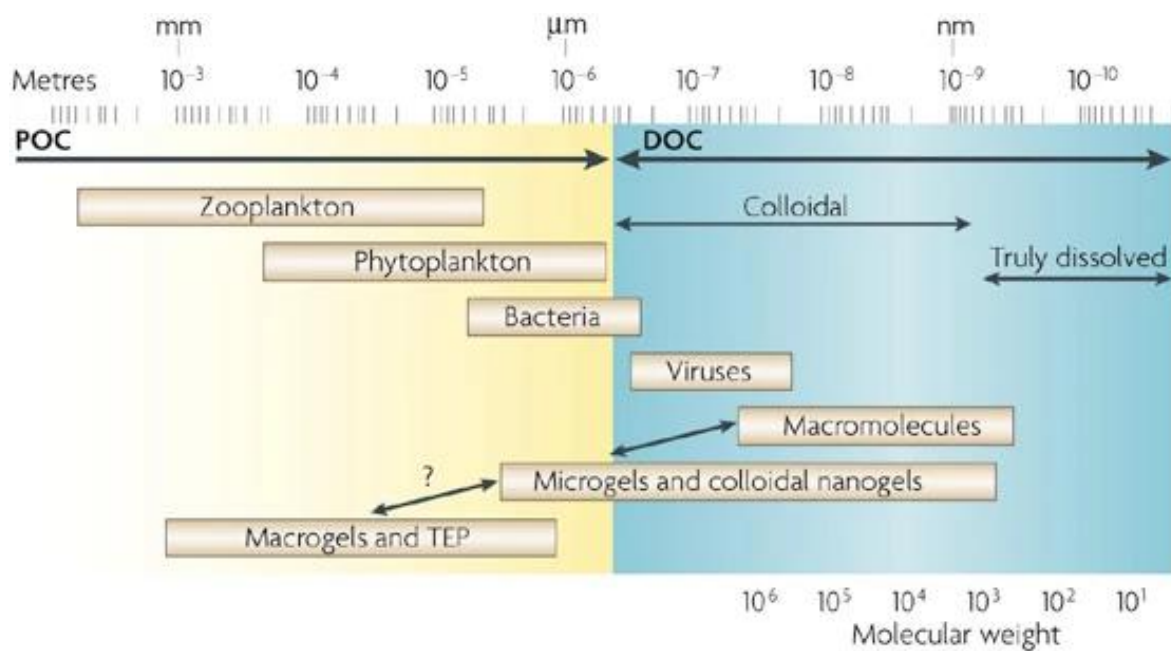
Figure 1.2: Spatial scale of organic matter distribution. Diagram outlining the spatial scales of various biological components within the marine microenvironment in relation to the partitioning of organic matter into particulate (POC) and dissolved (DOC) fractions. Figure from (Azam and Malfatti, 2007).

1.1.4 Dissolved organic matter

The residence times of various DOM molecules have variable lifespans within the marine microenvironment, and are influenced by the physico-chemical conditions, biomolecular diversity, and the microbial community structure. DOM is generally classified into three categories: labile, semi-labile and refractory DOM. On short timescales, marine microbes produce and consume "labile" DOM, which at any moment is < 0.2 Pg of the global organic carbon budget, and over longer timescales, excess production and deposition of carbon contributes to the accumulation of "semi-labile" DOM (Hansell and Carlson, 2014). Semi-labile DOC is that fraction of DOC that is present in surface waters but not at depths greater than 1000 m (Hansell and Carlson, 2014). The residence times of semi-labile DOC spans from months to several years, compared to refractory DOC (rDOC) is removed on timescales from decades to millennia. In the deep ocean, DOC has been measured to be several thousand years old, with an estimated turnover time ~16,000-30,000 years (Williams and Druffel, 1987;Druffel et al., 1992;Hansell and Carlson, 2014). Only biologically recalcitrant DOC persists for transportation to the deep ocean and sediments. Few of the newly produced DOC survive until 1000m depth, indicating that most of the DOC species are degraded in the surface waters (Hansell, 2013). DOC lability is dependent on and changes with nutrient conditions, temperature, light conditions, and community structures (Hansell and Carlson, 2014). Labile DOM can also undergo abiotic transformations that prevent microbial degradation and promote recalcitrant rDOC formation, extending its residence time (Keil and Kirchman, 1994).

Most marine DOM can be processed and respired by marine heterotrophic bacteria, or photochemically oxidized, or is transported to the ocean depths and buried in the sediments. A significant fraction of marine DOC persists in the water column from hours to millennia (Hansell and Carlson, 2014). Some of the labile organic carbon is converted through successive reactive transformation of the molecular species into refractory DOC, contributing to the larger pool of less reactive DOC in ambient seawater. The labile fraction of the DOC pool accounts for approximately 1% of the total DOC pool (662 ± 32 Pg C in size) and is characterized by its rapid consumption and turnover (Williams and Druffel, 1987;Hansell and Carlson, 1998;Hansell et al., 2009;Hansell, 2013). A significant percentage of the global primary production is released as labile DOM, which is then subsequently respired by or incorporated within microbial biomass. Grazing, cell lysis, and other secretory process are additional sources for labile DOM into seawater.

1.1.5 Microbial demand for DOM

Marine heterotrophic bacteria are a dominant sink for labile DOM. Low molecular weight biomolecular constituents of labile DOM, such as amino acids, sugars, organic acids, ATP, vitamins, and simple biopolymers, can be readily hydrolyzed and assimilated by microbes (Mopper and Stahovec, 1986). The high demand for these labile DOC molecular species from the microbial community keeps the constituents at steady-state concentrations, typically at nanomolar concentrations, in the ambient seawater (Fuhrman, 1987;Skoog and Benner, 1997;Kaiser and Benner, 2009).

Marine algae and bacteria can produce polysaccharides and proteins that can potentially persist for several years (Fry et al., 1996;Ogawa et al., 2001;Jiao et al., 2010) High molecular weight DOM carbohydrate amendments to marine assemblages stimulates bacterial carbon utilization by successive taxa, suggestive of partitioning semi-labile DOM amongst different taxa within a community (McCarren et al., 2010). This suggests that specific microbial species and community composition influence the composition and availability of labile and semi-labile DOM pools. Proteins account for approximately 50% of the organic carbon and 80% of the organic nitrogen in marine microbes, which contribute to the marine DOM when released by predation or viral lysis (Hansell and Carlson, 2014). Amino acids are rapidly metabolized and incorporated by marine bacteria from radiocarbon experiments (Fuhrman, 1987) and a significant fraction of total hydrolysable amino acids (THAA) are metabolized over short time scales by extracellular peptidase activity and spatio-temporal changes in THAA (Amon et al., 2001). . Simple sugar molecules and homopolysaccharides are rapidly degraded and readily taken up by bacteria, through selective hydrolyzation by surface enzymes (Rich et al., 1996;Aluwihare et al., 1997;Meon and Kirchman, 2001).

Labile DOM is available generally to marine heterotrophic microorganisms, but can include specific DOM molecular species, released from photoautotrophs, that can elicit specific growth responses from select taxa of a microbial assemblage (Cottrell and Kirchman, 2000a;Cottrell and Kirchman, 2000b;Sarmento and Gasol, 2012). Specific DOM released by heterotrophic bacteria can enhance the growth of certain marine photoautotrophs, like B vitamins and siderophores. (Vraspir and Butler, 2009;Tang et al.,

2010;Bertrand et al., 2011;Helliwell et al., 2011;Bertrand et al., 2012). The organic nitrogen and phosphorus in the marine DOM are stored, rather than immediately available to bacteria, and increasing the timescales for bioavailability of organic nitrogen, phosphorus and trace metals in the water column (Hansell and Carlson, 2014). Marine microbes are critical players in the biochemical and physical transformation of DOM within the surface waters and in regulating the carbon flux between carbon dioxide respiration and organic carbon sequestration.

1.1.6 Marine microbial surfaces

The diversity of microorganisms and their underlying spatial patterns generate and contribute to varying microenvironments and ecological processes, that drive and adapt to macroscale chemical gradients and climate-related changes (Cavicchioli et al., 2019;Ibarbalz et al., 2019). There are an estimated 1×10^{29} bacterial cells in the ocean, where in every cubic millimeter of surface seawater, there are typically 10000 viruses, 1000 bacteria, 100 *Prochlorococcus* cyanobacteria cells, 10 *Synechococcus* cyanobacteria cells, and 10 protists (Azam et al., 1983;Azam and Malfatti, 2007;Pomeroy et al., 2007). As unicellular organisms, each microbial cell is surrounded by a biological membrane acting as a distinct biotic boundary separating its internal contents from the ambient seawater microenvironment surrounding it. Marine bacterial surfaces are the dominant biotic surface in the ocean with approximately 0.1–1 m^2 bacterial surface area per m^3 of seawater, forming a significant boundary region that influences DOM biomolecular and colloidal interactions.

Unicellular microorganisms are the predominant type of organisms in the surface waters of the ocean, a significant fraction of which are planktonic or free-living bacteria. The classification of microbial organisms is divided into autotrophic or heterotrophic based on nutrient requirements. Autotrophs do not require an organic source of energy and can synthesize biomass and organic compounds from inorganic carbons sources. In comparison, heterotrophs require external sources of organic molecules for energy and generating biomass. These prokaryotic organisms have a single outer membrane to interface with the external environment, involved in the detection of external stimuli, uptake of biomolecular compounds, and secretion of internal compounds. Marine bacteria are the only compartment of the marine food web that has access to DOM pool and are capable of its uptake, consumption, and integration for processing in microbial biomass production. Within the aggregate microbial activity, individual bacteria encounter cell-cell interactions and microscale DOM hotspots, exhibiting various adaptive strategies in response to such potential encounters.

1.1.7 Microbial membrane structure

As prokaryotic organisms, marine bacteria have a unicellular structure with their biomass contained within one primary compartment, and no internal membrane-enclosed compartments. They are gram-negative cells, with the bacterial cell envelope structure consisting of an outer membrane, peptidoglycan cell wall, and an inner membrane. Generally, the inner membrane is composed of a phospholipid bilayer and outer membrane is composed of glycolipids and lipopolysaccharides. The aqueous compartment enclosed

between the inner and outer membranes, surrounding the peptidoglycan cell wall, known as the periplasm. Proteins and enzymes involved in the metabolic processing and transport of sugars and amino acids are located within the periplasmic space. The outer membrane contains lipoproteins, proteins with lipid moieties on certain amino acid residues, and integral β-barrel proteins, for the diffusion and transport of small molecules like amino acids and mono- and disaccharides.
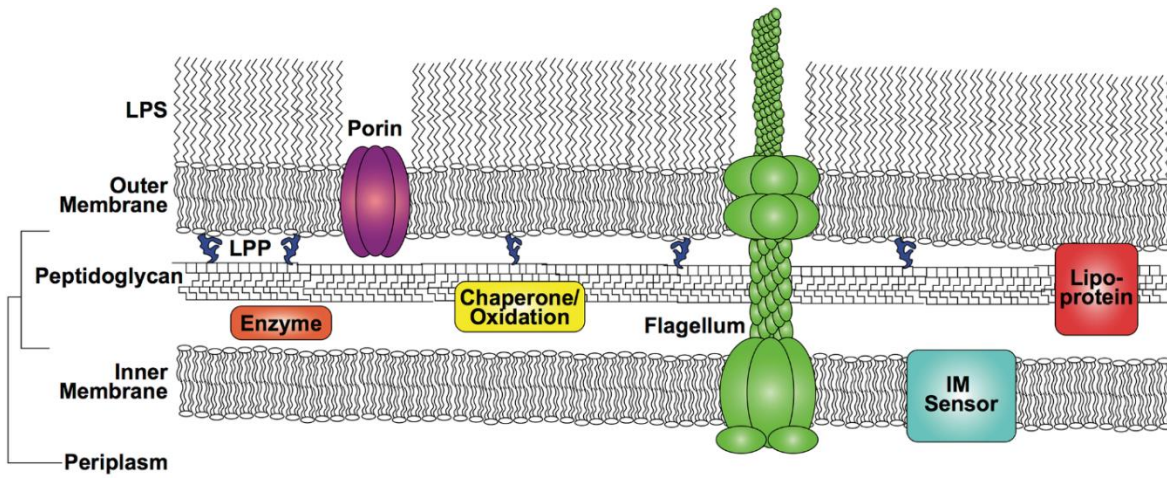
Figure 1.3: Bacterial membrane structure. Structure of gram-negative bacterial membrane structure, detailing the basic organization of the outer membrane, periplasm, and inner membrane. Figure from (Miller and Salama, 2018).

Bacteria can form architecturally complex communities termed as biofilms where cells grow in multicellular aggregates and are encased in an extracellular matrix of secreted proteins, polysaccharides, and other organic polymers. Proteins, like TasA and curli protein, can form amyloid filaments, which have a structural role in and are critical for biofilm formation in *B. subtilis* and *E. coli* respectively (Chapman et al., 2002;Barnhart and Chapman, 2006;Branda et al., 2006). Pili and fimbriae are cellular appendages that are used for cell adherence onto each other or other surfaces and facilitate biofilm formation. The matrix surrounding cells within biofilms is composed of extracellular polymers of polysaccharides, proteins, and extracellular DNA, providing structural support to the biofilm architecture (Flemming and Wingender, 2010). Bacterial cells can breakdown and remodel the extracellular matrix through the expression of hydrolytic enzymes for specific biopolymers, improving the dissolution, distribution, and utilization of nutrients. The coupling of enzymatic breakdown and expression of membrane-bound transporters renders bacterial surfaces (individually and communally) as reactive zones for transformation of organic molecules and potentially a hotspot for DOM formation.

1.1.8 Microbial utilization of organic matter

Microbial surfaces are reactive to extracellular DOM molecules in seawater and responsive to fluctuations and adapting to changes in their concentration levels. The ability of a microbe to adapt to the changing biochemical landscape and DOM levels can determine the likelihood of survival for specific individual bacteria and cumulatively influence the evolution of the microbial community structure. The concentration of DOC in the deep

waters is about 40 µM, with surface seawater DOC levels around 60–80 µM, and can rise to levels greater than 100 µM (Ogawa and Tanoue, 2003). There are many sources of DOM that promote the formation of microscale hotspots, with elevated DOM levels, within surface waters that exist on spatial scale of microns to meters and persists on temporal scales from seconds and minutes to hours. The sources of such discrete DOM hotspots include the processes of algal exudation, sloppy feeding, lysis, microgels and colloids, which can all contribute to the stochastic formation of transient nutrient hotspots and fluctuations in available DOM levels in ambient seawater. The spatio-temporal scales of the discrete events of DOM hotspot formation and dissolution can influence the response and changes of microbial communities to varying degrees.

A major source of DOM is the extracellular release of organic matter produced by phytoplankton primary production (Baines and Pace, 1991;Myklestad, 2000). Extracellular released DOM is carbon rich and is comprised of low molecular weight (LMW) and high molecular weight (HMW) DOM, with one hypothesis characterizing the release DOM based on an overflow model where the DOM exudation is correlated to photosynthesis rates (Baines and Pace, 1991;Sambrotto et al., 1993). Another model for released DOM is the passive diffusion model where a concentration gradient of DOM, primarily composted of LMW dissolved amino acids and neutral sugars, is present and correlated with phytoplankton biomass and relatively greater in smaller cells. (Kriest and Oschlies, 2007;Hansell and Carlson, 2014;Thornton, 2014). The terms "phycosphere" and "detritosphere" have been used to describe these naturally occurring DOM-enriched regions and the associated microbial interactions around phytoplankton and phytoplankton detritus,

respectively. Within the extracellular released DOM, carbohydrates account for 80%, along with the released peptides and amino acids, which in turn can become precursor substrates for the formation of transparent exopolymer particles (TEP) (Mague et al., 1980;Myklestad, 2000;Passow, 2002a;Engel et al., 2004). TEP are organic particles that can induce microbial interactions and attachment and undergo aggregation and form larger and enhance sinking particle fluxes and organic carbon transfer to the ocean depths (Passow, 2002b).

Marine phytoplankton fix approximately 50 Pg C per year into organic matter which is initially incorporated into metazoan and protist biomass and supports the heterotrophic organisms in marine food web (Chavez et al., 2010). Herbivory of phytoplankton releases nascent DOM into ambient seawater with organic carbon that originated from fixed carbon dioxide whereas bacteriovory essentially releases DOM from bacterial biomass as recycled form of DOM (Nagata and Kirchman, 1992;Kawasaki and Benner, 2006). From the physical breakage of the food source, sloppy feeding during phytoplankton grazing by copepods accounts for a loss of 49% of the DOC into the ambient seawater, with an additional loss of 6% through DOC leakage from the fecal pellets (Møller et al., 2003). As predator-to-prey size ratio increases above a specific threshold, less DOC is produced from the spillover after feeding (Møller, 2007). Zooplankton grazing of POC releases around $10 – 30\%$ as DOC into ambient seawater, which is comparable to and, in certain situations, exceeds the extracellular release of DOC by phytoplankton (Thornton, 2014;Steinberg and Landry, 2017). In addition to enriched hotspots generated from protozoan and metazoan feeding, their egesta also form transient DOM hotspots for heterotrophic bacteria, where the expelled organic matter become nutrients for bacteria and stimulate bacterial growth and production.

Marine snow and other large organic particles are naturally occurring DOM hotspots, active with heightened microbial activity. Marine snow particles are aggregates of natural polymers, larger than 500 µm, that grow bigger over time through aggregation with free polymers and other aggregates and can reach up to a few meters in size (Alldredge and Gotschalk, 1990). These polymeric aggregates can form from the physical coagulation of phytoplankton cells and detritus, fecal pellets, miscellaneous polymers, and smaller component particles. These particles host bacterial cell populations around $10^7 – 10^8$ cells in size, around 1-2 orders of magnitude greater in abundance than free-living bacteria surrounding seawater (DeLong et al., 1993). 3D visualizations of these aggregates show a diverse community and variable composition of polymers within each individual marine snow particle (Flintrop et al., 2018). Reaching a sufficiently large size, the aggregates sink down into the water taking the associated organic matter from the surface waters to the subsurface and deeper waters. The sinking marine snow particles, with elevated levels of bacterial abundance, enzymatic activity, and respiration, generate rich plumes of nutrients and diffusing DOM, forming chemical gradients that can benefit chemotactic motile bacteria (Ploug and Grossart, 2000;D'ambrosio et al., 2014). This process can lead to the proliferation and vertical stratification of bacteria associated with the marine snow particles, and other sinking POC and their degradation.

1.1.9 Bacterial interactions with aggregates and particles

Biopolymeric particle aggregates of carbohydrates, proteins, and lipids are partially broken down and solubilized by attached bacteria, releasing DOM into the ambient seawater.

(Alldredge and Gotschalk, 1990;Smith et al., 1995;Skoog and Benner, 1997;Alldredge, 1998;Grossart and Ploug, 2001;Kiørboe and Jackson, 2001;Simon et al., 2002;Kiørboe et al., 2003). Bacteria digest the biopolymers in POM into DOM using strategies such as the production and secretion of ectoenzymes as members of particle-attached microbial assemblages express specific proteases, β-glucosidase, and chitinase (Karner and Herndl, 1992;Smith et al., 1992;Arnosti, 2011). Another bacterial strategy is the expression of membrane-bound hydrolytic enzymes, or ectohydrolases, (e.g. protease, glucosidase, lipase, phosphatase, nuclease, and chitinase) to solubilize concentrated pockets of biopolymers, which can generate variable patterns and heterogeneity in DOM distribution (Hollibaugh and Azam, 1983;Martinez et al., 1996;Kirchman and White, 1999;Arrieta and Herndl, 2001;Nagata et al., 2003;Arnosti et al., 2005;Cottrell et al., 2005;Obayashi and Suzuki, 2005;Azam and Malfatti, 2007). The solubilization of larger particles releases a rich nutrient plume that is rich in DOM and is 10-100 times larger than particle volume, providing substrate nutrients for free bacterioplankton, presenting a significant influence on DOM availability over greater spatial scales in the marine environment (Cho and Azam, 1988;Kiørboe and Jackson, 2001). The microbial influence on hydrolysis and remineralization rates of sinking particles attenuates the sinking carbon flux and DOC sequestration in deeper waters. The hydrolytic degradation of HMW polymers can produce DOM that can be more readily consumed by free bacterioplankton. Differential solubilization of organic nitrogen and phosphorus results in a qualitative transformation of sinking aggregates and their physical composition, and consequentially changes the

18

evolution and particle interaction of associated and colonized microbial communities (Smith et al., 1995;Grossart and Ploug, 2001;Simon et al., 2002).

Marine viruses are ubiquitous in the marine surface ocean and can infect and lyse prokaryotic organisms and can impact the cycling of micro and macro nutrients (Wommack and Colwell, 2000;Suttle, 2007;Middelboe, 2008;Breitbart, 2011). Within the global ocean, an estimated 10^{30} phages infect prokaryotes at 10^{23} infections per second, killing 5-40% of prokaryotes daily (Suttle, 1994;2007;Middelboe, 2008). The viral lysis of prokaryotic hosts releases an estimated ~3-20 Pg of DOC cumulatively from cell lysate into seawater each year(Wilhelm and Suttle, 1999). This lysate is labile organic matter comprised of dissolved DNA, dissolved free amino acids (DFAA), and dissolved combined amino acids (DCAA), and carbohydrates among cellular debris and colloidal particles (Weinbauer and Peduzzi, 1995;Shibata et al., 1997;Middelboe and Jørgensen, 2006;Holmfeldt et al., 2010). Individual lysis events form discrete microscale DOM hotspots for bacterioplankton, where up to 28% of the viral lysate is converted to bacterial biomass (Middelboe et al., 2003).

Marine gels are 3D networks of complex heterogenous polydisperse mixture of biopolymers with seawater as the solvent with dissolved organic matter (Chin et al., 1998;Pace et al., 2012;Verdugo, 2012). HMW DOM molecules can spontaneously form chemical and physical gels that are held together by crosslinking and interconnected tangles (Verdugo, 2012). These self-assembled microgels can swell or collapse in response to physical and chemical changes in environmental conditions. 10% of DOC is in dynamic and reversible assembly equilibrium, suggesting that marine polymer gels can account for ~70 Gt C of the global DOC pool (Verdugo, 2012). Polymer gels physically vary in size from

small nanogels and microgels, which range between nanometers to several microns, and can extend up to a few meters (Verdugo et al., 2004;Svetličić et al., 2005). There are polyanionic polysaccharides, proteins, nucleic acids, and other amphiphilic and hydrophobic components within marine gels that contribute to variety and heterogeneity in local surface properties (Chin et al., 1998;Orellana et al., 2007;Ding et al., 2008;Orellana et al., 2011). DOM can adsorb onto the surface of microgels, depending on the local properties, reshaping, and influencing their properties and potential for microbial interactions (Long and Azam, 1996;Ogawa et al., 2001;Azam and Malfatti, 2007). Some refractory DOM can potentially form a partial scaffold or coating for the gel architecture, rendering select parts inaccessible or resistant to microbial interaction and degradation (Chin et al., 2004;Azam and Malfatti, 2007)). Ideal as DOM hotspots, attached bacteria on microgel surfaces can hydrolyze and break down the gel via surface ectohydrolases, generating labile DOM for nutrient uptake with enzyme activity (Smith et al., 1992;Long and Azam, 1996;Azam and Malfatti, 2007).

The molecular species in nascent DOM in ambient seawater have varying lability and residence lifetimes within the marine microenvironment, presenting varying metabolic utility for individual heterotrophic bacteria. Adsorption of labile DOC to colloidal surfaces can alter its lability and microbial accessibility (Kirchman et al., 1989;Nagata and Kirchman, 1996). Submicron particles (0.4 – 1.0 µm) are abundant in seawater, present in concentrations ranging from $10^6 – 10^7$ per ml (Isao et al., 1990;Wells and Goldberg, 1991;Nagata and Koike, 1995). Organic marine colloids, smaller than 120 nm in size, are present at concentrations between $10^7 – 10^9$ per ml in surface seawater and decreases with depth, where the vertical stratification of these colloids suggests potential influences of

particle aggregation and biological interaction (Wells and Goldberg, 1991). These particles are mostly organic in composition, with some trace metals (Fe, Al, Co) present, and contribute to the formation of microbe-sized agglomerates involved in sedimentation and biological interactions (Wells and Goldberg, 1991;1993). The colloidal fraction of DOC, consisting of organic constituents of colloids and organic colloids, represents an estimated 10–40% of the total DOC in seawaters (Benner et al., 1992;Guo and Santschi, 1997). Visualizing and understanding the microbial interactions with and responses to organic colloids can improve our understanding of the biological factors and mechanisms underlying the processes that determine the outcome of this fraction of DOM.

1.1.10 Significance of colloidal DOM

The general behavior of microbes and interactions with colloidal particles within the marine microenvironment is relatively underdeveloped subject of microbial ecology. The variability in biochemical composition, the surface structures and properties, and the abundance of colloids can potentially influence microbial behavior and responses in myriad ways. For example, marine colloids can cover microbial surfaces by attaching to the exopolysaccharides or outer membrane layer, potentially influencing the physical size and hydrodynamic properties of cells. In this process they interactive with or block surface receptors but also deliver nutrients via surface-adsorbed DOM to microbes for utilization. Colloids that consist of refractory DOM can potentially adsorb onto microbial surfaces, obstructing surface receptors, transporters, and enzymes, impeding their activity and uptake of surface organic material. Furthermore, the sloughing of biomaterial from microbial

surfaces can generate additional colloids for that can undergo physical aggregation or biological interactions with other microbial surfaces and colloids. The combined processes of nascent organic colloidal DOM production and degradation, with physical aggregation and biological interactions influencing this cycling, result in dynamic changes in the surface, biochemical and physical properties of the marine microenvironment for individual bacteria.

1.2 High resolution microscopy of marine bacteria

Microscopy is a common and versatile technique in microbial ecology that has been used conventionally to visualize and characterize the natural assemblages of phytoplankton, bacteria, and viruses within the marine microenvironment and their interactions. Briefly, in light microscopy, a sample specimen is illuminated by a light source, and in its interaction with light and attenuates some physical properties of the incident light rays (e.g. amplitude, phase, direction). The resulting light emitted from the sample is focused be a series of lenses into a detector such as the human eye or a charge-coupled device (CCD) camera sensor. In fluorescence microscopy, fluorescent molecules in sample specimen are illuminated by a specific wavelength of light, which upon excitation, emit light at a longer wavelength, which is picked up by a detector. Various color and fluorescent stains have been deployed for light and fluorescence microscopy-based visualization of marine microenvironmental components. The structure of marine aggregates can be visualized and studied by use of polysaccharide-specific stains that have revealed transparent exopolymer particles (TEP), up to 100 µm in size and up to 5000 particles mL^{-1} in abundance, that provide abiotic sources of organic matter for microbial utilization (Alldredge et al., 1993). Coomassie stained

particles (CSP) are proteinaceous particles, occasionally overlapping with TEP, that populate the marine microenvironment and interact with heterotrophic bacteria as nitrogen-rich substrates (Long and Azam, 1996). Fluorescent stains offer an additional approach to visualize other transparent particles and structures within the marine microenvironment can be potential hotspots of microbial diversity and activity (Samo et al., 2008). Nucleic acid stains such DAPI have been used to visualize and enumerate marine bacteria by fluorescently labelling DNA, in various marine microbial systems, including coral mucus associated bacteria (Garren and Azam, 2010). SYBR Green I, another fluorescent nucleic acid stain, has demonstrated utility in rapid and accurate enumeration of marine viruses, which are typically 20 – 200 nm in size (Noble and Fuhrman, 1998). Fluorescent microscopy can be a simple, rapid method to visualize bacterial structures and motility, e.g. NanoOrange protein stain as a means to demonstrate bacterial flagella (Grossart et al., 2000).

Light microscopy is limited in part by the physical properties of light and the ability of optical components to gather and focus the light onto the sensor. The spatial resolution limit using visible light is approximately 250 nanometers. Furthermore, fluorescence microscopy is limited in part by the fluorescence properties of the labelling molecules, such as the excitation and emission spectra and stability, and the biochemical properties that influence how the fluorescent molecules interact with biological components. These properties restrict the potential combinations for labeling and detecting the various biological components in marine microenvironments. The optics-based microscopy techniques are partially limited in their application for imaging environmental biological samples due to the labelling strategy employed to mark specific biomolecules and by the

physical diffraction limit of visible light, restricting the detected spatial resolution to 250 nm.

Non-optical microscopy techniques are alternative nano-imaging approaches for visualizing microbes and other biological and environmental components, in samples that are obscured due to the physical resolution limitations of light-based microscopy. Electron microscopy methods have been extensively used to visualize the submicron structures and features of the marine microorganisms and microenvironment. Briefly, electron microscopy techniques use a beam of electrons to interact with a sample specimen and reconstruct an image from the scattered or transmitted electrons, depending on the specific technique. Such methods generally require significant sample preparation and processing that may introduce artefacts and distort some features. Contrast agents are necessary to introduce electron-rich atoms to interact with electron beam and visualize features within biological specimens; for example, sputter-coated metals are applied to coat structures to enhance features and to prevent degradation under the electron beam exposure in scanning electron microscopy (SEM). In transmission electron microscopy (TEM), heavy metals can be used to stain samples to introduce contrast by deviating the electron beam trajectory and attenuating the signal. Electron microscopy techniques are typically performed vacuum or non-physiological environmental conditions and offer an alternative view of the biological structures and surfaces from light and fluorescence microscopy-based techniques at finer spatial resolutions. Electron microscopy techniques have be applied in the characterization of marine viruses and their spatial distribution (Cochlan et al., 1993;Lander et al., 2012). As another class of non-optical microscopy techniques, scanning probe microscopies use

physical interactions and forces to image sample specimens and can offer high spatial resolution in near-physiological conditions without significant sample preparation and related artefacts.

1.2.1 Fundamentals of atomic force microscopy

Atomic force microscopy (AFM) is a technique that reproduces a topographic image from the movement a probe tip raster scanning across a sample surface, while maintaining constant force with an error-correcting feedback controller adjusting tip-sample distance (Binnig et al., 1986). The scanning probe is typically a sharp microfabricated tip on the end of a silicon or silicon nitride microcantilever, with a tip radius < 10 nm at the apex. For operation, the probe moves into contact with the sample surface using piezoelectric actuators, as the physical forces exerted between the atoms of the AFM tip and sample surface result in the deflection of the microcantilever. The detection is typically detected by optical beam detection method, where a laser is reflected off the microcantilever into a detector and small deflections result in movements of the laser spot on the detector area. Once in contact, the probe laterally scans across the sample surface while maintaining contact, as measured by a constant microcantilever deflection, using piezoelectric actuators for lateral movement. A constant applied force and deflection of the AFM probe is maintained by a feedback controller making vertical adjustments to tip-sample distances and force. When the applied force is higher than a desired set point, the tip-sample distance is increased and when it is lower, the distance is decreased. The sample surface is reconstructed from the movement of the scanning probe as it travels with feedback maintaining a constant

deflection and applied force. Typically, AFM operates using the repulsion van der Waals forces as the force feedback during image scanning. Other forces can also be applied to force feedback, which gives versatility to AFM imaging as an imaging modality. AFM is generally independent of sample labelling as it operates on the detection of physical interactions. The technique does not require significant sample preparation other than immobilizing the sample onto a flat substrate to support against applied imaging forces. One advantage of AFM is the feature of operating in near-physiologic conditions, allowing for the observation of biological structures and surfaces in the native states (Kindt et al., 2002;Liu and Wang, 2010). This advantage has allowed for AFM to characterize microbial cell surfaces, dynamics of surface proteins, the evolution of cell shape, and changes in the cell envelope in various microbial systems (Viljoen et al., 2020).
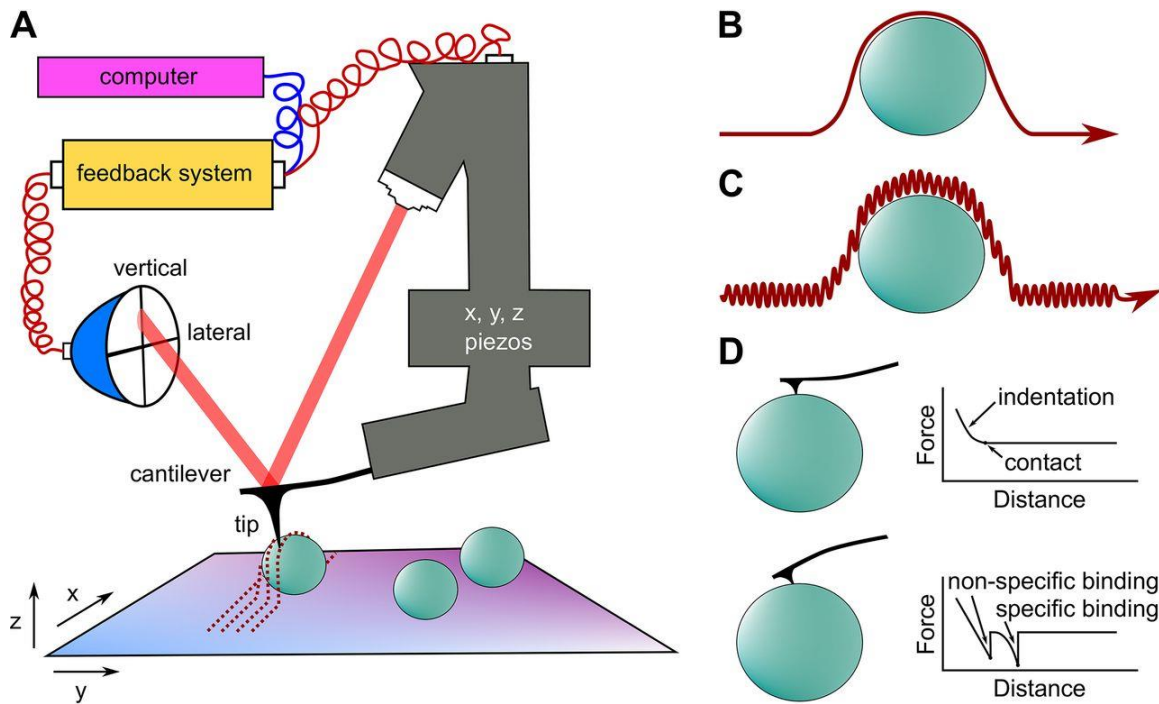
Figure 1.4: Principles of AFM operation. A) An overview schematic of an atomic force microscope in context of scanning a sample surface consisting of cells attached to a flat substrate. The AFM probe movement is controlled via piezoelectric actuators in x, y, and z directions. The interaction force between the tip and sample surface results in a cantilever deflection, which is detected by a quadrant detector. The vertical and lateral deflection signals are input into a feedback control system for piezoactuated adjustment and a computer for data collection. B) The movement path (red line) of the AFM tip when maintaining direct contact with the sample surface. C) The movement path (red line) when AFM tip maintains intermitted contact with the sample surface when the AFM probe is oscillated for dynamic imaging. D) Examples of force-distance curves when the AFM tip interacts with a sample surface in force spectroscopy. The upper and lower figures show a typical force-distance profile during an extension movement of the tip towards the sample surface and a retraction movement of the tip away from the surface, respectively. Figure from (Viljoen et al., 2020).

1.2.2 Nanomechanical measurements

Atomic force micrograph data are topographic images that provide quantitative height data and measurements for the surface profile of local sample surface regions. The AFM probe functions as a force detector and applicator simultaneously, as an inherent feature of its operating principle. Images are generated from the coordination of piezoactuated lateral scanning movement and force feedback control. Isolated vertical movement of the AFM probe at discrete spatial points and the resulting force-displacement profiles provide force spectroscopy data about the local mechanical properties of the sample and insight into the qualitative characteristics and differences at a nanoscale spatial resolution (Xu et al., 2018). Briefly, the applied force is calculated using Hooke's law, $F = -k \times \delta$, were the applied force, F, is equivalent to the product of the microcantilever spring constant k (measured in N/m), and its vertical deflection δ (measured in nm). Analysis of the resulting force-displacement profile yields measures of certain nanomechanical properties, such as modulus, deformation, and adhesion. The corresponding force and displacement measurements during the vertical movement of AFM force spectroscopy, i.e., an extension-retraction cycle of the AFM tip during its interaction with the sample, can be transformed and fit to mechanical models to estimate the elastic modulus. The integrated area between the extension and retraction profiles gives a quantitative measure for the mechanical energy dissipated in that interaction cycle. Other properties like the deformation and adhesion force can also be extracted from this data profile; the deformation from the vertical difference during the zero-force points between the two curves and the adhesion from the peak minimum force during the cycle. The nanomechanical capabilities of AFM have been

applied to microbial cell mechanics investigations to study the force and adhesion response of various bacterial structures and appendages (Dufrêne et al., 2021).

The alignment of individual force curve profiles and image pixels yields nanomechanical data maps that correlate topographic features with local nanomechanical properties in the sample. In one such method, peak force tapping (PFT) AFM, the AFM probe is vertically oscillated at high frequencies in a sinusoidal motion, where the probe interacts with the sample surface at the bottom of the cycle in discrete tapping cycles. In each tapping cycle, the force profile is extracted and processed to determine the peak force applied by the AFM tip and to extract mechanical properties. The integrated surface topography and nanomechanical data visualization allow for correlations between observed features and quantitative measurements regarding the material properties of biological systems at a nanometer spatial resolution (Dufrêne et al., 2013). These measured nanomechanical properties offer empirical observations and insight regarding qualitative differences and variations in biological surfaces by utilizing the visualization and quantitative measure of local material properties. One application of peak force tapping AFM is in the characterization of marine diatom cells regarding the biomineralization of silica in seawater and the nanomechanical response at a subcellular level (Pletikapić et al., 2012).

1.2.3 Applications in marine microbial ecology

As an emerging method for nanoscale imaging in marine microbiology, atomic force microscopy expands the observational capabilities for scientific investigations and offers

augmented visualizations of the various biological components of the marine microenvironment and their respective interactions in natural conditions (Taylor, 2019). In one application, the finer nanoscale structures of marine diatoms and their mechanical properties have studied using AFM (Pletikapić et al., 2011;Radić et al., 2011).AFM imaging has been used to visualize surfaces and features of marine microbes with nanometer resolution, appending studies of bacterial morphology with precise quantitative measurements of microbial biovolumes in natural marine assemblages (Nishino et al., 2004;Malfatti and Azam, 2009;Malfatti et al., 2010).

Additional marine applications for AFM have been in the characterization of marine gels and diatom-derived extracellular polymers and the investigation of marine viruses collected from California coastal waters (Kuznetsov et al., 2010;Kuznetsov et al., 2012;Pletikapić et al., 2012). The high-resolution capability of AFM imaging has also been utilized for observing and characterizing organic colloids and biopolymers from natural waters (Santschi et al., 1998;Wilkinson et al., 1999). Structural studies and live-cell imaging with AFM have yielded a new perspective workings of the marine microenvironment and its constituents. AFM studies investigating the interactions of these various components of the marine microenvironment offer a novel method for studying what marine bacteria are doing in their natural environment.

Illuminating the finer details and aspects of individual components within marine microenvironments, AFM imaging has been used to observe morphological details in host-phage interactions for marine bacterium *Roseobacter denitrificans* OCh114 and for phytoplankton *Phaeocystis globosa* (Zhang et al., 2012;Sheik et al., 2013). Malfatti and

Azam (2009) using AFM showed potential symbiotic interactions between heterotrophic marine bacteria and *Synechococcus* cells, which has implications in bacterial networks and associations within seawater (Malfatti and Azam, 2009). Seo et al. (2007) used AFM to observe marine bacterial capture of submicron particles and the relative frequency within natural bacterial populations, which has implications for the degradation of colloidal organic particles (Seo et al., 2007).

The application of AFM is uniquely suited for studying what individual bacteria are doing within the marine microenvironment. With minimal modifications and direct physical imaging, an AFM perspective offers detailed view of bacterial cells and structures within a natural context. With a finer understanding, more specific hypotheses can be developed and tested regarding bacterial mechanisms and behaviors in response to colloidal particles. The delineation of various bacterial response can yield clarity and more concrete knowledge beyond the current general knowledge regarding bacterial influence over colloidal organic matter cycling in the ocean.

1.3 References

Alldredge, A. (1998). The carbon, nitrogen and mass content of marine snow as a function of aggregate size. *Deep Sea Research Part I: Oceanographic Research Papers* 45**,** 529-541.

Alldredge, A.L., and Gotschalk, C.C. (1990). The relative contribution of marine snow of different origins to biological processes in coastal waters. *Continental Shelf Research* 10**,** 41-58.

Alldredge, A.L., Passow, U., and Logan, B.E. (1993). The abundance and significance of a class of large, transparent organic particles in the ocean. *Deep Sea Research Part I: Oceanographic Research Papers* 40**,** 1131-1140.

Aluwihare, L.I., Repeta, D.J., and Chen, R.F. (1997). A major biopolymeric component to dissolved organic carbon in surface sea water. *Nature* 387**,** 166.

Amon, R.M., Fitznar, H.-P., and Benner, R. (2001). Linkages among the bioreactivity, chemical composition, and diagenetic state of marine dissolved organic matter. *Limnology and Oceanography* 46**,** 287-297.

Arnosti, C. (2011). Microbial extracellular enzymes and the marine carbon cycle. *Annual review of marine science* 3**,** 401-425.

Arnosti, C., Durkin, S., and Jeffrey, W. (2005). Patterns of extracellular enzyme activities among pelagic marine microbial communities: implications for cycling of dissolved organic carbon. *Aquatic Microbial Ecology* 38**,** 135-145.

Arrieta, J.M., and Herndl, G.J. (2001). Assessing the diversity of marine bacterial β-glucosidases by capillary electrophoresis zymography. *Applied and environmental microbiology* 67**,** 4896-4900.

Azam, F., Fenchel, T., Field, J.G., Gray, J., Meyer-Reil, L., and Thingstad, F. (1983). The ecological role of water-column microbes in the sea. *Marine ecology progress series***,** 257-263.

Azam, F., and Malfatti, F. (2007). Microbial structuring of marine ecosystems. *Nature Reviews Microbiology* 5**,** 782.

Baines, S.B., and Pace, M.L. (1991). The production of dissolved organic matter by phytoplankton and its importance to bacteria: patterns across marine and freshwater systems. *Limnology and Oceanography* 36**,** 1078-1090.

Barnhart, M.M., and Chapman, M.R. (2006). Curli biogenesis and function. *Annu. Rev. Microbiol.* 60**,** 131-147.

Bauer, J., and Bianchi, T. (2011). 5.02—dissolved organic carbon cycling and transformation. *Treatise on estuarine and coastal science. Academic Press, Waltham***,** 7-67.

Benner, R., Pakulski, J.D., Mccarthy, M., Hedges, J.I., and Hatcher, P.G. (1992). Bulk chemical characteristics of dissolved organic matter in the ocean. *Science* 255**,** 1561-1564.

Bertrand, E.M., Allen, A.E., Dupont, C.L., Norden-Krichmar, T.M., Bai, J., Valas, R.E., and Saito, M.A. (2012). Influence of cobalamin scarcity on diatom molecular physiology and identification of a cobalamin acquisition protein. *Proceedings of the National Academy of Sciences* 109**,** E1762-E1771.

Bertrand, E.M., Saito, M.A., Lee, P.A., Dunbar, R.B., Sedwick, P.N., and Ditullio, G.R. (2011). Iron limitation of a springtime bacterial and phytoplankton community in the Ross Sea: implications for vitamin B12 nutrition. *Frontiers in microbiology* 2**,** 160.

Binnig, G., Quate, C.F., and Gerber, C. (1986). Atomic force microscope. *Physical review letters* 56**,** 930.

Branda, S.S., Chu, F., Kearns, D.B., Losick, R., and Kolter, R. (2006). A major protein component of the Bacillus subtilis biofilm matrix. *Molecular microbiology* 59**,** 1229-1238.

Breitbart, M. (2011). Marine viruses: truth or dare. *Annual review of marine science*, 4, 425-448.

Burdige, D.J. (2007). Preservation of organic matter in marine sediments: controls, mechanisms, and an imbalance in sediment organic carbon budgets? *Chemical reviews* 107**,** 467-485.

Cavicchioli, R., Ripple, W.J., Timmis, K.N., Azam, F., Bakken, L.R., Baylis, M., Behrenfeld, M.J., Boetius, A., Boyd, P.W., and Classen, A.T. (2019). Scientists' warning to humanity: microorganisms and climate change. *Nature Reviews Microbiology* 17**,** 569-586.

Chapman, M.R., Robinson, L.S., Pinkner, J.S., Roth, R., Heuser, J., Hammar, M., Normark, S., and Hultgren, S.J. (2002). Role of Escherichia coli curli operons in directing amyloid fiber formation. *Science* 295**,** 851-855.

Chavez, F.P., Messié, M., and Pennington, J.T. (2010). Marine primary production in relation to climate variability and change.

Chin, W.-C., Orellana, M.V., Quesada, I., and Verdugo, P. (2004). Secretion in unicellular marine phytoplankton: demonstration of regulated exocytosis in Phaeocystis globosa. *Plant and cell physiology* 45, 535-542.

Chin, W.-C., Orellana, M.V., and Verdugo, P. (1998). Spontaneous assembly of marine dissolved organic matter into polymer gels. *Nature* 391, 568.

Cho, B.C., and Azam, F. (1988). Major role of bacteria in biogeochemical fluxes in the ocean's interior. *Nature* 332, 441.

Cochlan, W.P., Wikner, J., Steward, G.F., Smith, D.C., and Azam, F. (1993). Spatial distribution of viruses, bacteria and chlorophyll a in neritic, oceanic and estuarine environments. *Marine Ecology-Progress Series* 92, 77-77.

Cottrell, M.T., and Kirchman, D.L. (2000a). Natural assemblages of marine proteobacteria and members of the Cytophaga-Flavobacter cluster consuming low- and high-molecular-weight dissolved organic matter. *Appl Environ Microbiol* 66, 1692-1697.

Cottrell, M.T., and Kirchman, D.L. (2000b). Natural assemblages of marine proteobacteria and members of the Cytophaga-Flavobacter cluster consuming low-and high-molecular-weight dissolved organic matter. *Applied and environmental microbiology* 66, 1692-1697.

Cottrell, M.T., Yu, L., and Kirchman, D.L. (2005). Sequence and expression analyses of Cytophaga-like hydrolases in a Western arctic metagenomic library and the Sargasso Sea. *Applied and environmental microbiology* 71, 8506-8513.

D'ambrosio, L., Ziervogel, K., Macgregor, B., Teske, A., and Arnosti, C. (2014). Composition and enzymatic function of particle-associated and free-living bacteria: a coastal/offshore comparison. *The ISME journal* 8, 2167-2179.

Delong, E.F., Franks, D.G., and Alldredge, A.L. (1993). Phylogenetic diversity of aggregate-attached vs. free-living marine bacterial assemblages. *Limnology and oceanography* 38, 924-934.

Ding, Y.-X., Chin, W.-C., Rodriguez, A., Hung, C.-C., Santschi, P.H., and Verdugo, P. (2008). Amphiphilic exopolymers from Sagittula stellata induce DOM self-assembly and formation of marine microgels. *Marine Chemistry* 112, 11-19.

Druffel, E.R., Williams, P.M., Bauer, J.E., and Ertel, J.R. (1992). Cycling of dissolved and particulate organic matter in the open ocean. *Journal of Geophysical Research: Oceans* 97**,** 15639-15659.

Dufrêne, Y.F., Martínez-Martín, D., Medalsy, I., Alsteens, D., and Müller, D.J. (2013). Multiparametric imaging of biological systems by force-distance curve–based AFM. *Nature methods* 10**,** 847-854.

Dufrêne, Y.F., Viljoen, A., Mignolet, J., and Mathelié-Guinlet, M. (2021). AFM in cellular and molecular microbiology. *Cellular Microbiology***,** e13324.

Engel, A., Thoms, S., Riebesell, U., Rochelle-Newall, E., and Zondervan, I. (2004). Polysaccharide aggregation as a potential sink of marine dissolved organic carbon. *Nature* 428**,** 929.

Flemming, H.-C., and Wingender, J. (2010). The biofilm matrix. *Nature reviews microbiology* 8**,** 623-633.

Flemming, H.-C., and Wuertz, S. (2019). Bacteria and archaea on Earth and their abundance in biofilms. *Nature Reviews Microbiology* 17**,** 247-260.

Flintrop, C.M., Rogge, A., Miksch, S., Thiele, S., Waite, A.M., and Iversen, M.H. (2018). Embedding and slicing of intact in situ collected marine snow. *Limnology and Oceanography: Methods* 16**,** 339-355.

Fry, B., Hopkinson Jr, C.S., Nolin, A., Norrman, B., and Zweifel, U.L. (1996). Long-term decomposition of DOC from experimental diatom blooms. *Limnology and Oceanography* 41**,** 1344-1347.

Fuhrman, J. (1987). Close coupling between release and uptake of dissolved free amino acids in seawater studied by an isotope dilution approach. *Mar. Ecol. Prog. Ser* 37**,** 45-52.

Garren, M., and Azam, F. (2010). New method for counting bacteria associated with coral mucus. *Applied and environmental microbiology* 76**,** 6128-6133.

Grossart, H.-P., and Ploug, H. (2001). Microbial degradation of organic carbon and nitrogen on diatom aggregates. *Limnology and oceanography* 46**,** 267-277.

Grossart, H.-P., Steward, G.F., Martinez, J., and Azam, F. (2000). A simple, rapid method for demonstrating bacterial flagella. *Applied and environmental microbiology* 66**,** 3632-3636.

Gruber, N., Gloor, M., Fletcher, S.E.M., Doney, S.C., Dutkiewicz, S., Follows, M.J., Gerber, M., Jacobson, A.R., Joos, F., and Lindsay, K. (2009). Oceanic sources, sinks, and transport of atmospheric CO2. *Global Biogeochemical Cycles* 23.

Guo, L., and Santschi, P.H. (1997). Composition and cycling of colloids in marine environments. *Reviews of Geophysics* 35**,** 17-40.

Hansell, D.A. (2013). Recalcitrant dissolved organic carbon fractions. *Annual Review of Marine Science* 5**,** 421-445.

Hansell, D.A., and Carlson, C.A. (1998). Deep-ocean gradients in the concentration of dissolved organic carbon. *Nature* 395**,** 263.

Hansell, D.A., and Carlson, C.A. (2014). *Biogeochemistry of marine dissolved organic matter.* Academic Press.

Hansell, D.A., Carlson, C.A., Repeta, D.J., and Schlitzer, R. (2009). Dissolved organic matter in the ocean: A controversy stimulates new insights. *Oceanography* 22**,** 202-211.

Helliwell, K.E., Wheeler, G.L., Leptos, K.C., Goldstein, R.E., and Smith, A.G. (2011). Insights into the evolution of vitamin B12 auxotrophy from sequenced algal genomes. *Molecular biology and evolution* 28**,** 2921-2933.

Hollibaugh, J., and Azam, F. (1983). Microbial degradation of dissolved proteins in seawater 1. *Limnology and Oceanography* 28**,** 1104-1116.

Holmfeldt, K., Titelman, J., and Riemann, L. (2010). Virus production and lysate recycling in different sub-basins of the Northern Baltic Sea. *Microbial ecology* 60**,** 572-580.

Houghton, R. (2007). Balancing the global carbon budget. *Annu. Rev. Earth Planet. Sci.* 35**,** 313-347.

Ibarbalz, F.M., Henry, N., Brandão, M.C., Martini, S., Busseni, G., Byrne, H., Coelho, L.P., Endo, H., Gasol, J.M., and Gregory, A.C. (2019). Global trends in marine plankton diversity across kingdoms of life. *Cell* 179**,** 1084-1097. e1021.

Isao, K., Hara, S., Terauchi, K., and Kogure, K. (1990). Role of sub-micrometre particles in the ocean. *Nature* 345**,** 242.

Jiao, N., Herndl, G.J., Hansell, D.A., Benner, R., Kattner, G., Wilhelm, S.W., Kirchman, D.L., Weinbauer, M.G., Luo, T., and Chen, F. (2010). Microbial production of recalcitrant dissolved organic matter: long-term carbon storage in the global ocean. *Nature Reviews Microbiology* 8**,** 593.

Jurado, E., Dachs, J., Duarte, C.M., and Simo, R. (2008). Atmospheric deposition of organic and black carbon to the global oceans. *Atmospheric Environment* 42**,** 7931-7939.

Kaiser, K., and Benner, R. (2009). Biochemical composition and size distribution of organic matter at the Pacific and Atlantic time-series stations. *Marine Chemistry* 113**,** 63-77.

Karner, M., and Herndl, G.J. (1992). Extracellular enzymatic activity and secondary production in free-living and marine-snow-associated bacteria. *Marine Biology* 113**,** 341-347.

Kawasaki, N., and Benner, R. (2006). Bacterial release of dissolved organic matter during cell growth and decline: molecular origin and composition. *Limnology and Oceanography* 51**,** 2170-2180.

Keil, R.G., and Kirchman, D.L. (1994). Abiotic transformation of labile protein to refractory protein in sea water. *Marine Chemistry* 45**,** 187-196.

Kindt, J.H., Sitko, J.C., Pietrasanta, L.I., Oroudjev, E., Becker, N., Viani, M.B., and Hansma, H.G. (2002). Methods for biological probe microscopy in aqueous fluids. *Methods Cell Biol* 68**,** 213-229.

Kiørboe, T., and Jackson, G.A. (2001). Marine snow, organic solute plumes, and optimal chemosensory behavior of bacteria. *Limnology and Oceanography* 46**,** 1309-1318.

Kiørboe, T., Tang, K., Grossart, H.-P., and Ploug, H. (2003). Dynamics of microbial communities on marine snow aggregates: colonization, growth, detachment, and grazing mortality of attached bacteria. *Applied and Environmental Microbiology* 69**,** 3036-3047.

Kirchman, D.L., Henry, D.L., and Dexter, S.C. (1989). Adsorption of proteins to surfaces in seawater. *Marine chemistry* 27**,** 201-217.

Kirchman, D.L., and White, J. (1999). Hydrolysis and mineralization of chitin in the Delaware Estuary. *Aquatic Microbial Ecology* 18**,** 187-196.

Kriest, I., and Oschlies, A. (2007). Modelling the effect of cell-size-dependent nutrient uptake and exudation on phytoplankton size spectra. *Deep Sea Research Part I: Oceanographic Research Papers* 54**,** 1593-1618.

Kuznetsov, Y.G., Chang, S.-C., Credaroli, A., Martiny, J., and Mcpherson, A. (2012). An atomic force microscopy investigation of cyanophage structure. *Micron* 43, 1336-1342.

Kuznetsov, Y.G., Martiny, J.B., and Mcpherson, A. (2010). Structural analysis of a Synechococcus myovirus S-CAM4 and infected cells by atomic force microscopy. *Journal of general virology* 91, 3095-3104.

Lander, G.C., Baudoux, A.-C., Azam, F., Potter, C.S., Carragher, B., and Johnson, J.E. (2012). Capsomer dynamics and stabilization in the T= 12 marine bacteriophage SIO-2 and its procapsid studied by CryoEM. *Structure* 20, 498-503.

Liu, S., and Wang, Y. (2010). Application of AFM in microbiology: a review. *Scanning* 32, 61-73.

Long, R.A., and Azam, F. (1996). Abundant protein-containing particles in the sea. *Aquatic Microbial Ecology* 10, 213-221.

Mague, T., Friberg, E., Hughes, D., and Morris, I. (1980). Extracellular release of carbon by marine phytoplankton; a physiological approach1. *Limnology and Oceanography* 25, 262-279.

Malfatti, F., and Azam, F. (2009). Atomic force microscopy reveals microscale networks and possible symbioses among pelagic marine bacteria. *Aquatic Microbial Ecology* 58, 1-14.

Malfatti, F., Samo, T.J., and Azam, F. (2010). High-resolution imaging of pelagic bacteria by atomic force microscopy and implications for carbon cycling. *The ISME journal* 4, 427-439.

Martinez, J., Smith, D.C., Steward, G.F., and Azam, F. (1996). Variability in ectohydrolytic enzyme activities of pelagic marine bacteria and its significance for substrate processing in the sea. *Aquatic Microbial Ecology* 10, 223-230.

Mccarren, J., Becker, J.W., Repeta, D.J., Shi, Y., Young, C.R., Malmstrom, R.R., Chisholm, S.W., and Delong, E.F. (2010). Microbial community transcriptomes reveal microbes and metabolic pathways associated with dissolved organic matter turnover in the sea. *Proceedings of the National Academy of Sciences* 107, 16420-16427.

Meon, B., and Kirchman, D.L. (2001). Dynamics and molecular composition of dissolved organic material during experimental phytoplankton blooms. *Marine Chemistry* 75, 185-199.

Middelboe, M. (2008). *Microbial disease in the sea: effects of viruses on carbon and nutrient cycling.* Princeton, NJ, USA: Princeton University Press.

Middelboe, M., and Jørgensen, N.O. (2006). Viral lysis of bacteria: an important source of dissolved amino acids and cell wall compounds. *Journal of the Marine Biological Association of the United Kingdom* 86**,** 605-612.

Middelboe, M., Riemann, L., Steward, G.F., Hansen, V., and Nybroe, O. (2003). Virus-induced transfer of organic carbon between marine bacteria in a model community. *Aquatic Microbial Ecology* 33**,** 1-10.

Mikaloff Fletcher, S.E., Gruber, N., Jacobson, A.R., Doney, S.C., Dutkiewicz, S., Gerber, M., Follows, M., Joos, F., Lindsay, K., and Menemenlis, D. (2006). Inverse estimates of anthropogenic CO2 uptake, transport, and storage by the ocean. *Global Biogeochemical Cycles* 20.

Miller, S.I., and Salama, N.R. (2018). The gram-negative bacterial periplasm: Size matters. *PLoS biology* 16**,** e2004935.

Møller, E.F. (2007). Production of dissolved organic carbon by sloppy feeding in the copepods Acartia tonsa, Centropages typicus, and Temora longicornis. *Limnology and Oceanography* 52**,** 79-84.

Møller, E.F., Thor, P., and Nielsen, T.G. (2003). Production of DOC by Calanus finmarchicus, C. glacialis and C. hyperboreus through sloppy feeding and leakage from fecal pellets. *Marine Ecology Progress Series* 262**,** 185-191.

Mopper, K., and Stahovec, W.L. (1986). Sources and sinks of low molecular weight organic carbonyl compounds in seawater. *Marine Chemistry* 19**,** 305-321.

Myklestad, S.M. (2000). "Dissolved organic carbon from phytoplankton," in *Marine chemistry*. Springer), 111-148.

Nagata, T., and Kirchman, D. (1996). Bacterial degradation of protein adsorbed to model submicron particles in seawater. *Marine Ecology Progress Series* 132**,** 241-248.

Nagata, T., and Kirchman, D.L. (1992). Release of dissolved organic matter by heterotrophic protozoa: implications for microbial food webs. *Arch. Hydrobiol. Beih. Ergebn. Limnol* 35**,** 99-109.

Nagata, T., and Koike, I. (1995). Marine colloids: Their roles in food webs and biogeochemical fluxes. *Biogeochemical processes and ocean flux in the western Pacific***,** 275-292.

Nagata, T., Meon, B., and L. Kirchman, D. (2003). Microbial degradation of peptidoglycan in seawater. *Limnology and Oceanography* 48**,** 745-754.

Nishino, T., Ikemoto, E., and Kogure, K. (2004). Application of atomic force microscopy to observation of marine bacteria. *Journal of oceanography* 60**,** 219-225.

Noble, R.T., and Fuhrman, J.A. (1998). Use of SYBR Green I for rapid epifluorescence counts of marine viruses and bacteria. *Aquatic Microbial Ecology* 14**,** 113-118.

Obayashi, Y., and Suzuki, S. (2005). Proteolytic enzymes in coastal surface seawater: significant activity of endopeptidases and exopeptidases. *Limnology and oceanography* 50**,** 722-726.

Ogawa, H., Amagai, Y., Koike, I., Kaiser, K., and Benner, R. (2001). Production of refractory dissolved organic matter by bacteria. *Science* 292**,** 917-920.

Ogawa, H., and Tanoue, E. (2003). Dissolved organic matter in oceanic waters. *Journal of Oceanography* 59**,** 129-147.

Orellana, M.V., Matrai, P.A., Leck, C., Rauschenberg, C.D., Lee, A.M., and Coz, E. (2011). Marine microgels as a source of cloud condensation nuclei in the high Arctic. *Proceedings of the National Academy of Sciences* 108**,** 13612-13617.

Orellana, M.V., Petersen, T.W., Diercks, A.H., Donohoe, S., Verdugo, P., and Van Den Engh, G. (2007). Marine microgels: Optical and proteomic fingerprints. *Marine chemistry* 105**,** 229-239.

Pace, M.L., Reche, I., Cole, J.J., Fernández-Barbero, A., Mazuecos, I.P., and Prairie, Y.T. (2012). pH change induces shifts in the size and light absorption of dissolved organic matter. *Biogeochemistry* 108**,** 109-118.

Passow, U. (2002a). Production of transparent exopolymer particles (TEP) by phyto-and bacterioplankton. *Marine Ecology Progress Series* 236**,** 1-12.

Passow, U. (2002b). Transparent exopolymer particles (TEP) in aquatic environments. *Progress in oceanography* 55**,** 287-333.

Pletikapić, G., Berquand, A., Radić, T.M., and Svetličić, V. (2012). Quantitative nanomechanical mapping of marine diatom in seawater using peak force tapping atomic force microscopy 1. *Journal of phycology* 48**,** 174-185.

Pletikapić, G., Radić, T.M., Zimmermann, A.H., Svetličić, V., Pfannkuchen, M., Marić, D., Godrijan, J., and Žutić, V. (2011). AFM imaging of extracellular polymer

release by marine diatom Cylindrotheca closterium (Ehrenberg) Reiman & JC Lewin. *Journal of molecular recognition* 24**,** 436-445.

Ploug, H., and Grossart, H.P. (2000). Bacterial growth and grazing on diatom aggregates: Respiratory carbon turnover as a function of aggregate size and sinking velocity. *Limnology and Oceanography* 45**,** 1467-1475.

Pomeroy, L.R., Leb. Williams, P.J., Azam, F., and Hobbie, J.E. (2007). The microbial loop. *Oceanography* 20**,** 28-33.

Radić, T.M., Svetličić, V., Žutić, V., and Boulgaropoulos, B. (2011). Seawater at the nanoscale: marine gel imaged by atomic force microscopy. *Journal of Molecular Recognition* 24**,** 397-405.

Rich, J.H., Ducklow, H.W., and Kirchman, D.L. (1996). Concentrations and uptake of neutral monosaccharides along 14 W in the equatorial Pacific: contribution of glucose to heterotrophic bacterial activity and the DOM flux. *Limnology and Oceanography* 41**,** 595-604.

Sambrotto, R.N., Savidge, G., Robinson, C., Boyd, P., Takahashi, T., Karl, D.M., Langdon, C., Chipman, D., Marra, J., and Codispoti, L. (1993). Elevated consumption of carbon relative to nitrogen in the surface ocean. *Nature* 363**,** 248.

Samo, T.J., Malfatti, F., and Azam, F. (2008). A new class of transparent organic particles in seawater visualized by a novel fluorescence approach. *Aquatic Microbial Ecology* 53**,** 307-321.

Santschi, P.H., Balnois, E., Wilkinson, K.J., Zhang, J., Buffle, J., and Guo, L. (1998). Fibrillar polysaccharides in marine macromolecular organic matter as imaged by atomic force microscopy and transmission electron microscopy. *Limnology and Oceanography* 43**,** 896-908.

Sarmento, H., and Gasol, J.M. (2012). Use of phytoplankton-derived dissolved organic carbon by different types of bacterioplankton. *Environmental microbiology* 14**,** 2348-2360.

Seo, Y., Ikemoto, E., Yoshida, A., and Kogure, K. (2007). Particle capture by marine bacteria. *Aquatic microbial ecology* 49**,** 243-253.

Sheik, A., Brussaard, C., Lavik, G., Foster, R., Musat, N., Adam, B., and Kuypers, M. (2013). Viral infection of Phaeocystis globosa impedes release of chitinous star-like structures: quantification using single cell approaches. *Environmental microbiology* 15**,** 1441-1451.

Shibata, A., Kogure, K., Koike, I., and Ohwada, K. (1997). Formation of submicron colloidal particles from marine bacteria by viral infection. *Marine Ecology Progress Series* 155**,** 303-307.

Simon, M., Grossart, H.-P., Schweitzer, B., and Ploug, H. (2002). Microbial ecology of organic aggregates in aquatic ecosystems. *Aquatic microbial ecology* 28**,** 175-211.

Skoog, A., and Benner, R. (1997). Aldoses in various size fractions of marine organic matter: Implications for carbon cycling. *Limnology and Oceanography* 42**,** 1803-1813.

Smith, D.C., Simon, M., Alldredge, A.L., and Azam, F. (1992). Intense hydrolytic enzyme activity on marine aggregates and implications for rapid particle dissolution. *Nature* 359**,** 139.

Smith, D.C., Steward, G.F., Long, R.A., and Azam, F. (1995). Bacterial mediation of carbon fluxes during a diatom bloom in a mesocosm. *Deep Sea Research Part II: Topical Studies in Oceanography* 42**,** 75-97.

Steinberg, D.K., and Landry, M.R. (2017). Zooplankton and the ocean carbon cycle. *Annual Review of Marine Science* 9**,** 413-444.

Suttle, C.A. (1994). The significance of viruses to mortality in aquatic microbial communities. *Microbial ecology* 28**,** 237-243.

Suttle, C.A. (2007). Marine viruses—major players in the global ecosystem. *Nature Reviews Microbiology* 5**,** 801.

Svetličić, V., Žutić, V., and Zimmermann, A.H. (2005). Biophysical scenario of giant gel formation in the Northern Adriatic Sea. *Annals of the New York Academy of Sciences* 1048**,** 524-527.

Tang, Y.Z., Koch, F., and Gobler, C.J. (2010). Most harmful algal bloom species are vitamin B1 and B12 auxotrophs. *Proceedings of the National Academy of Sciences***,** 201009566.

Taylor, G.T. (2019). Windows into microbial seascapes: Advances in nanoscale imaging and application to marine sciences. *Annual review of marine science* 11**,** 465-490.

Thornton, D.C. (2014). Dissolved organic matter (DOM) release by phytoplankton in the contemporary and future ocean. *European Journal of Phycology* 49**,** 20-46.

Verdugo, P. (2012). Marine microgels. *Annual Review of Marine Science* 4**,** 375-400.

Verdugo, P., Alldredge, A.L., Azam, F., Kirchman, D.L., Passow, U., and Santschi, P.H. (2004). The oceanic gel phase: a bridge in the DOM–POM continuum. *Marine Chemistry* 92**,** 67-85.

Viljoen, A., Foster, S.J., Fantner, G.E., Hobbs, J.K., and Dufrêne, Y.F. (2020). Scratching the surface: bacterial cell envelopes at the nanoscale. *MBio* 11**,** e03020-03019.

Vraspir, J.M., and Butler, A. (2009). Chemistry of marine ligands and siderophores. *Annual review of marine science* 1**,** 43-63.

Weinbauer, M.G., and Peduzzi, P. (1995). Effect of virus-rich high molecular weight concentrates of seawater on the dynamics of dissolved amino acids and carbohydrates. *Marine Ecology Progress Series* 127**,** 245-253.

Wells, M.L., and Goldberg, E.D. (1991). Occurrence of small colloids in sea water. *Nature* 353**,** 342.

Wells, M.L., and Goldberg, E.D. (1993). Colloid aggregation in seawater. *Marine Chemistry* 41**,** 353-358.

Wilhelm, S.W., and Suttle, C.A. (1999). Viruses and nutrient cycles in the sea: viruses play critical roles in the structure and function of aquatic food webs. *Bioscience* 49**,** 781-788.

Wilkinson, K.J., Balnois, E., Leppard, G.G., and Buffle, J. (1999). Characteristic features of the major components of freshwater colloidal organic matter revealed by transmission electron and atomic force microscopy. *Colloids and Surfaces A: Physicochemical and Engineering Aspects* 155**,** 287-310.

Williams, P.M., and Druffel, E.R. (1987). Radiocarbon in dissolved organic matter in the central North Pacific Ocean. *Nature* 330**,** 246-248.

Wommack, K.E., and Colwell, R.R. (2000). Virioplankton: viruses in aquatic ecosystems. *Microbiology and molecular biology reviews* 64**,** 69-114.

Xu, K., Sun, W., Shao, Y., Wei, F., Zhang, X., Wang, W., and Li, P. (2018). Recent development of PeakForce Tapping mode atomic force microscopy and its applications on nanoscience. *Nanotechnology Reviews* 7**,** 605-621.

Zhang, Y., Zhang, F., Yang, J., and Jiao, N. (2012). Host responses of a marine bacterium, Roseobacter denitrificans OCh114, to phage infection. *Archives of microbiology* 194**,** 323-330.

Chapter 2 Bacterial nanotubes as intercellular linkages in marine assemblages

2.1 Abstract

Several types of bacterial appendages, e.g., pili and fimbriae, are known for their role in promoting interactions and aggregation with particles and bacteria in the ocean. First discovered in *Bacillus subtilis* and *Escherichia coli*, but novel to marine bacteria, bacterial nanotubes are hollow tubular structures connecting cell pairs that allow for the internal transport of cytoplasmic metabolites across the connecting structure. While the significance of nanotubes in exchange of cytoplasmic content has been established in non-marine bacteria, their occurrence and potential ecological significance in marine bacteria has not been reported. Using multiple high-resolution microscopy methods (atomic force microscopy, scanning and transmission electron microscopy), we have determined that marine bacteria isolates and natural assemblages from nearshore upper ocean waters can express bacterial nanotubes. In marine isolates *Pseudoalteromonas* sp. TW7 and *Alteromonas sp*. ALTSIO, individual bacterial nanotubes measured 50–160 nm in width and extended 100–600 nm between connected cells. The spatial coupling of different cells via nanotubes can last for at least 90 minutes, extending the duration of interaction events between marine bacteria within natural assemblages. The nanomechanical properties of bacterial nanotubes vary in adhesion and dissipation properties, which has implication for structural and functional variability of these structures in their ability to stick to surfaces and respond to mechanical forces. Nanotube frequency is low among cells in enriched natural

assemblages, where nanotubes form short, intimate connections, < 200 nm, between certain neighboring cells. Bacterial nanotubes can form the structural basis for a bacterial ensemble and function as a conduit for cytoplasmic exchange (not explicitly studied here) between members for multicellular coordination and expression. The structural measurements and nanomechanical analyses in this study also extends knowledge about the physical properties of bacterial nanotubes and their consequences for marine microenvironments. The discovery of nanotube expression in marine bacteria has significant potential implications regarding intimate bacterial interactions in spatially-correlated marine microbial communities.

2.2 Introduction

Marine microbial communities are comprised cumulatively of extremely abundant (10^{29} estimated bacteria in the global ocean) and diverse cells that shape the biological and biogeochemical landscapes of the oceans through interactions with their biotic and abiotic environments (Azam et al., 1994;Azam and Malfatti, 2007;Flemming and Wuertz, 2019). Numerous microbial associations and interactions drive and regulate carbon and nutrient fluxes in the ocean via the microbial loop through the production, transformation, and remineralization of organic matter. The aggregate of marine microbes' activity is a major force structuring the global ocean ecosystems that varies spatially and temporally. Therefore, a fundamental goal in microbial oceanography is to understand how microbes interact with their organic matter field, including other microbes, and larger organisms —and with what ecosystem consequences.

This is a formidable challenge given the enormous complexity of the organic matter pool in the ocean, the diversity of potential interactions, and the range of spatial scales of influence—from nanometers to the ocean basins. Further, the occurrence of organic matter is compositionally, spatially, and temporally variable with feedbacks to the interacting microbes. The global ocean dissolved organic matter-carbon (DOM-C) inventory is huge, being comparable to the entire atmospheric CO_2-C pool. Yet, the concentration of readily utilizable DOM is only few tens of µM-C with individual molecular species occurring at sub-pM to nM (Benner and Kaiser, 2003;Wakeham et al., 2003;Kaiser and Benner, 2008;Zark et al., 2017). So, the challenge for pelagic marine bacteria is to grow and persist at the expense of such vanishingly low concentrations of DOM. This has raised the question whether pelagic bacteria gain metabolic and growth advantage by interacting with colloids and particulate detritus to solubilize them, thus generating microscale loci of high DOM. Furthermore, submicron-sized colloids, present at ~10^8 particles mL^{-1} in ambient seawater (Wells and Goldberg, 1991) and likely even greater in phycospheres and detritospheres, might attach to bacterial surface and appendages, generating nanoscale hotspots of organic matter directly on cell surface.

Marine bacteria also interact with co-occurring bacteria as sources of organic nutrients and energy employing a variety of strategies and mechanisms. Bacteria are highly abundant in surface seawater (~10^6 mL^{-1}) and on marine snow (~10^9 mL^{-1}) so bacteria-bacteria separation on average is ~100 µm in the surface ocean and ~10 µm on marine snow. Some bacterial interactions involve the coordination of biological activity and phenotypic expression in groups of bacteria due to quorum sensing. Bacteria-bacteria antagonistic

interactions involving several types of secretion systems have also been reported in marine bacterial communities (Russell et al., 2014;Green and Mecsas, 2016;Klein et al., 2020). Other contact-dependent mechanisms involving physical intercellular connections (e.g., pili and microbial nanowires) for bacteria-bacteria interactions and activity have been extensively studied. Bacterial pili promote bacterial adhesion to surfaces; type IV pili translocate biomolecules between two connected cells (Pelicic, 2008;Lukaszczyk et al., 2019). *Geobacter sulfurreducens* and *Shewanella oneidensis* produce electrically conductive pili to connect cells over micrometer distances. with the capability of extracellular electron transfer for mediating cell-cell communication (Sure et al., 2016). *S. oneidensis* forms nanowires ~10 nm in diameter from outer membrane extensions that connect cells for direct electron transfer (Pirbadian et al., 2014). Extracellular bridges have been observed in *Myxococcus xanthus* as outer membrane vesicles fuse into appendages (Remis et al., 2014). Similar appendages form in marine flavobacteria due to "pearling" of membrane vesicles 50–80 nm in diameter and 80–100 nm in length forming chain-like appendages 0.5–2 µm long. (Fischer et al., 2019).

We have been testing the hypothesis that some marine bacterial surface appendages might additionally serve to capture and concentrate colloidal organic matter from seawater and the bacterium could then enzymatically solubilize and utilize these concentrates of colloidal particles (Patel et al, in preparation). During this study employing atomic force microscopy in order to visualize colloids associating with bacterial appendages in real time, we noticed intercellular connections among bacterial cells involving surface appendages that did not match the characteristics of previously described surface appendages of marine

bacteria. However, these intercellular appendages were similar to bacterial nanotubes first discovered in *Bacillus subtilis* and *Escherichia coli* (Dubey and Ben-Yehuda, 2011). These authors named the appendages "bacterial nanotubes" after analogous structures like tunneling nanotubes that had previously been reported in eukaryotic cells; these dynamic connections facilitate exchange of intracellular contents in various cell types (e.g., neuronal cells, endothelial cells, myogenic satellite cells) (Gousset et al., 2009;Tavi et al., 2010;Astanina et al., 2015;Alarcon-Martinez et al., 2020).

Dubey and Ben-Yehuda discovered that *B. subtilis* and *E. coli* can produce intercellular nanotubes, where adjacent cells form connections with hollow tubular structures that mediate direct transfer of biomolecules (Dubey and Ben-Yehuda, 2011). They showed that bacterial nanotubes are fundamentally distinct from other physical microbial connections involving extracellular appendages, e.g., pili, flagella, and elongated membrane extensions. They described two types of nanotubes: thick tubes connecting distal cell pairs and thin tubes 30–130 nm wide and up to 1 µm long arrayed to connect cells (Dubey and Ben-Yehuda, 2011). Nanotubes were functioning as conduits for the intercellular exchange of cytoplasmic material, including plasmids and proteins, between neighboring cells (Dubey et al., 2016). Nanotubes can also connect interspecies pairs in mixed cultures of *B. subtilis*, *E. coli*, and *Staphylococcus aureus*, increasing the potential for complex cell interactions within a mixed microbial community (Dubey and Ben-Yehuda, 2011). Pande et al. (Pande et al., 2015) found that interspecies nanotubes can accommodate mutually beneficial bidirectional molecular transport in co-cultured auxotrophic mutants of *E. coli* and another terrestrial bacterium *Acinetobacter baylyi* under nutrient limiting conditions. Bacterial

nanotubes can directly deliver tRNase toxin and cell wall hydrolases into recipient cells as an asymmetric competitive or cooperative microbial strategy (Stempler et al., 2017;Baidya et al., 2020). As direct connections and conduits for intercellular exchanges of macromolecules, bacterial nanotubes offer opportunities for coordinated biological activity within groups of microbial cells.

Our finding of nanotube expression in marine bacteria prompted us to begin to address their influence on how bacteria interact with the organic matter (including other bacteria) and on the microscale physical structure of pelagic marine ecosystems. Bacterial nanotubes could be a novel microbial strategy for creating and/or exploiting DOM hotspots in the pelagic ocean, by establishing hollow connections between cells and enabling intercellular exchanges of cytoplasmic macromolecules, offering interesting opportunities for coordinated biological activity. We report first observations of intercellular nanotubes in marine bacterial isolates and within natural marine assemblages using atomic force microscopy (AFM).

The application of AFM on live cells enabled us to visualize these structures that have escaped prior observation, and the potential to probe their biomechanical properties and functionality due to AFM force application and sensing capabilities. Using complementary microscopy techniques AFM, SEM and TEM, we show these structures are hollow and could accommodate the transport and exchange of internal cellular material. We also found additional types of contact-dependent linkages complementary to bacterial nanotubes in tethering bacteria into networks, sometimes between morphologically different cells. Our findings add to understanding of bacterial interactions with other bacteria,

pertaining to the potential density and diversity of nanotubes and other intercellular connections in bacterial assemblages.

2.3 Materials and Methods

2.3.1 Bacterial cultures

Samples with natural marine assemblages were prepared from seawater collected off Ellen Browning Scripps Memorial Pier (San Diego, CA, USA). Samples (100 mL) were filtered upon a 0.2-µm polycarbonate filters and resuspended in 10 mL of 0.2-µm filtered autoclaved seawater (FASW) and enriched with Marine Broth 2216 liquid medium (Becton, Dickinson and Company, MD, USA) to adjust the final concentration to 1% or 10% marine broth. Enriched seawater cultures were incubated on a shaker (150 rpm) at room temperature for 20 hours before sample preparation for AFM without any further modification.

Marine bacterial isolates Alteromonas sp. ALTSIO, Pseudoalteromonas sp. TW7, and α-proteobacteria isolates sp. La5 and La6 (isolated from seawater collected from Scripps Pier) were cultured in Marine Broth 2216 liquid medium. Bacterial cells were sampled from cultures at mid-exponential phase and centrifuged at 3000 g for 5 minutes. Pelleted cells were resuspended in FASW in 40-50% of the initial volume and used in sample preparations.

2.3.2 Cell sample preparation for AFM

Cleaned glass coverslips were treated with poly-D-lysine by placing a 10 µL droplet of a 1 mg/ml solution between a pair of coverslips and separating to air dry. A sample region

for cells was demarcated with a hydrophobic barrier by outlining a circle with a liquid blocker PAP pen. A volume of 200 to 250 µL of cell suspension was deposited upon the poly-D-lysine-coated glass coverslip and incubated at room temperature for 30 mins to 1 hour. The cell suspension was exchanged for fresh FASW buffer using a pair of syringes simultaneously to gently replace the media and then promptly fixed with 20 µL of 37% formalin (final conc. ca. 4%) for 15 mins. Sample coverslips were then rinsed with 5 mL of pure water and then air dried prior to microscopy preparation and analysis.

2.3.3 Atomic Force Microscopy

AFM is an emerging microscopic method that employs a scanning probe for investigating nanoscale biological structures and physical interactions in near-native conditions (Liu and Wang, 2010;Aguayo et al., 2015;Dufrêne et al., 2021;Zhou et al., 2021). Briefly, an ultrasharp tip on a microcantilever is brought into physical contact with a sample surface with actuator movement. The repulsive atomic forces between the AFM tip and sample surface registers as a deflection in the microcantilever, which is measured and monitored by optical beam deflection. Upon contact, the AFM tip images the sample topography by laterally scanning across the surface and maintaining constant force by applying feedback control to adjust tip-sample distance with piezoelectric actuators. In addition to the reconstructed surface topography, the feedback error from the difference between the setpoint force and actual imaging forces can be reconstructed into an error mode image that emphasize sharp changes in the surface.

In non-imaging applications, AFM can measure local force profiles by simultaneous measuring the tip-sample distance and tip forces during extension and retraction movements of the tip with respect to the surface at various spatial points. Adhesive properties can be measured empirically as the maximum attraction force experienced by the tip during its retraction away from the surface. The local deformation of the sample area is measured as the vertical difference between the points of contact in an extension-retraction cycle, where the net tip force is zero. Additionally, energy dissipated from the tip into the sample, a localized mechanical property, can be assessed qualitatively by computing from the difference in integrated area of extension and retraction force-distance curves.

Quantitative Nanomechanical MappingTM (QNM) is a dynamic AFM imaging modality that integrates topographic imaging and nanomechanical characterization (Pittenger and Slade, 2013). Briefly, the AFM tip is sinusoidally oscillated at frequencies higher than image scan rates. In this movement, the tip experiences tapping events of brief contact with the surface at the peak of its movement. The force is monitored during the tapping cycle to measure the peak force applied. Individual tapping cycles are converted into force-distance curves and analyzed to measure sample nanomechanical properties.

Sample coverslips were secured on glass coverslips with adhesive tabs and imaged using a Dimension FastScan Atomic Force Microscope (Bruker, Santa Barbara, CA). AFM imaging was performed in QNM mode using ScanAsyst-Air probes (Bruker, spring constant: 0.4 N/m, nominal tip radius: 2 nm). Briefly, the AFM tip was oscillated at a PeakForce Tapping frequency of 8 kHz during scanning with a tapping amplitude of 150 nm. Live cell

samples were imaged unfixed and in a 0.2-µm syringe-filtered FASW imaging media using ScanAsyst-Fluid Probes (spring constant: 0.7 N/m, tip radius: 20 nm). AFM images were collected at 1024x1024 pixel resolutions at 2 Hz scan rate unless otherwise specified. Raw AFM image data was processed with line flattening and plane fitting routines using Nanoscope Analysis (Bruker) and Gwyddion software (http://gwyddion.net). For select AFM images, Gwyddion software was used to generate SEM image-like presentations from AFM height data simulated by Monte Carlo integration (Klapetek et al., 2004). The length and width of nanotubes were measured from independent $10\,\mu m \times 10\,\mu m$ image scans, from 2 replicate samples for TW7 and ALTSIO isolates. The frequency of intercellular connections was determined as the number of interconnecting bacterial structures normalized by the number of cells within an AFM image scan. The average frequency was calculated from the harmonic mean of the observed frequencies from regions presenting intercellular connections.

2.3.4 Scanning and Transmission Electron Microscopy

Samples were prepared as specified above on glass coverslips for scanning electron microscopy (SEM) analysis and secured onto a SEM sample holder with carbon tape. Samples were sputter coated with chrome for 3 seconds and then imaged on a Zeiss Sigma 500 SEM microscope (Zeiss, Thornwood, New York).

Standard negative stain protocols were used to prepare bacterial samples, as specified above, for transmission electron microscopy (TEM) imaging. Briefly, samples were placed

in modified Karnovsky's fixative (2.5% glutaraldehyde and 2% paraformaldehyde in 0.15 M sodium cacodylate buffer, pH 7.4) for at least 4 hours, postfixed in 1% osmium tetroxide in 0.15 M cacodylate buffer for 1 hour and stained en bloc in 2% uranyl acetate for 1 hour. Samples were then dehydrated in ethanol, embedded in Durcupan epoxy resin (Sigma-Aldrich), sectioned at 50 to 60 nm on a Leica UCT ultramicrotome, and picked up on Formvar and carbon-coated copper grids. TEM sample grids were viewed on a FEI Tecnai Spirit G2 BioTWIN Transmission Electron Microscope equipped with an Eagle 4k CCD camera (FEI, Hillsboro, OR).

2.4 Results

2.4.1 Intercellular connectivity between marine bacteria

We observed during nanoscale imaging in native-like conditions with AFM numerous instances of bacterial nanotubes connecting cell pairs within surface populations of Pseudoalteromonas sp. TW7 and Alteromonas sp. ALTSIO cultured isolates. A study of bacterial nanotubes and their size measurements among TW7 and ALTSIO cells shows variability in their dimensions. Figure 2.1 shows representative AFM and SEM images of the various intercellular bacterial nanotubes in TW7 and ALTSIO cultured cells. Nanotubes visually classified from intercellular connections were individually measured from AFM height images. Histograms of nanotube length and width were derived from 71 nanotubes and are shown in Figure 2.1 ($n_{TW7} = 47$, $n_{ALTSIO} = 24$). The nanotube lengths range 100–600 nm, and the widths range 50–160 nm (measured by the half maximum width at the connection midpoint). A single outlier case with a length of 918 nm observed in ALTSIO

cells was excluded from the length distribution. A single peak was observed in the unimodal observed frequency distributions for nanotube widths, with a peak within the 60–120 nm range, for both ALTSIO and TW7 bacterial isolates (Figuire 2.1E, 2.1G). The nanotube length distributions differed between TW7 and ALSTIO and were observed as bimodal and unimodal distributions, respectively. Two peaks were observed in TW7 nanotube length distribution (Figure 2.1H), around 150–200 nm and 350–450 nm, with a separation threshold at approximately 250 nm. In comparison, ALTSIO nanotubes had relatively shorter lengths, with a range of 100–350 nm, and the distribution peak between 100–200 nm (Figure 2.1F). The heights of bacterial nanotubes between cells range between 18–250 nm, where connections > 150 nm in width are correlated with a greater height. Nanotubular connections with a measured height less than 100 nm are likely due to the intercellular structure settling on the substrate surface along its span. In addition to nanotubes, there were various observations of wide, short intercellular connections between cells lacking a tubular appearance; such features had widths greater than 150 nm and lengths lower than 250 nm and potentially consist of polymers forming a physical linkage between cells.

Figure 2.1: **Image and size distributions of marine bacteria nanotubes.** Images of bacterial nanotubes in marine isolates *Pseudoalteromonas* sp. TW7 (**A, C**) and *Alteromonas* sp. ALTSIO (**B, D**) reveal various nanotubes and physical connections between adjacent cells (**A, B**: AFM; **C, D**: SEM). Observed frequencies of nanotube width and length measurements are shown for ALTSIO (**E, F**) and TW7 (**G, H**) cells. Frequency values were calculated from fractions of all ALTSIO (n=24) and TW7 (n=47) nanotubes. Bin sizes for width and length graphs are 20 and 50 nm, respectively.
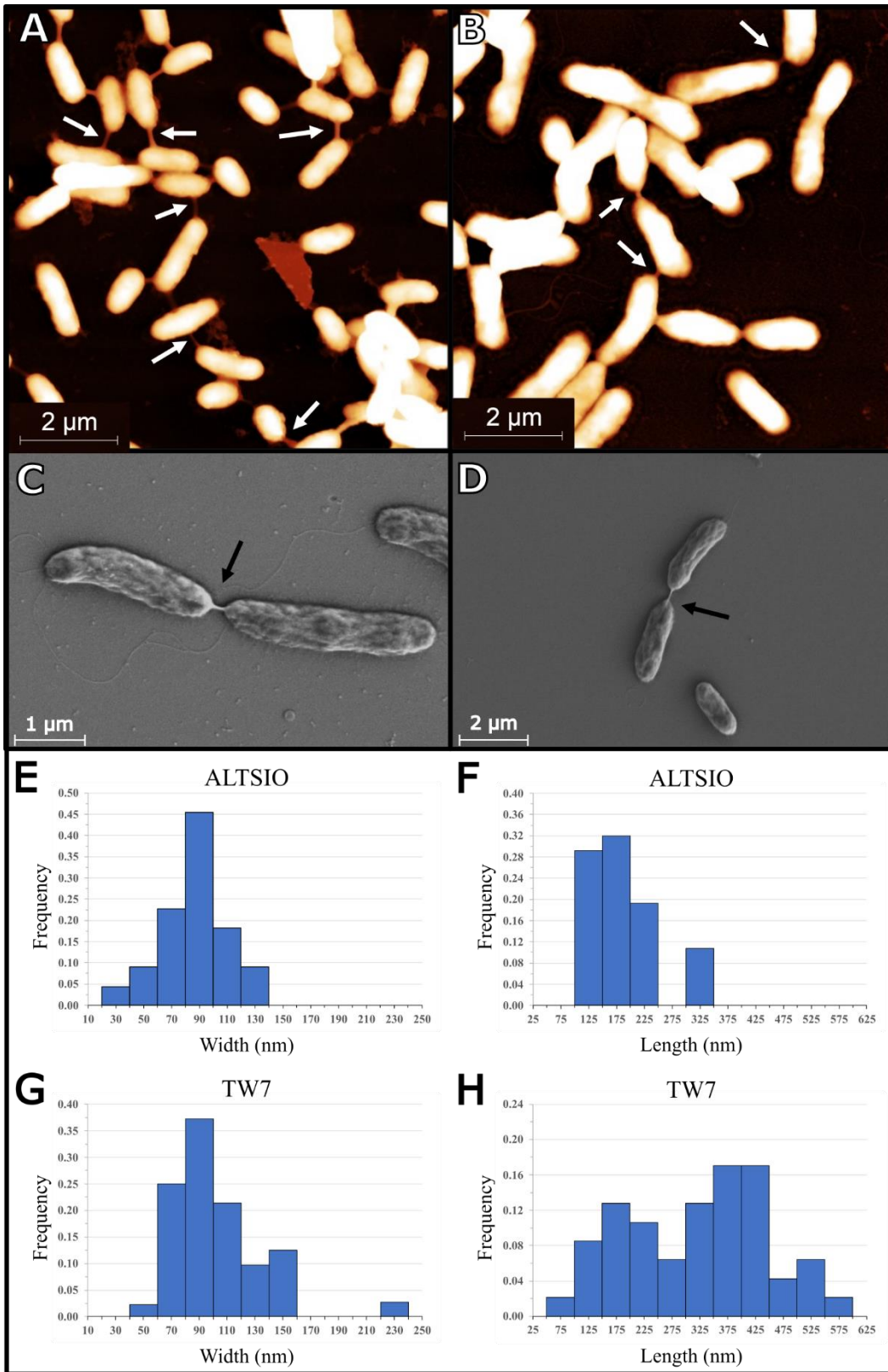
2.4.2 Connection frequency

The average frequency of general intercellular connections per bacterial cell was 0.11 for TW7 (n_{cells} = 501) and 0.07 for ALTSIO (n_{cells} = 545), which include bacterial nanotubes and general physical linkages (i.e., not tubes). The range of observed frequencies in TW7 cells are 0.03–0.68 connections per cell (n_{images} = 11) and in ALTSIO cells are 0.02–0.50 connections per cell (n_{images} = 17). Of these observed intercellular connections, 67% for TW7 ($n_{nanotubes}$ = 47) and 44% for ALTSIO ($n_{nanotubes}$ = 24), were classified as individual nanotubular structures based on reported descriptions, resulting in an average frequency of 0.07 and 0.03 of nanotubes per bacterial cell for the respective bacterial isolates. These connections are classifiable as nanotubes based on singular connection between two cells, a linear span, well-defined edges, and with a consistent width and devoid of deviation along its span.

The cultured isolates have a much higher frequency compared to bacterial cell assemblages from enriched seawater, in which two instances of nanotubes were observed (see Figure 2.4). This observed data is potentially impacted by the misclassification of some observed bacterial nanotubes due to misidentifying physical linkages with the similar physical dimensions and characteristics.

2.4.3 Bacterial networks

In AFM images, we observed distributed groups of TW7 cells interconnected via bacterial nanotubes forming a tentative microbial network (Figure 2.1). Most cells with nanotubes are connected to one or two other cells with few cells connected to more cell

partners. Additional representative images of marine bacteria isolates expressing bacterial nanotubes are shown in Figure 2.S2. AFM topographic images and their representative SEM image-like representations, generated by Monte Carlo simulation using Gwyddion image analysis software (Klapetek et al., 2004), show other instances of bacterial nanotubular connections and extended interconnectivity found in different groups of TW7 and ALTSIO cells.

Nanotubes can extend bacterial networks beyond single pairs, to longer serial connections of cells and, less frequently, bacterial hubs that connect to multiple cells. Variability in intercellular connections was observed within bacterial cell neighborhoods, with nanotubes and other instances of physical intercellular connections were also observed connecting cell pairs, as shown in Figure 2.S3.

In addition to TW7, and ALTSIO cells, nanotube expression was observed in 2 separate α-proteobacterial isolates (La5 and La6) cultured from natural seawater collected from Scripps Pier (San Diego, CA, US) (Figure 2.S4). Individual bacterial nanotubes were detected using fluorescence microscopy by co-staining TW7 and ALTSIO cells with NanoOrange and FM 4-64FX to label proteins and lipids, respectively, as shown in Figure 2.S5. In images processed by a smoothing operation and Mexican hat filter, individual structures appear as faint linear connections between the greater fluorescence intensity of cell membrane regions, with varying labelling efficacy of protein and lipid stains.

2.4.4 TEM images showing membrane contiguity

Nanotube were observed as contiguous extensions of bacterial cell membrane connecting two cells, with or without intercellular material, in TEM imaging of negatively stained section off TW7 cells, shown in Figure 2.2. An example of paired TW7 cells connected by a bacterial nanotube is shown. This representative connection, with measured length of 250 nm and width of 200 nm, has an interior channel with labeled cellular material that is 100 nm in width. The membrane continuity of nanotubes is suggestive of connected cytoplasmic compartments of participating cells. Cellular material can be shared between the two cells as shown in the TEM images. The measured channel is large enough to support the direct transfer of large cytoplasmic materials, such as large particles, aggregates, and potentially bacterial microcompartments. Nanotubular connections form part of extended cellular connectivity, with occasional material transfer between TW7 cells, as shown in Figure 2.S6 depicting a labeled particle and polymer in transfer between connecting cells.
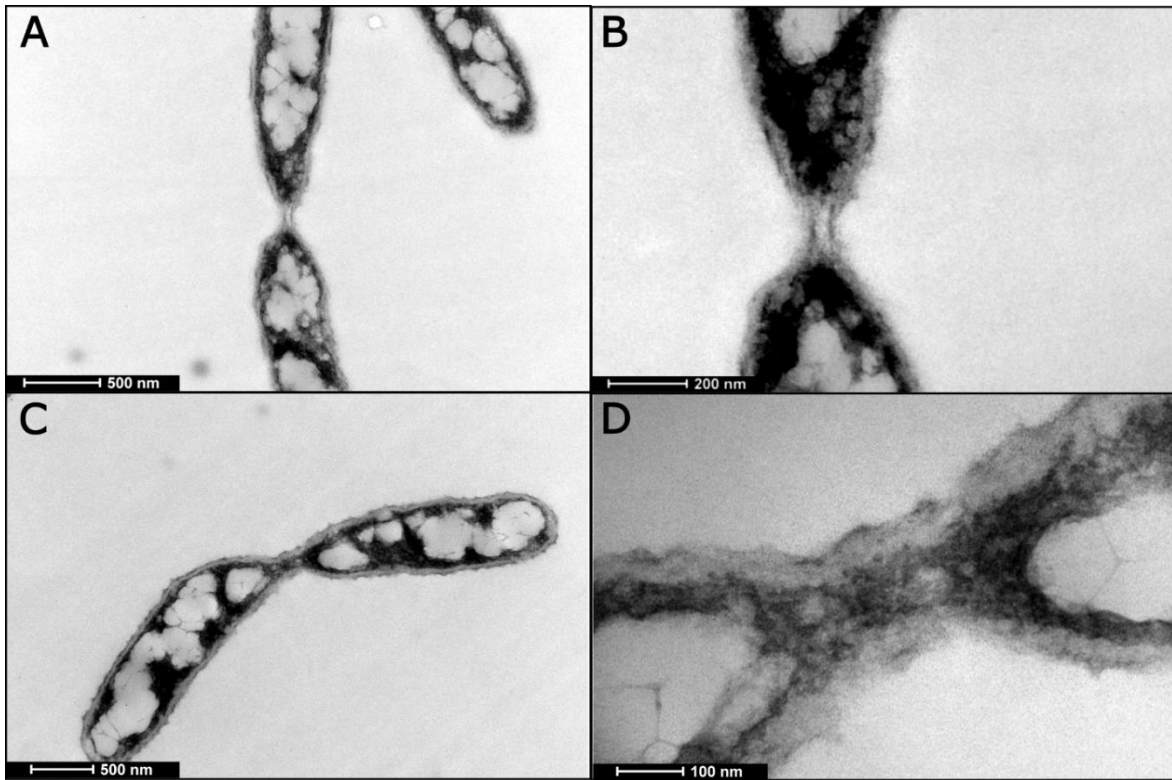
Figure 2.2: **Nanotubes as hollow connection between cells.** TEM images of negatively stained samples of TW7 cells expressing bacterial nanotubes. (**A**) A representative nanotube presenting a hollow tubular structure and lacking internal cellular material. (**B**: magnified image of nanotube). (**C**) Labelled cellular material transferred across select bacterial nanotubes. (**D**: magnified image of labeled cellular material within nanotube).

2.4.5 Physical characteristics of nanotubes

We measured the nanomechanical properties of bacterial nanotubes among TW7 cells using the force measuring capabilities of AFM to quantify the maximum adhesion force and energy dissipated at each pixel point. The measured adhesion forces are surface properties that are relevant to the attachment and interaction with biotic and abiotic elements of the marine microenvironment (e.g., colloidal particles and microbial surfaces). The dissipated energy is a qualitative mechanical property quantifying the energy loss in the indentation of the surface, that shows the spatial distribution and relative differences in the viscoelastic properties of the sample surface. Figure 2.3 shows the AFM data of TW7 cells, with corresponding error mode, adhesion, and dissipation images, where the nanotubes have varying mechanical properties compared to the connecting cell bodies. Additional nanomechanical data for TW7 cells and nanotubes are shown in Supplemental Figures 7 and 8. In both figures of nanomechanical images, prominent bacterial nanotubes are present along with other intercellular connections that bear some similarities with nanotubes. The alternate intercellular connections are primarily low-lying structures that resemble nanotubes in their direct span between two cells, with parallel edges and lack kinks or deviations along their length. The low-lying connections are entirely flattened upon the substrate with minimal height profile and present a nanomechanical profile of tubular connections. The adhesion and dissipation data are inconsistent where the edges are comparable to cells and nanotubes with less definition, and the midline properties resemble the substrate. The confounding interstitial features can be misinterpreted as nanotubes from

nanomechanical data images but lack the structural definition and physical size of bacterial nanotubes.

Figure 2.3: **Nanomechanical perspective of nanotube structures.** Atomic force micrographs and corresponding nanomechanical data images of TW7 cells expressing intercellular bacterial nanotubes (white arrows). (Height, Peak force error, Dissipation, and Adhesion images labelled accordingly). Additional low-lying intercellular tubular connections (black arrows) were observed amount cells expressing nanotubes. Image scan sizes are 3 µm × 3 µm.
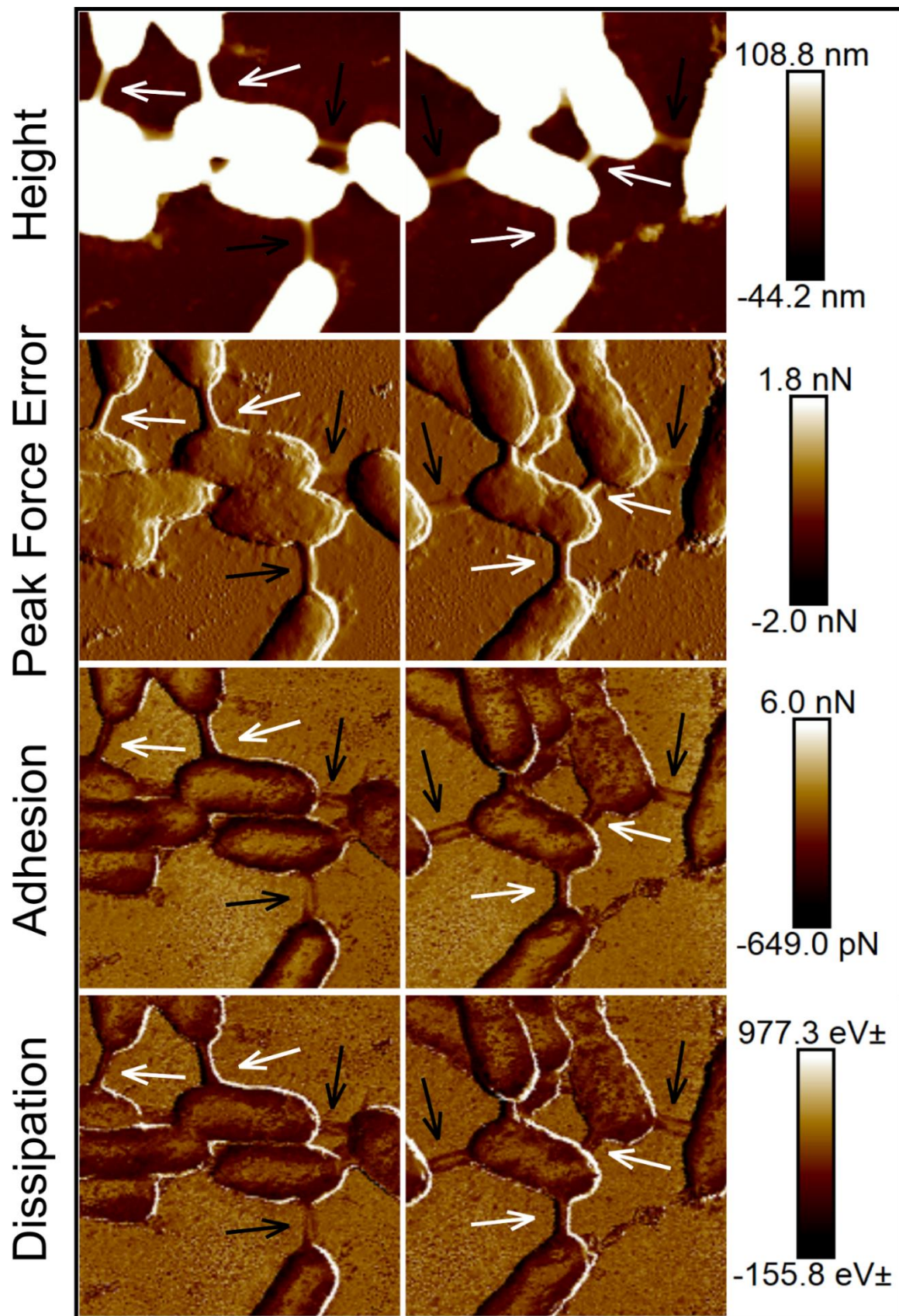
Time-lapse fluid imaging of live TW7 cells (Figure 2.S9) revealed an intercellular nanotube connecting a pair of live cells within a filtered autoclaved seawater medium. The presence of this nanotube suggests that these structural connections between cells can persist for periods of at least 90 minutes. The measured nanomechanical properties of this nanotube (Figure 2.9) appear to be consistent over the duration of imaging and in relation to the properties of the connecting cells, suggesting they do not undergo drastic changes over such periods of time.

This observation indicates that nanotubes can withstand a certain degree of applied AFM scanning forces and tip movement effects, suggesting a level of stability that can potentially hold cells together and move concertedly. Representative line traces of the nanotube (depicted in Figure 2.9) height and nanomechanical data are shown and summarily plotted over successive image scans in Figure 2.S10. The measured nanomechanical data shows slight differences in the adhesion, deformation and dissipation measured relative to the connective connected cell. This can be partially attributed to the influence of the background substrate and the slight differences observed can be obscured by the variability in the intercellular variation in nanomechanical properties. There is little variation in relative nanomechanical property changes relative to the microbial surface properties over time.

2.4.6 Interspecies bacterial connections

Bacterial nanotubes were less frequent in natural bacterial assemblages from seawater samples compared to ALTSIO and TW7 marine bacterial isolates. AFM imaging of natural seawater enriched with 1% Marine Broth 2216 shows two unique cell pairs

connected by a bacterial nanotube in Figure 2.4. Samples were prepared by cell deposition and fixing the cells in place after 10 minutes. The incubation period involved in preparation suggests nanotube production occurs between bacterial cells in suspension instead of stimulated production after cell attachment to the glass surface.
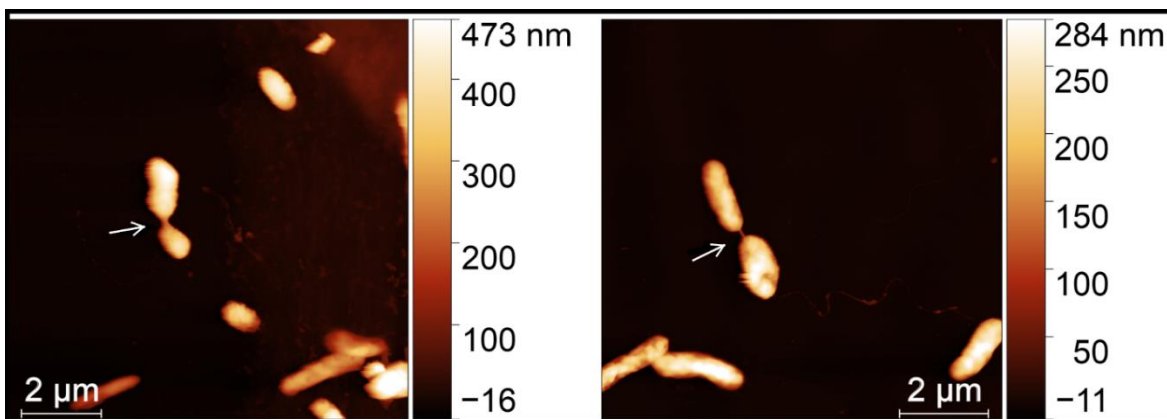
Figure 2.4: Individual connections in bacteria from seawater assemblage. Independent cell pairs from a natural bacterial assemblage from enriched seawater connected by a bacterial nanotube (white arrow). AFM images scan sizes are 10 µm × 10 µm.

SEM is an alternative or complementary technique to confirm the presence of nanotubes and for measuring the frequency and occurrence of nanotube connections. In a cell mixture of cultured TW7 cells and cells from enriched natural assemblages (at a 1:1 ratio), SEM images show putative interspecies linkages between morphologically distinct cells, connecting the longer, thinner TW7 bacteria with the smaller, wider natural assemblage bacteria. SEM data shows TW7 cells mixed with that natural assemblage created a microbial network and connected microbial consortium as shown in Figure 2.5. The linkages appear to connect individual cells to a cluster of other cells, holding separate cells together, creating a degree of physical coordination or spatial restriction between the individual cells. Similarly, cell monolayers of natural bacterial assemblages from enriched seawater have multiple instances of small groups of cells with very short intercellular bacterial nanotubes connecting cells of different sizes and shapes as shown in Figure 2.6. Within the close neighborhood of bacterial cells in monolayer, select pairs of cells are connected by bacterial nanotubes as observed in the height and nanomechanical data images.

Figure 2.5: **Connections between cells of different morphologies**. Scanning electron micrographs of cell mixtures of TW7 and natural assemblages from enriched seawater (1% liquid Marine Broth 2216) show various nanotubes (black arrows) formed between cells of different morphologies. Select cells express greater interconnectivity with adjacent cells in denser cell neighborhoods via multiple bacterial nanotubes (white arrows). Scale bars provided.
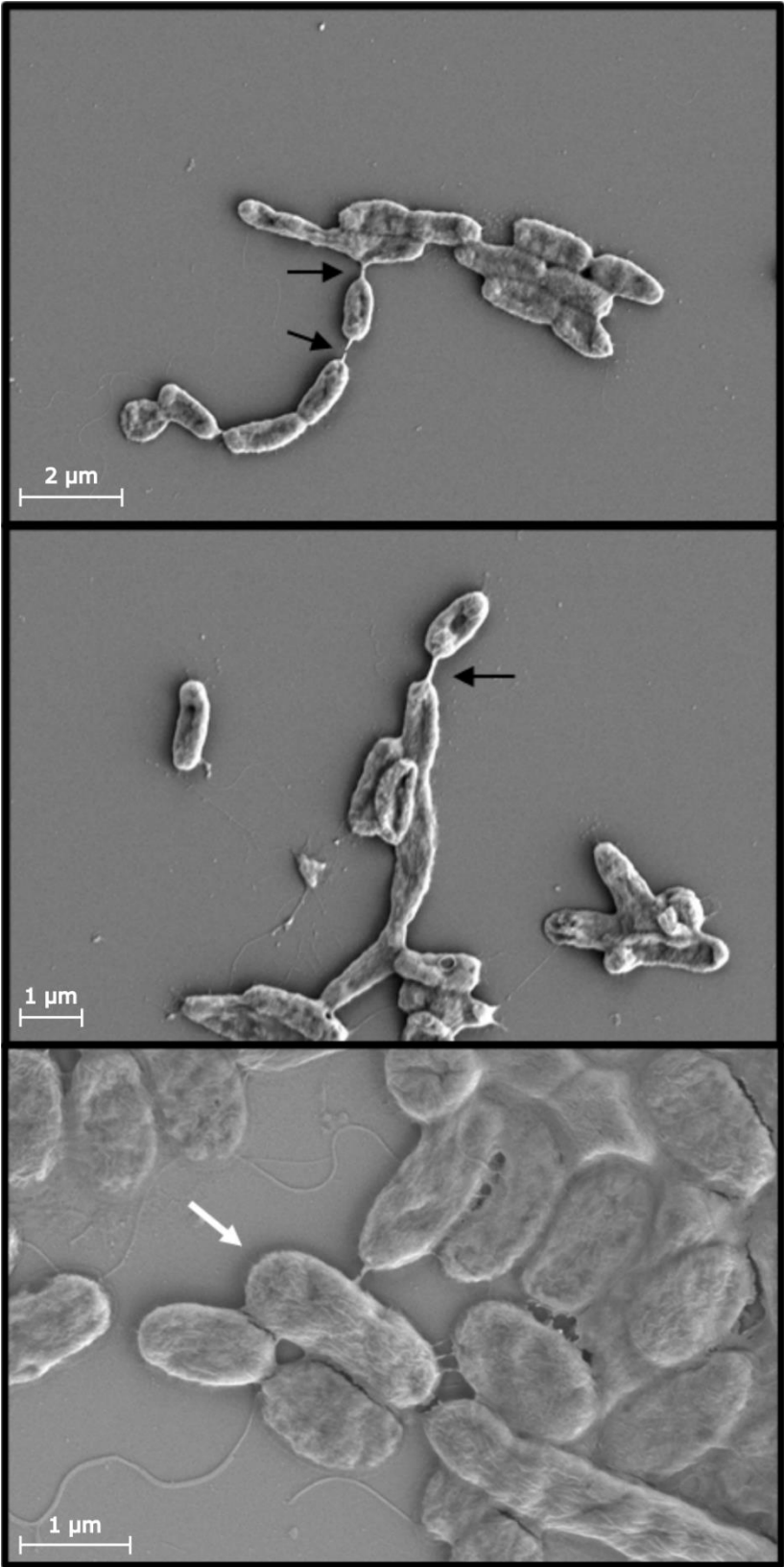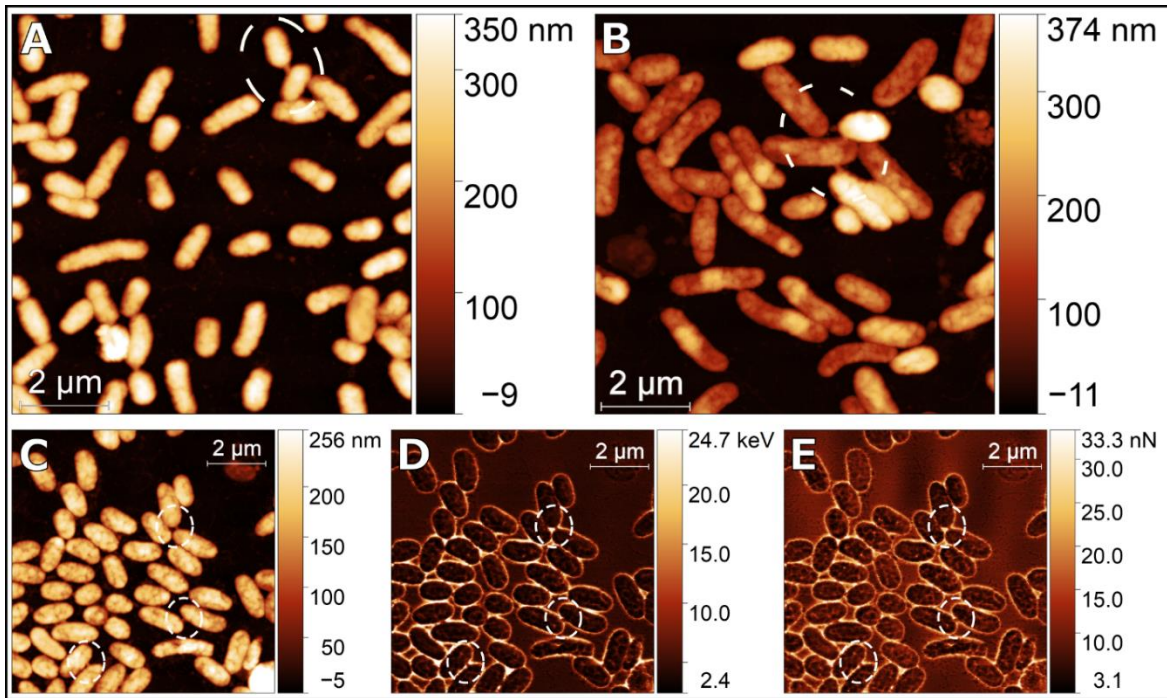
Figure 2.6: **Group connectivity in bacteria by short nanotubular connections. (A, B)** Atomic force micrograph images (height) of natural bacterial assemblages attached onto a glass coverslip surface as a cell monolayer, with select few cells present intimate physical connections with neighboring cells, via bacterial nanotubes (white regions). **(C)** The short nanotube connections (within outlined white regions) are present and more readily observed within dissipation **(D)** and adhesion **(E)** nanomechanical data images. Scale bars provided.

2.4.7 Structural variability of nanotubes and intercellular linkages

There were two distinct types of intercellular linkages, bacterial nanotubes and other mechanical linkages (i.e., not tubes), that are distinguished by their shape, quantity and mechanical properties. Individually nanotubes are tubular structures that solely extend between two cells (across ~200–400 nm), as opposed to connecting more than two cells. Furthermore, as singular structures, nanotubes position two cells a set distance apart and do not divide or conjoin to form multiple parallel structures. In contrast, mechanical linkages lack a distinct tubular shape, span a shorter distance, form multiple parallel linkages, and promote additional connections to hold cells together, as shown in Figure 2.S11. Observed adhesion forces and measured dissipation energies on the mechanical linkages were greater compared to the cell surface. Instances of intercellular linkages were observed to coalesce with each other to form contiguous surfaces between adjoining cells (Figure 2.S11). Additionally, complex arrangements of nanotubes and intercellular linkages were observed in interstitial spaces between cells in larger bacterial networks and aggregates (Figure 2.S12).

2.5 Discussion

2.5.1 Nanotubes form intimate physical connections between marine bacteria

This is the first report of nanotube-based physical connectivity between marine bacteria cells. The compounded connectivity between cell pairs and microbial ensembles contributes to connecting individual cells to denser cell clusters and aggregates over longer spatial scales (> 10 µm). The intercellular connections are separable into two categories,

bacterial nanotubes, and more generic mechanical linkages (Figure 2.S3). Bacterial nanotubes are identifiable from their visual characteristic tubular structure with a linear span and consistent width, devoid of kinks or deviations, as initially observed in B. subtilis and E. coli cells by Dubey and Ben-Yehuda (Dubey and Ben-Yehuda, 2011). Nanotubes are distinguishable from other intercellular connections potentially formed from exopolymers and occupy the interstitial space as observed in archaea (Jahn et al., 2008). From our observations, the widths and lengths of marine bacterial nanotubes fall within the range of 50 – 160 nm and 200 – 600 nm, respectively, with few exceptions, conforming to previous reports by Dubey and Ben-Yehuda (Dubey and Ben-Yehuda, 2011). Other generic mechanical linkage connections are generally wider and shorter. The heights along the midsection of the nanotubes range from 18 – 250 nm and could be a potential physical criterion for distinguishing them as bacterial nanotubes, apart from other bacterial structures and appendages. One significant distinction is that in AFM height images other bacterial structures are generally unsupported and tend to lie flat on the background substrate whereas nanotubes are supported at both ends by the two connected bacterial cell bodies.

Nanotubes in marine isolates were < 600 nm long, and much shorter among surface-attached cells from enriched natural bacterial assemblages. The short span of bacterial nanotubes can contribute to a limited overall size of interconnected bacterial networks in an ensemble structure. Such constraints may be more common and significant in marine bacterial isolates compared to B. subtilis and E. coli nanotubes, which extend up to 1 µm (Dubey and Ben-Yehuda, 2011). This implies an upper bound on nanotube length in marine bacteria.

2.5.2 Frequency of nanotubes

The average frequency of nanotube connections observed in TW7 and ALTSIO were 0.07 and 0.03 nanotube cell-1, respectively. For comparison, general intercellular connections (not-tube) were on average 0.10 and 0.07 connections cell-1 (Figure 2.1). The frequency of nanotubes was variable from the observed regions (average of ~28 cells per 10 µm ×10 µm area). Apart from few regions of dense interconnectivity as outliers, our frequency range of intercellular connections was 0.02 – 0.10 nanotube cell-1 for surface-attached bacterial isolates in enriched microenvironments. We estimate that our frequency measurements may be 10-100-fold overestimated due to sample preparation selectively removing unattached cells, lacking nanotube expression. On the other hand, sample preparation methods that involve physical processes such as filtration and centrifugation likely disrupt nanotubes and hence contribute to underestimation of nanotube-based cellular connections. The combined influence of high cell seeding density and bacterial surface adsorption via deposition contribute to conditions conducive to intercellular nanotube observation.

In addition to γ-proteobacteria isolates TW7 and ALTSIO, we also tested two cultured α-proteobacteria isolated from seawater from Scripps Pier and found them to be positive for nanotube expression (Figure 2.S4). Furthermore, we observed individual bacterial nanotubes connecting cells from enriched natural seawater (Figure 2.4). We did not conduct a (technically challenging) systematic survey of marine bacteria isolates or natural assemblages for their nanotube expression. However, the protocols developed here lend

themselves to expanding the range of species for nanotube expression. It should therefore be possible to test the hypothesis that nanotube expression is a general phenotype expressed within natural marine assemblages. Our observed frequency of nanotubes in TW7 and ALTSIO isolates was greater compared to seawater assemblages. This could be because some bacterial species have higher relative rates of nanotube expression. But it is more likely due to different nutrient and growth conditions. Thus, a systematic test of the generality of nanotube expression in marine bacteria (or bacteria from any other environment, e.g., as soil or human microbiome) is feasible, technically challenging, but desirable. However, detailed and mechanistic studies of a limited number of isolates or model natural systems should be a priority.

2.5.3 Cytoplasmic transfer between cells via nanotubes

Previous biochemical and molecular dynamics studies (Dubey and Ben-Yehuda, 2011;Pande et al., 2015) have established that bacterial nanotubes allow for direct exchange of cellular components. Our study is mainly focused on the ecological and biogeochemical implications of nanotube expression taking advantage of the capabilities of multiple imaging modalities. Our TEM images of TW7 nanotubes (Figure 2.2), show clearly delineated tube boundaries and stained cellular materials within the nanotubes. While not capturing its dynamics, the images are consistent with intercellular transfer of cytoplasmic and/or periplasmic materials between the two cells. We observed varying degrees of negatively stained material within the hollow interior of different nanotubes. Small molecules in bacterial cytoplasm should be readily diffusible across the nanotubes unless there are

regulatory mechanisms constraining molecular exchange. Furthermore, the large with of intercellular nanotubes of the intercellular connections (ca. 50 – 160 nm) could accommodate directional transfer between the two cells of components such as protein aggregates and bacterial microcompartments. Individual cells connecting to cell clusters via a nanotube (e.g., Figure 2.1) may derive benefit from connecting to a cell cluster, potentially gaining access to a pool of greater biochemical diversity. Transmission of metabolites and signaling molecules across nanotube-connected bacterial ensembles could promote biological coordination and synchronicity

2.5.4 Fluorescence detection of nanotube

In addition to AFM visualization, marine bacterial nanotubes in TW7 and ALTSIO samples are detectable to a limited extent using confocal fluorescence microscopy via co-staining proteins and lipids (Figure 2.S5). Both isolates showed nanotubes labeled by the protein stain NanoOrange; by visual inspection of the fluorescent micrographs, the staining intensity in the nanotubes and the cells was comparable. Only the TW7 cell nanotube was labelled by the lipophilic FM 4-64FX membrane stain, suggesting that the TW7 nanotubes have similar levels of lipid components compared to other cell membrane regions. The differential staining with FM 4-64FX may be due to differences in structure and relative composition of lipophilic and proteinaceous components in nanotubes.

Fluorescence-based detection have limited utility in delineating nanotubes from other labelled membrane regions between marine bacterial cells. The use of nonspecific protein and lipid stains is influenced by nonlocalized fluorescence detection around the

connection. Furthermore, overstaining cellular material via nonspecific fluorescence labelling limits image contrast of nanotube structures, posing significant challenges for detection in more complex environmental samples with this strategy. Determining specific proteins that are associated with nanotube structures, such as flagellar CORE proteins and YmdB phosphodiesterase, for specific fluorescence targeting may be a viable strategy to enhance discovery rates of nanotubes in marine bacterial assemblages via fluorescent microscopy (Dubey et al., 2016;Bhattacharya et al., 2019). Further studies are needed to refine the ability to detect and observe nanotube structures within marine microenvironments to determine their functionality, development, and ecological significance in marine bacterial communities.

2.5.5 Insights into nanomechanical properties of bacterial nanotubes

Multiparametric AFM imaging has potential utility in characterizing bacterial nanotubes using physical characteristics (length and width) and nanomechanical properties (adhesion and dissipation). In general, bacterial nanotubes have defined edges (Figure 2.3, Peak Force Error images), and present lower adhesion and dissipation compared to cell surfaces, and greater contrast from background substrates (Figure 2.3: Adhesion, Dissipation images). Nanomechanical data images can provide better visual contrast for identifying bacterial nanotubes in larger surveyed areas compared to height or peakforce error images (Figures 2.S7 & 2.S8A). In nonideal conditions, identifying nanotubes associated with other materials and features from topography data can be challenging. Identifying intercellular nanotubes in such cases from characteristic nanomechanical data is desirable, such as, for

example, a potential nanotube structure embedded within interstitial material (Figure 2.S11 E-G). Nanomechanical characterization of bacterial nanotubes can be confounded by additional features such as low-lying interstitial connection, which resemble tubular structures with less distinct edges and inconsistent adhesion and dissipation properties (Figure 2.S8B). The characterization of bacterial nanotubes is dependent on the physical structures imaged, where freestanding structures are readily identifiable compared to more obscured counterparts. Furthermore, characterization of altered nanotube structures due to development or environmental changes cannot be performed solely from AFM topography data. For example, characterizing the low-lying tubular features that resemble nanotubes (Figures 2.3 and 2.S8B) and their function in relation to nanotubes cannot be accomplished by AFM imaging. Further investigation is needed to determine how nanomechanical properties of bacterial nanotubes differ among bacterial species and other comparable structures in microbial communities. Further, the protocols developed here could be applied to similar interrogations of bacteria adapted to other environments (e.g., whether salinity of the environment influences the nanomechanical properties of the nanotubes).

2.5.6 Extended physical coordination

Bacterial nanotubes influence the physical interactions occurring between two cells, as opposed to indirect coordination and interactions through e.g., polymers, gel matrices or surfaces. Nanotubes can contribute to the development of a spatial structure within a microbial community by connecting cells and maintaining their relative positions and separation distances over time. Nanotubes were persisted for at least 90 minutes (Figure

2.S9) a significant duration in the lives of adjoined bacteria. Nanotube expression can extend the duration of an interaction of bacterial cells and potentially supporting and amplifying and possibly regulating any biological effects of interactions. Interconnected bacterial ensembles can potentially have significant consequences as they move in a concerted manner through a dynamic microenvironment. One possibility is the concerted interaction and attachment of cells to the surfaces of organic particles and polymeric gels. Nanotube based bacteria microaggregates could serve as nuclei for the generation of pre-colonized marine snow. (10^8–10^9 bacteria mL^{-1}) in coastal marine surface waters by attracting motile bacteria as well as colloids and particles. The concerted metabolic action of nanotube associated bacteria could contribute to the biogeochemical dynamics of marine snow.

Nanotubes expression between interconnected ensembles of bacterial cells presents ecological benefits through functional multicellularity. The interaction extends into physical coordination as bacterial nanotubes establish some degree of ordering and spatial organization of cells, as their positioning and movement within the microenvironment is constrained. The physical network of cells forms a larger interactive biological surface, altering the flow of ambient fluid and promoting interstitial organic matter attachment and buildup between connecting cell bodies (e.g., Figure 2.S12). Complex intercellular connections formed from multiple parallel nanotubes and intercellular linkages can form an interaction surface for interstitial particles and polymers and nucleate bacterial aggregates.

2.5.7 Interspecies connectivity

Interspecies bacterial nanotubes as observed by Dubey and Ben-Yehuda (Dubey and Ben-Yehuda, 2011) and by us here raise questions on how common they might be in the ocean, as they can bring together and connect various constituents of marine assemblages . Such connections can build interconnected multispecies bacterial ensembles, as observed from connections between morphologically different cells in SEM and AFM images (Figures 2.5 and 2.6). These physical intercellular connections could support the spatial and biochemical coupling of different microbial species by allowing for intimate exchange of metabolites and cytoplasmic material across these structures over short spatial scales (< 1 µm). Biochemical coupling via bacterial nanotubes of different species has been previously demonstrated in auxotrophic cell mutants exchanging the necessary compounds (Pande et al., 2015). Metabolite interchange and distribution between connected bacterial ensemble may be influenced by nanotube width (ca. 50–160 nm), where the interior surface chemistry may provide selective passage of molecules.

Within an interconnected microbial ensemble, nanotubes can form a foundational structure and basis for transient or collapsible bacterial microaggregates, capable of accommodating individual cells into the larger group. Bacterial nanotubes have been shown to be manifested structures associated with cell death, forming due to biophysical forces, with potential altruistic benefits to other neighboring bacteria (Pospíšil et al., 2020). Nanotubes, as manifestations from cell death, can form a scaffold around the released cell contents or surround live cells and promote released organic matter aggregation, generating a hotspot of organic matter. Nanotube expression can provide benefits of transient symbioses

to individual cells forming physical connections that accommodate metabolite interchange between members of bacterial assemblages.

2.5.8 Limited knowledge and open questions

Little is known about the structural and physiological characteristics of marine bacterial nanotubes and their ecological role within the marine microenvironment. Production of bacterial nanotubes in B. subtilis cells is known to involve the CORE protein complex involved in flagellar production and is associated with YmdB phosphodiesterase activity (Dubey et al., 2016;Bhattacharya et al., 2019). More work is needed to elucidate the conditions and factors necessary for nanotube expression in marine bacteria considering that these structures have only been observed with low frequency among surface-attached cells in our study. This limits our understanding to nanotube structures between surface-attached bacteria and may not directly relate to their formation, development, and mechanisms of actions in planktonic bacteria and natural microenvironments. As back-of-the envelop calculation with an estimated 10^{29} bacteria in the ocean and a conservative estimated frequency of bacterial nanotubes of 10^{-4} or 10^{-5}, there may be 10^{24}–10^{25} nanotubes at any given time connecting bacterial cells and forming innumerable interconnected multicellular bacterial ensembles throughout the ocean. The variability of nanotube expression across bacterial species has significant implications for their relevance in cooperative strategies and multicellular behavior of within mixed communities.

In conclusion, the discovery of nanotubes in marine bacteria has novel implications for microbial oceanography and biogeochemistry. Nanotube-mediated exchange of

82

cytoplasmic contents between bacteria changes how we think about the in-situ physiology and growth regulation of bacteria in the sea. Nanotube-based bacteria-bacteria and bacteria-organic-matter interactions may result in collapsible structures at the microscale. This could enhance the aggregation of microbes and colloidal organic matter and their downward flux. in the ocean. Finally, nanotube-based interactions of bacteria in densely-populated environments (e.g., marine snow, coral mucus, marine sediments) offers a new view of the biochemical and biogeochemical dynamics within these microenvironments.

2.6 Supplementary Data

Figure 2.S1: Physical connectivity in marine bacteria over longer spatial scales. Atomic force micrograph of a marine bacterium isolate TW7 cells showing groups and clusters of cells connected by intercellular nanotubes. Interconnected cell pairs were connected to larger bacterial networks, establishing interconnectivity over a longer spatial scale. (Left: 30 µm × 30 µm scan size, right: 10 µm × 10 µm area marked by white square)
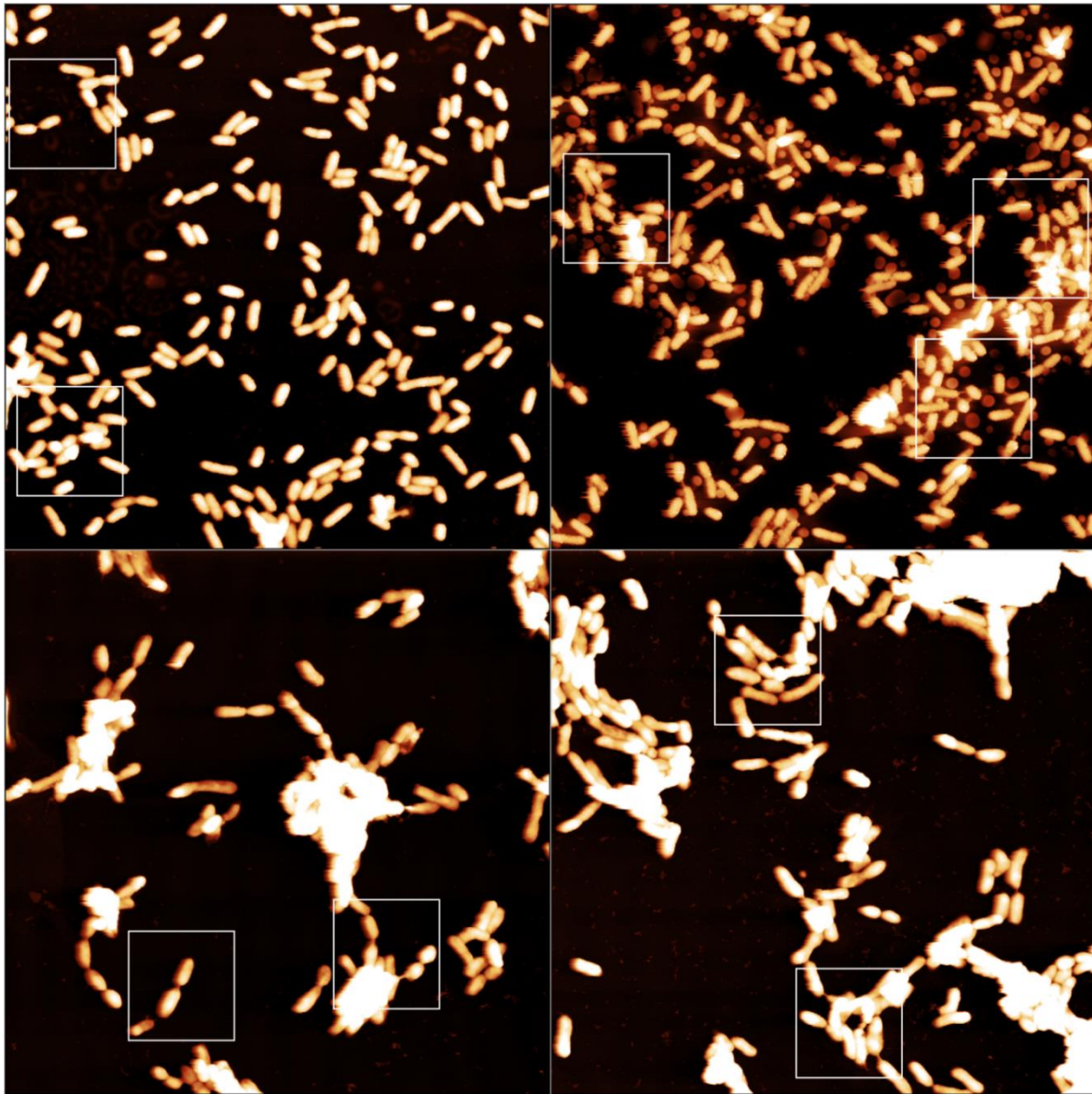
Figure 2.S2: Examples in nanotube-connections in groups of bacteria. Atomic force micrographs (height data) of marine bacterium isolates TW7 (top row) and ALTSIO (bottom row), and respective Monte Carlo simulated SEM image-like presentations for AFM images (Figure 2.S2, continued) for visualization purposes. showing additional examples of groups and clusters of cells expressing intercellular nanotube connections (located in regions marked white squares). In many instances, nanotubes are present in lone cell pairs, limited by low cell density. In areas with higher cell density, nanotubes connect cells in a serial manner, potentially forming a long chain of interconnected cells. Occasionally, few select cells express multiple nanotubes and develop increased interconnectivity within a small local neighborhood of cells. Image scan sizes are 30 µm x 30 µm.
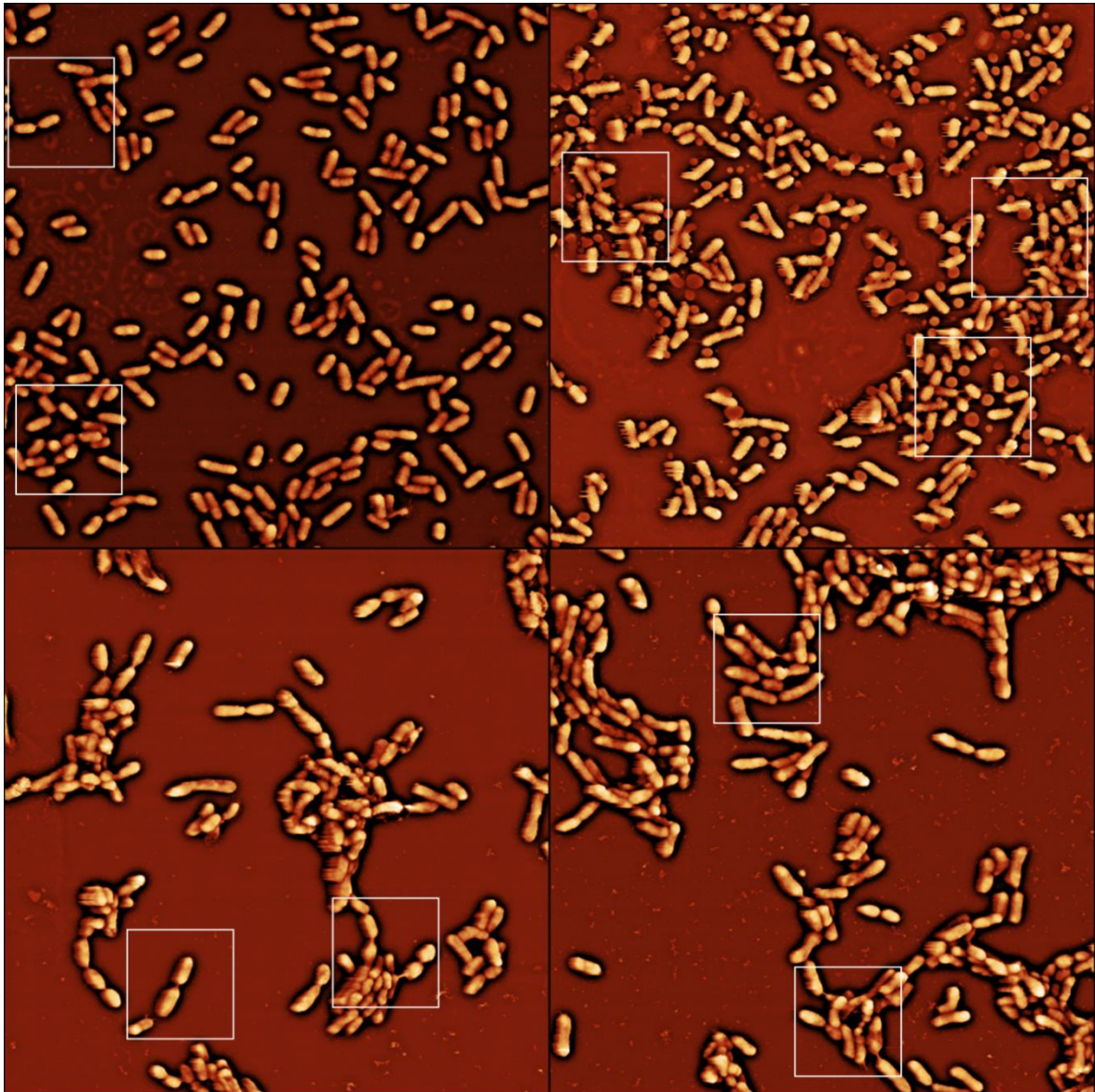
Figure 2.S2: Examples in nanotube-connections in groups of bacteria, continued.
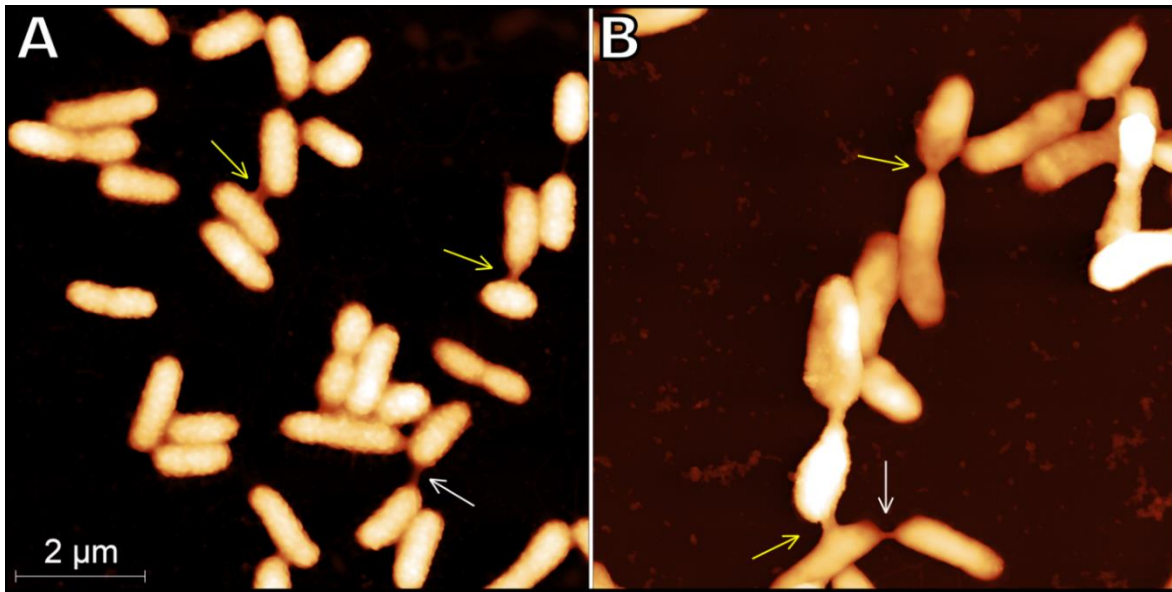
Figure 2.S3: Nanotubes and general mechanical linkages. Atomic force height micrographs of TW7 **(A)** and ALTSIO **(B)** cells show intercellular nanotubes and other general mechanical linkages (i.e., non-tubes). Bacterial nanotubes (white arrows) appear within the images as linear connections straight edges along their span. In comparison, general mechanical linkages (yellow arrows) are shorter connections with flared edges that bridge the interstitial space between cells.
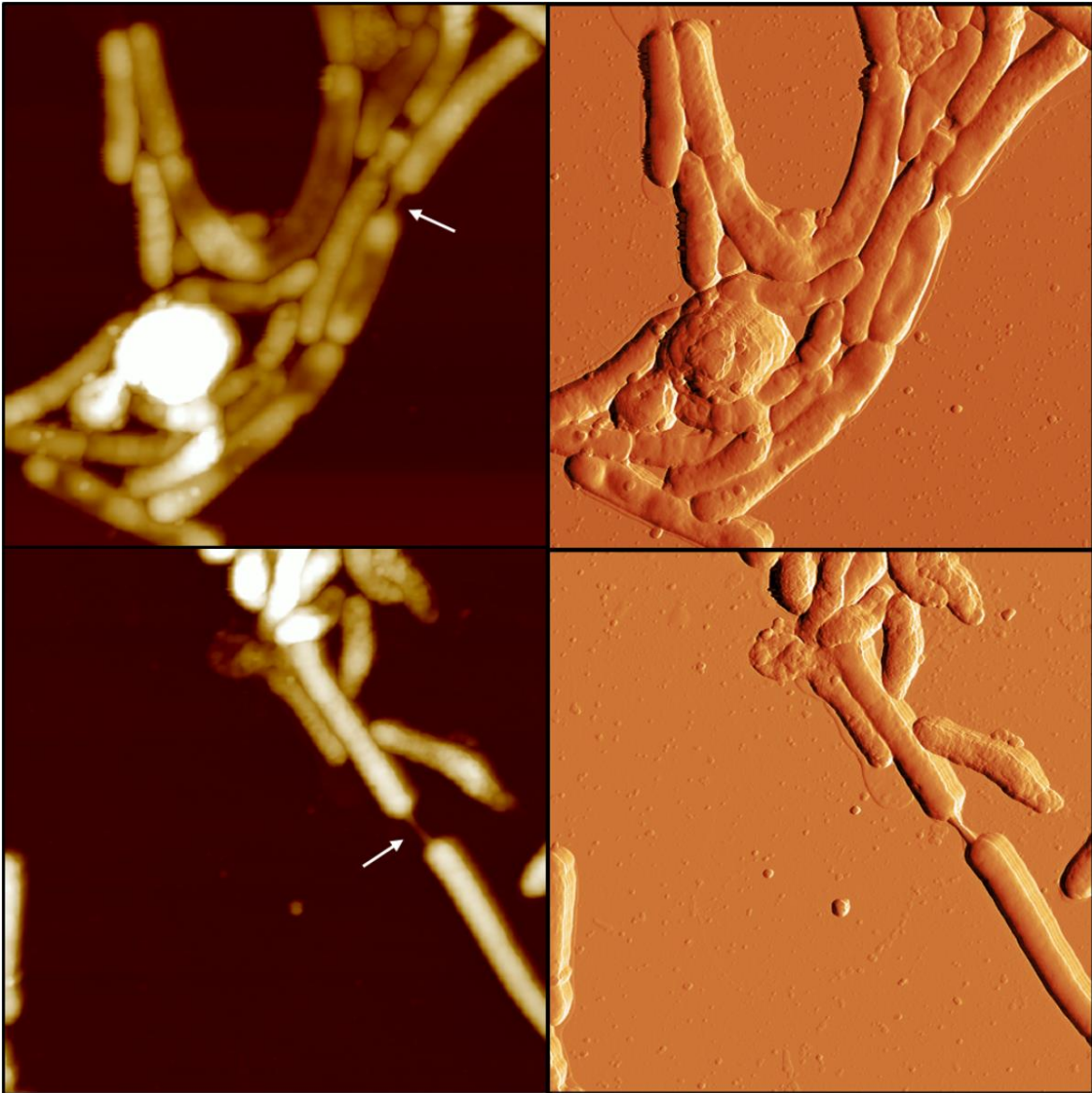
Figure 2.S4: Bacterial nanotubes in α-proteobacteria. Examples of bacterial nanotubes in two α-proteobacterial species, La5 (top row) and La6 (bottom row), isolated from natural seawater collected off Scripps Pier. The presence of bacterial nanotubes in α-proteobacteria and γ-proteobacteria isolates TW7 and ALTSIO suggests that nanotube expression is common among other marine bacteria. Image scan sizes are 10 µm × 10 µm and are shown as height images (left column) and error mode images (right column).
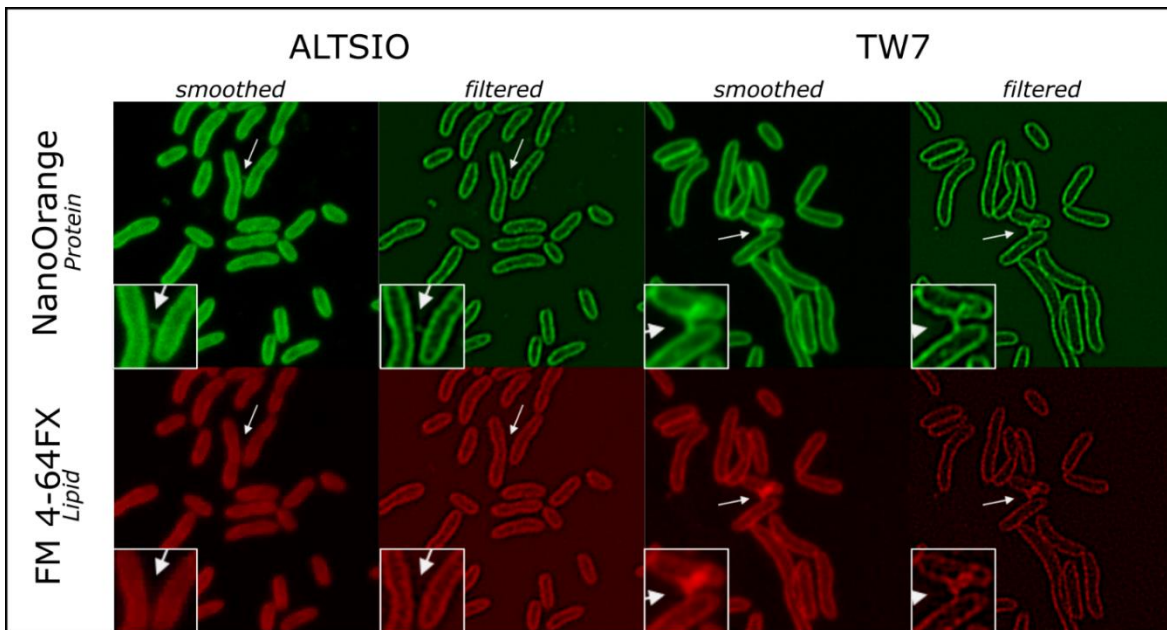
Figure 2.S5: Fluorescence images of bacterial nanotubes. Fluorescence co-staining of proteins (NanoOrange, top row) and lipids (FM 4-64FX, bottom row) in ALTSIO and TW7 cells on polylysine treated glass coverslips. (Smoothed images and images processed with a Mexican hat filter shown in image pairs). Nanotube structures (as seen in inset images) that are primarily labelled by the protein stain in both microbial isolates. ALTSIO cells lack colocalized lipid signal with the nanotube structure, suggesting lower lipid content compared to other regions of bacterial membranes. TW7 cells have with colocalized protein and lipid stains, suggesting that nanotubes are protein-rich and have lipids in their structure, comparable to the bacterial cell membrane. Image areas were cropped to 20 µm in size.
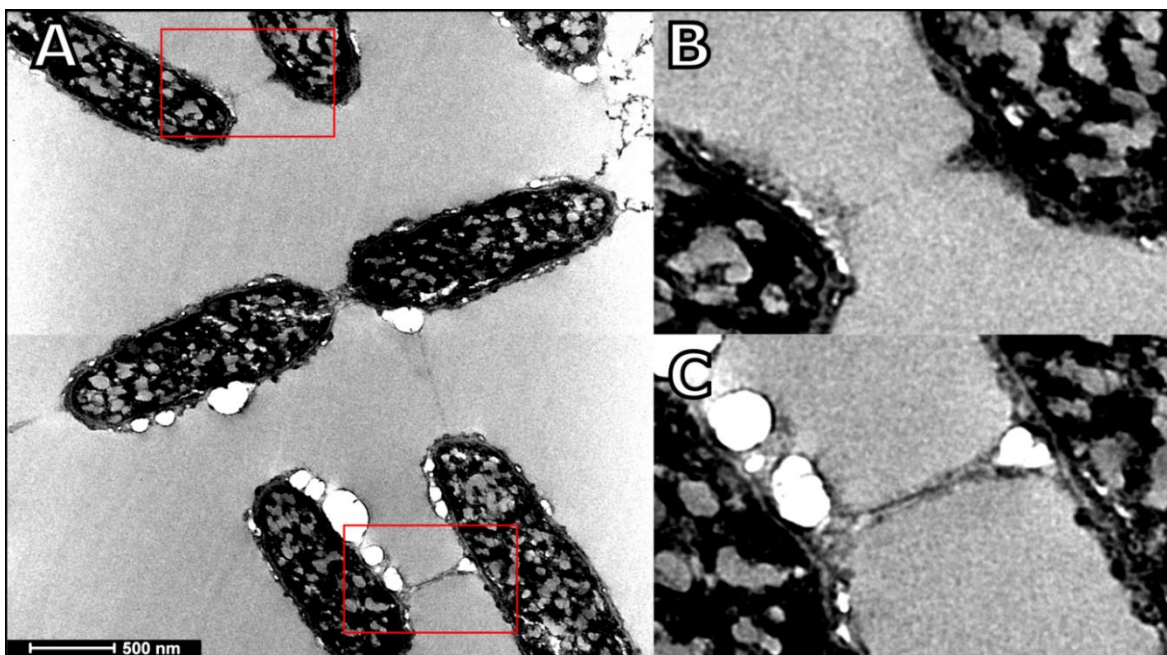
Figure 2.S6: Hollow physical network of nanotubes and connections in bacteria. **(A)** TEM image of negatively stained samples of TW7 cells show multiple intercellular connections (black arrows) expressed within a local neighborhood of cells, that may include bacterial nanotubes and provide physical interconnectivity and structure to the group of cells. **(B)** Traces of many intercellular connecting structures remain as faint or disappearing features, due to limitations from sample sectioning for microscopy. **(C)** In rare instances, connections may be observed with intercellular material between two cells, (e.g. stained linear polymer shown).
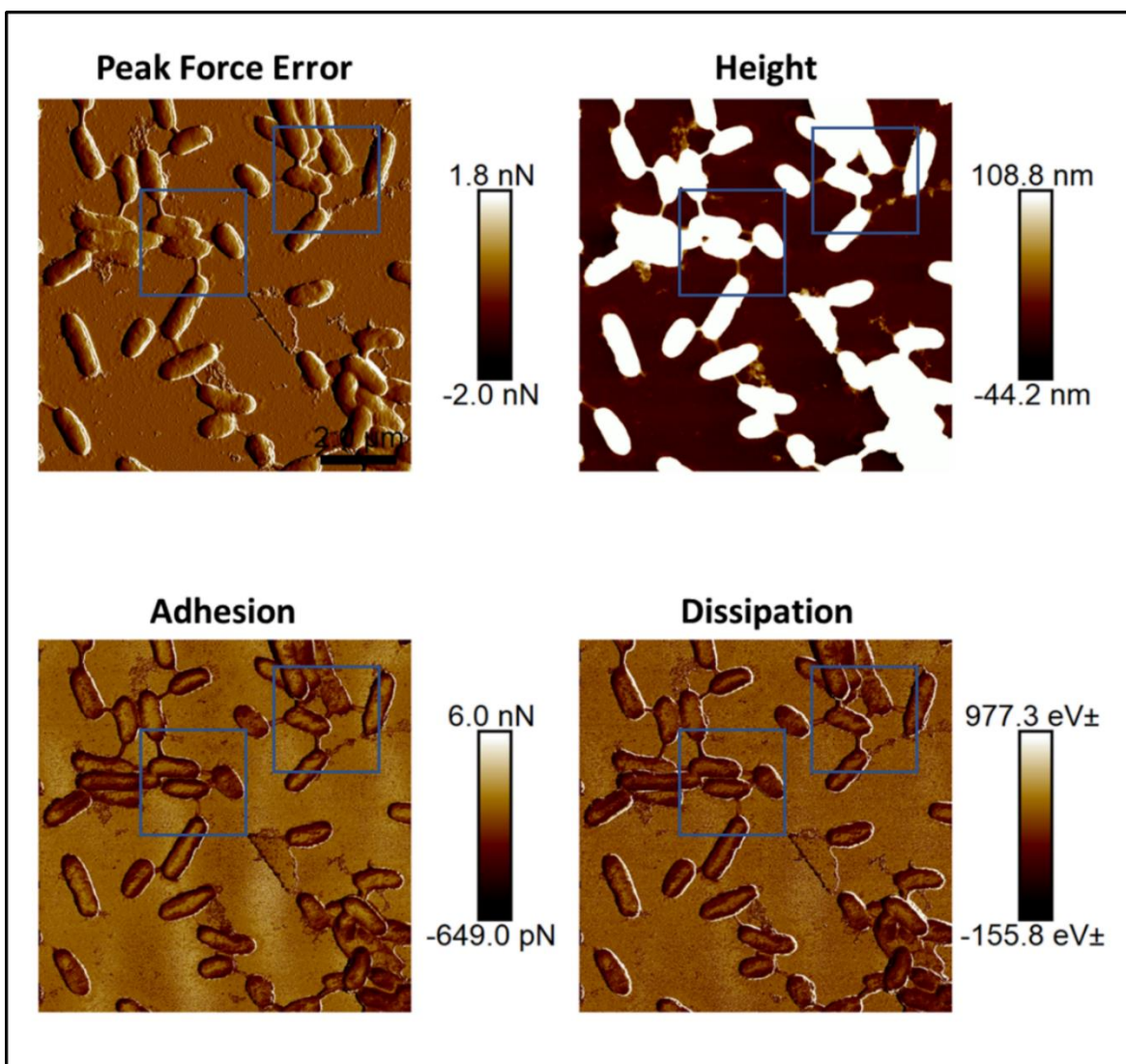
Figure 2.S7: Nanomechanical AFM image of bacteria nanotubes. Uncropped nanomechanical AFM data measured for a group of TW7 cells expressing intercellular bacterial nanotubes showing the diversity and variety of bacterial nanotube structures and properties. Areas marked by blue squares correspond to the AFM nanomechanical data shown in Figure 2.3. Image scan sizes are 10 µm × 10 µm.

Figure 2.S8: Variety in nanotube structure and nanomechanical properties. (A) Additional nanomechanical AFM data measured for a group of TW7 cells expressing intercellular bacterial nanotubes. Collected image scan sizes are 10 µm × 10 µm. Select regions, marked by blue squares and shown as magnified images in **(B)**, have many instances of bacterial nanotubes and connections that have varying nanomechanical properties. The mechanical signatures in the adhesion and dissipation data of interstitial low-lying connections (marked by arrows) differ from more prominent nanotubular connections between cells.
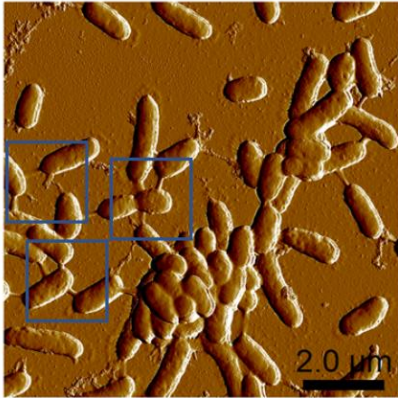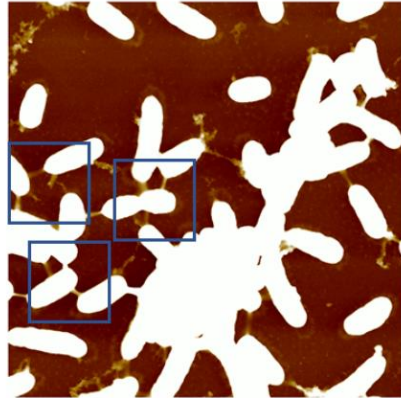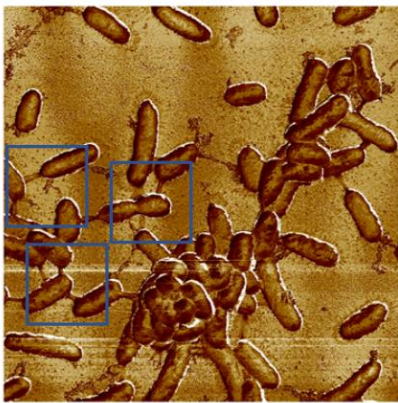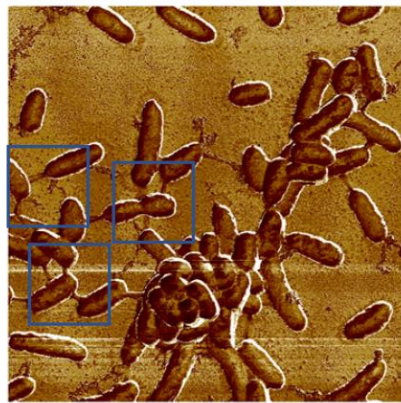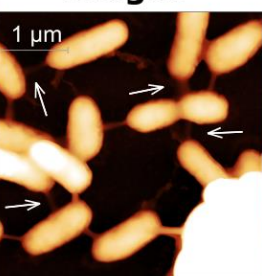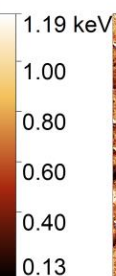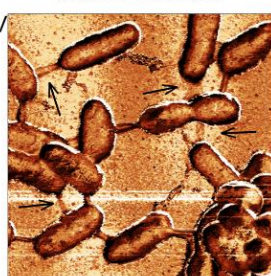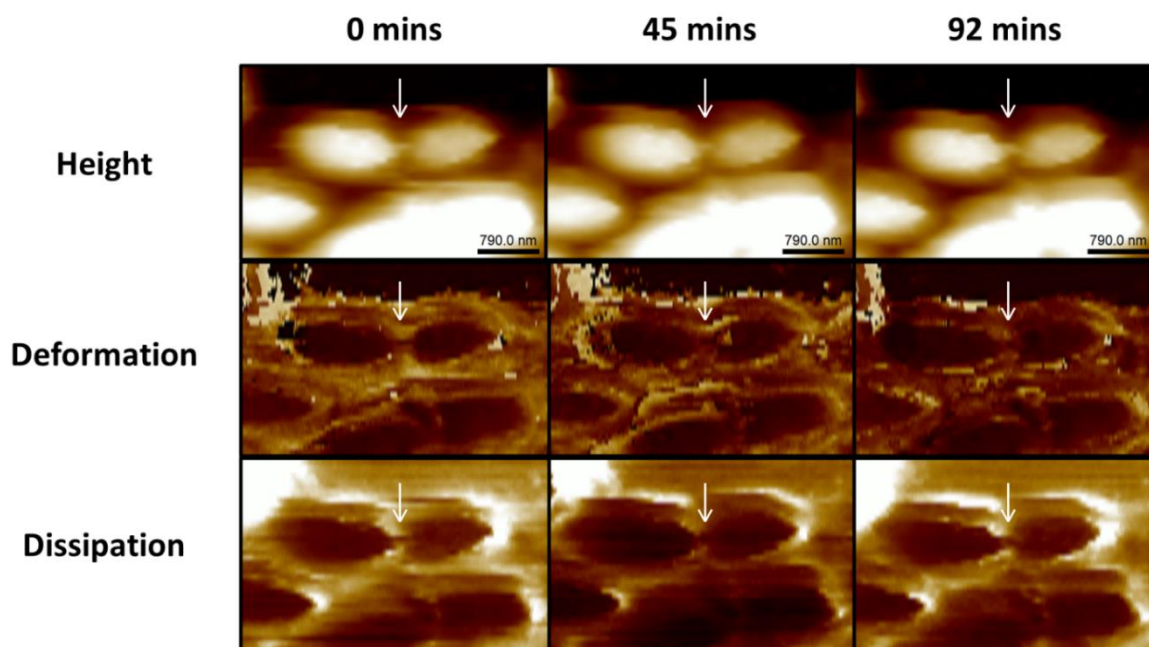
Figure 2.S9: Nanotube connection in live bacteria. Atomic force micrographs (top row) of live TW7 cells in filtered autoclaved seawater media connected by a short bacterial nanotube (white arrow, ca. 200 nm long) remains connected over substantial period. Select frames (at 0 mins, 45 mins, and 92 mins) from consecutively image time-lapse period of 92 minutes are shown with the corresponding adhesion and dissipated energy nanomechanical property maps. Data show a visible nanotube connection between the two live cells with mechanical properties distinct from background glass coverslip substrate and more similar to the cell surfaces. (Scale bars: 790 nm. Images are cropped sections from 15.7 µm × 15.7 µm scan size, acquired at 256x1024 at 0.5 Hz)
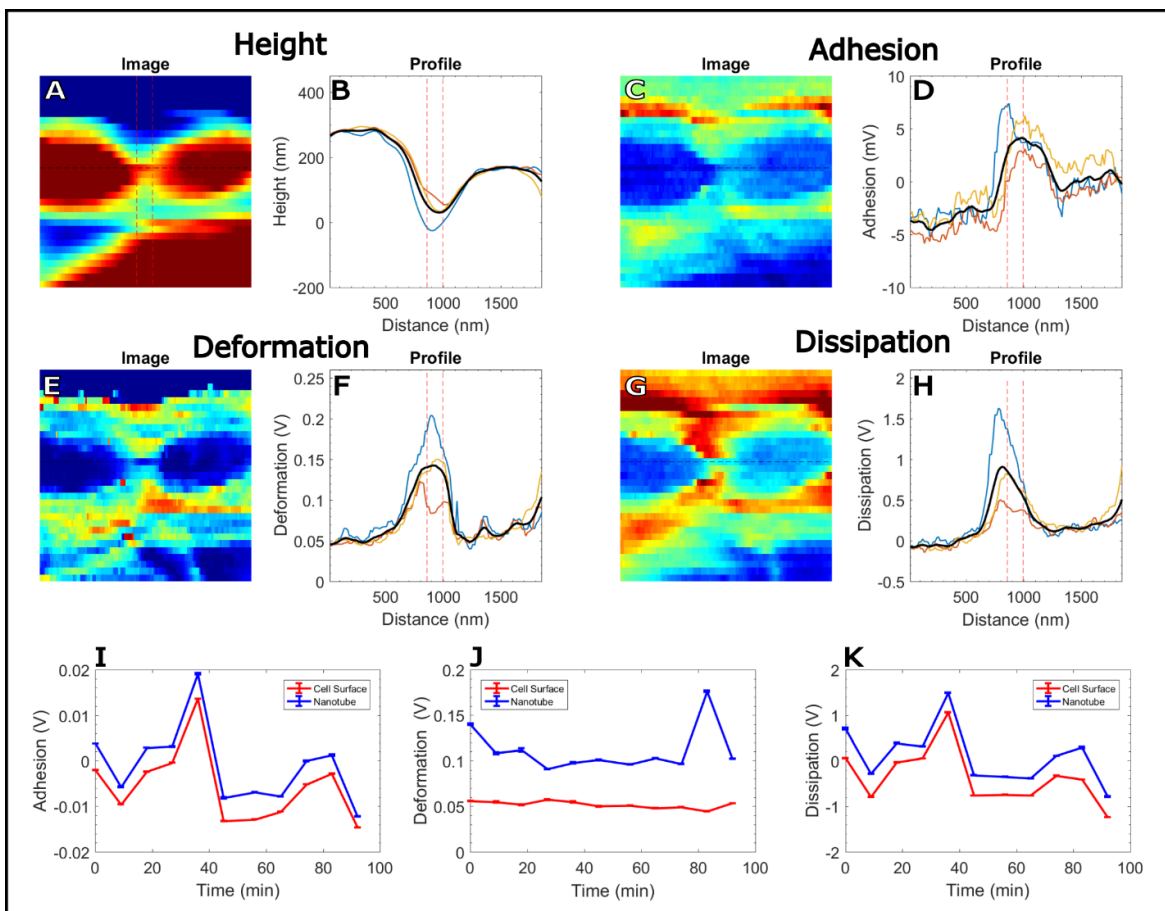
Figure 2.S10: Nanotube nanomechanical properties in live bacteria. Line trace data for an AFM height image for a bacterial nanotube connecting live TW7 cells collected for the time series shown in Figure 2.S9. Representative image and corresponding line profile graph pairs from the time series are shown for height data **(A, B)**, and adhesion **(C, D)**, deformation **(E, F)**, and dissipation data **(G, H)**. Profile graphs **(B, D, F, H)** show the 3 consecutive line traces spanning the bacterial nanotube in the image data (blue, yellow, and orange lines), along with an averaged line graph (black line). The central line trace marking the position of the nanotube is indicated by faint horizontal lines within images (in **A, C, E, G**) with ends of nanotube region marked by vertical red lines (in **A, B, D, F, H**). All AFM images **(A, C, E, G)** are 1.9 µm in size. **(I, J, K)** The nanomechanical data was summarily plotted for nanotube properties (I: adhesion, J: deformation, K: dissipation), in relation to cell surfaces over the time-lapse image series of the live TW7 cells. The properties were measured as averaged values from line segments covering the nanotube (blue) and cell surfaces (red). The line profiles show consistent relative properties between nanotubes and connected cells over time, with a consistent difference in nanotube and cell body nanomechanical properties. This suggests nanomechanical properties as potential signatures for identifying and differentiating bacterial nanotubes.
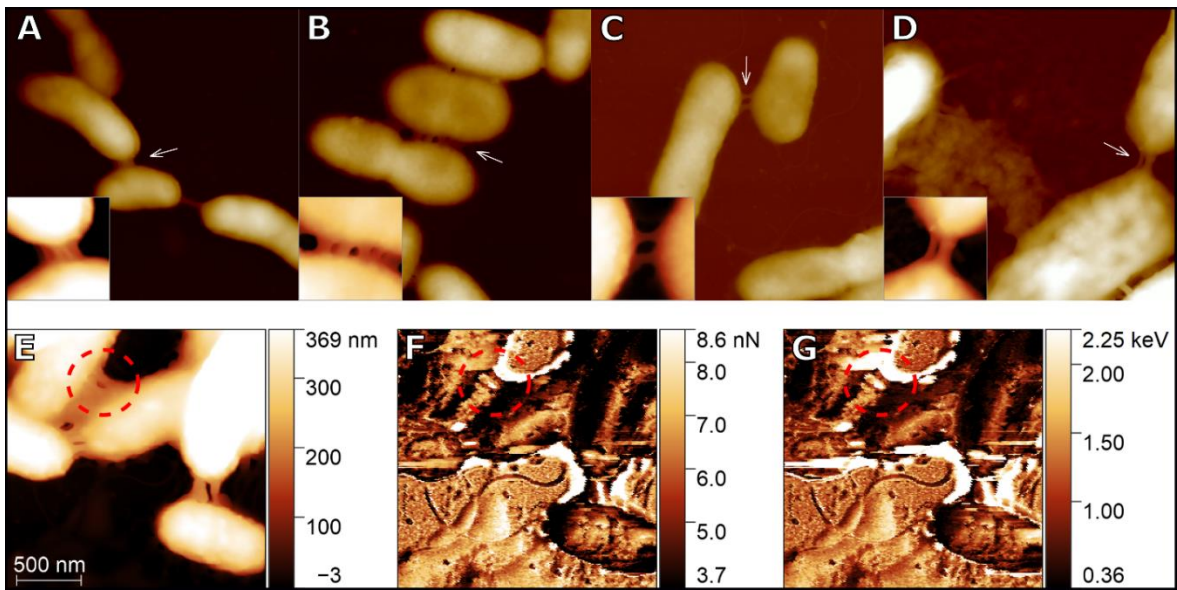
Figure 2.S11: Complex nanotubular connection structures. Complex nanotube structures appear as multiple physical connections form conjoint connections **(A)** or disjoint connections from parallel individual connections **(B)** (white arrows). The parallel connections within the compound structures can be formed from equal, symmetric **(C)** or unequal, asymmetric **(D)** connections (white arrows). In one complex intercellular connecting structure observed between TW7 cells **(E)**, the corresponding nanomechanical image maps (**F**: adhesion, **G**: dissipation) show variability in the adhesion and dissipation data in different areas of the connection. Such areas can present properties similar to the connecting cell bodies or background substrate. Nanomechanical data images reveal potentially obscured intercellular structures in one region (**E,F,G:** red region) suggesting partially covered bacterial nanotubes. Image scan sizes - **A**) image: 3.79 µm, inset: 586 nm; **B**) image: 3.63 µm, inset: 781 nm; **C**) image: 2.78 µm, inset: 626 nm; **D**) 3.7 µm, inset: 623 nm; **E-G**) 2.4 µm.
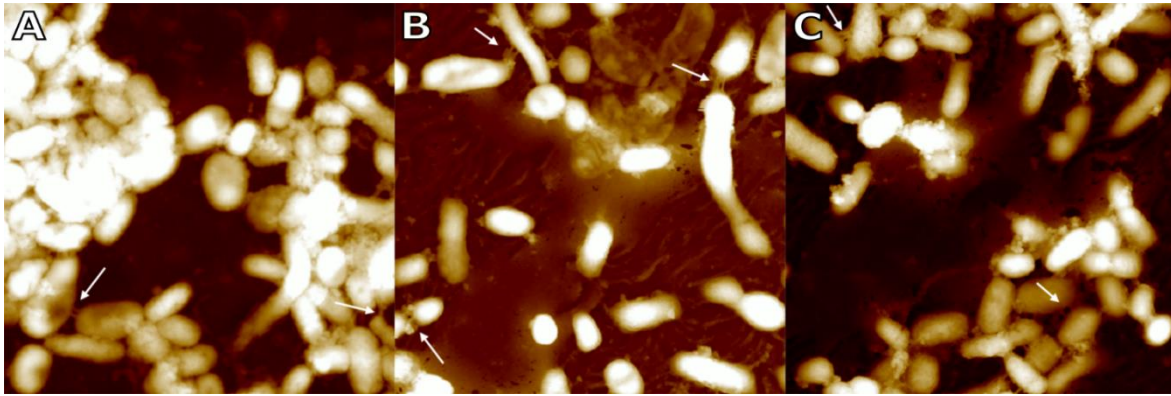
Figure 2.S12: Nanotubes substrates for organic matter attachment. Surface-attached ALTSIO cells when incubated for extended periods of time (4.5 h) on glass surfaces in enriched seawater form intercellular connections within the cell aggregates and organic matter deposited around individual cells. **(A-C)** Representative atomic force micrographs of cells and aggregates show many instances of intercellular connections and physical connectivity (white arrows) that may include or support bacterial nanotubes. AFM images are 10 µm × 10 µm scan size.

2.7 References

Aguayo, S., Donos, N., Spratt, D., and Bozec, L. (2015). Single-bacterium nanomechanics in biomedicine: unravelling the dynamics of bacterial cells. *Nanotechnology* 26**,** 062001.

Alarcon-Martinez, L., Villafranca-Baughman, D., Quintero, H., Kacerovsky, J.B., Dotigny, F., Murai, K.K., Prat, A., Drapeau, P., and Di Polo, A. (2020). Interpericyte tunnelling nanotubes regulate neurovascular coupling. *Nature* 585**,** 91-95.

Astanina, K., Koch, M., Jüngst, C., Zumbusch, A., and Kiemer, A.K. (2015). Lipid droplets as a novel cargo of tunnelling nanotubes in endothelial cells. *Scientific reports* 5**,** 1-13.

Azam, F., and Malfatti, F. (2007). Microbial structuring of marine ecosystems. *Nature Reviews Microbiology* 5**,** 782.

Azam, F., Smith, D., Steward, G., and Hagström, Å. (1994). Bacteria-organic matter coupling and its significance for oceanic carbon cycling. *Microbial Ecology* 28**,** 167-179.

Baidya, A.K., Rosenshine, I., and Ben-Yehuda, S. (2020). Donor-delivered cell wall hydrolases facilitate nanotube penetration into recipient bacteria. *Nature Communications* 11**,** 1-13.

Benner, R., and Kaiser, K. (2003). Abundance of amino sugars and peptidoglycan in marine particulate and dissolved organic matter. *Limnology and Oceanography* 48**,** 118-128.

Bhattacharya, S., Baidya, A.K., Pal, R.R., Mamou, G., Gatt, Y.E., Margalit, H., Rosenshine, I., and Ben-Yehuda, S. (2019). A ubiquitous platform for bacterial nanotube biogenesis. *Cell reports* 27**,** 334-342. e310.

Dubey, G.P., and Ben-Yehuda, S. (2011). Intercellular nanotubes mediate bacterial communication. *Cell* 144**,** 590-600.

Dubey, G.P., Malli Mohan, G.B., Dubrovsky, A., Amen, T., Tsipshtein, S., Rouvinski, A., Rosenberg, A., Kaganovich, D., Sherman, E., Medalia, O., and Ben-Yehuda, S. (2016). Architecture and Characteristics of Bacterial Nanotubes. *Dev Cell* 36**,** 453-461.

Dufrêne, Y.F., Viljoen, A., Mignolet, J., and Mathelié-Guinlet, M. (2021). AFM in cellular and molecular microbiology. *Cellular Microbiology***,** e13324.

Fischer, T., Schorb, M., Reintjes, G., Kolovou, A., Santarella-Mellwig, R., Markert, S., Rhiel, E., Littmann, S., Becher, D., and Schweder, T. (2019). Biopearling of interconnected outer membrane vesicle chains by a marine flavobacterium. *Applied and environmental microbiology* 85**,** e00829-00819.

Flemming, H.-C., and Wuertz, S. (2019). Bacteria and archaea on Earth and their abundance in biofilms. *Nature Reviews Microbiology* 17**,** 247-260.

Gousset, K., Schiff, E., Langevin, C., Marijanovic, Z., Caputo, A., Browman, D.T., Chenouard, N., De Chaumont, F., Martino, A., and Enninga, J. (2009). Prions hijack tunnelling nanotubes for intercellular spread. *Nature cell biology* 11**,** 328-336.

Green, E.R., and Mecsas, J. (2016). Bacterial secretion systems: an overview. *Virulence mechanisms of bacterial pathogens***,** 213-239.

Jahn, U., Gallenberger, M., Junglas, B., Eisenreich, W., Stetter, K.O., Rachel, R., and Huber, H. (2008). Nanoarchaeum equitans and Ignicoccus hospitalis: new insights into a unique, intimate association of two archaea. *Journal of bacteriology* 190**,** 1743-1750.

Kaiser, K., and Benner, R. (2008). Major bacterial contribution to the ocean reservoir of detrital organic carbon and nitrogen. *Limnology and Oceanography* 53**,** 99-112.

Klapetek, P., Necas, D., and Anderson, C. (2004). Gwyddion user guide. *Czech Metrology Institute* 2007**,** 2009.

Klein, T.A., Ahmad, S., and Whitney, J.C. (2020). Contact-dependent interbacterial antagonism mediated by protein secretion machines. *Trends in microbiology* 28**,** 387-400.

Liu, S., and Wang, Y. (2010). Application of AFM in microbiology: a review. *Scanning* 32**,** 61-73.

Lukaszczyk, M., Pradhan, B., and Remaut, H. (2019). "The biosynthesis and structures of bacterial pili," in *Bacterial Cell Walls and Membranes*. Springer), 369-413.

Pande, S., Shitut, S., Freund, L., Westermann, M., Bertels, F., Colesie, C., Bischofs, I.B., and Kost, C. (2015). Metabolic cross-feeding via intercellular nanotubes among bacteria. *Nature communications* 6**,** 6238.

Pelicic, V. (2008). Type IV pili: e pluribus unum? *Molecular microbiology* 68**,** 827-837.

Pirbadian, S., Barchinger, S.E., Leung, K.M., Byun, H.S., Jangir, Y., Bouhenni, R.A., Reed, S.B., Romine, M.F., Saffarini, D.A., and Shi, L. (2014). Shewanella oneidensis MR-1 nanowires are outer membrane and periplasmic extensions of the extracellular

electron transport components. *Proceedings of the National Academy of Sciences* 111**,** 12883-12888.

Pittenger, B., and Slade, A. (2013). Performing quantitative nanomechanical AFM measurements on live cells. *Microscopy today* 21**,** 12-17.

Pospíšil, J., Vítovská, D., Kofroňová, O., Muchová, K., Šanderová, H., Hubálek, M., Šiková, M., Modrák, M., Benada, O., and Barák, I. (2020). Bacterial nanotubes as a manifestation of cell death. *Nature communications* 11**,** 1-12.

Remis, J.P., Wei, D., Gorur, A., Zemla, M., Haraga, J., Allen, S., Witkowska, H.E., Costerton, J.W., Berleman, J.E., and Auer, M. (2014). Bacterial social networks: structure and composition of M yxococcus xanthus outer membrane vesicle chains. *Environmental microbiology* 16**,** 598-610.

Russell, A.B., Peterson, S.B., and Mougous, J.D. (2014). Type VI secretion system effectors: poisons with a purpose. *Nature reviews microbiology* 12**,** 137-148.

Stempler, O., Baidya, A.K., Bhattacharya, S., Mohan, G.B.M., Tzipilevich, E., Sinai, L., Mamou, G., and Ben-Yehuda, S. (2017). Interspecies nutrient extraction and toxin delivery between bacteria. *Nature communications* 8**,** 1-9.

Sure, S., Ackland, M.L., Torriero, A.A., Adholeya, A., and Kochar, M. (2016). Microbial nanowires: an electrifying tale. *Microbiology* 162**,** 2017-2028.

Tavi, P., Korhonen, T., Hänninen, S.L., Bruton, J.D., Lööf, S., Simon, A., and Westerblad, H. (2010). Myogenic skeletal muscle satellite cells communicate by tunnelling nanotubes. *Journal of cellular physiology* 223**,** 376-383.

Wakeham, S.G., Pease, T.K., and Benner, R. (2003). Hydroxy fatty acids in marine dissolved organic matter as indicators of bacterial membrane material. *Organic Geochemistry* 34**,** 857-868.

Wells, M.L., and Goldberg, E.D. (1991). Occurrence of small colloids in sea water. *Nature* 353**,** 342-344.

Zark, M., Christoffers, J., and Dittmar, T. (2017). Molecular properties of deep-sea dissolved organic matter are predictable by the central limit theorem: evidence from tandem FT-ICR-MS. *Marine Chemistry* 191**,** 9-15.

Zhou, G., Zhang, B., Tang, G., Yu, X.-F., and Galluzzi, M. (2021). Cells nanomechanics by atomic force microscopy: focus on interactions at nanoscale. *Advances in Physics: X* 6**,** 1866668.

Chapter 3 Bacterial surface interactions with organic colloidal particles: nanoscale hotspots of organic matter in the ocean

3.1 Abstract

Colloidal particles constitute a substantial fraction of organic matter in the global ocean and an abundant component of the organic matter interacting with bacterial surfaces. Using E. coli ribosomes as model colloidal particles, we applied high-resolution atomic force microscopy to probe bacterial surface interactions with organic colloids to investigate particle attachment and relevant surface features. We observed the formation of ribosome films associating with marine bacteria isolates and natural seawater assemblages, and that bacteria readily utilized the added ribosomes as growth substrate. In exposure experiments ribosomes directly attached onto bacterial surfaces as 40–200 nm clusters and patches of individual particles. We found that certain bacterial cells expressed surface corrugations that range from 50–100 nm in size, and 20 nm deep. Furthermore, our AFM studies revealed surface pits in select bacteria that range between 50–300 nm in width, and 10–50 nm in depth. Our findings suggest novel adaptive strategies of pelagic marine bacteria for colloid capture and utilization as nutrients, as well as storage as nanoscale hotspots of DOM.

3.2 Introduction

Organic colloids in surface waters of the global ocean play a significant role in the biogeochemical cycling of organic matter and for shaping the microenvironment for individual microorganisms (Guo and Santschi, 1997;Hara and Koike, 2000;Fukuda and

Koike, 2004). The abundance of organic colloids in marine surface waters (10^8–10^9 mL^{-1}; < 120 nm-sized) is two to three orders of magnitude higher than the abundance of free-living bacteria and colloid concentration decreases from the surface to deeper waters (Isao et al., 1990;Wells and Goldberg, 1991;1993;Nagata and Koike, 1995). Colloidal particles influence the availability and distribution of organic matter through their physical interactions with dissolved organic matter (DOM), influencing the aggregation and dissolution processes of larger organic particles (Chin et al., 1998;Passow, 2000;Klein et al., 2020). Their interactions with biotic and abiotic surfaces contributes to biofouling and modifying surface sites for increased likelihood of bacterial cell attachment and colonization (Kepkay, 1994). Bacteria are exposed to frequent interactions with more abundant colloids within their marine microenvironment. Adsorption and specific attachment of colloids can influence surface nutrient and DOM bioavailability, surface protein activity, and enzymatic degradation (Amon and Benner, 1994;Nagata and Kirchman, 1996;Schuster et al., 1998;Pan et al., 2020). Interactions of organic colloidal particles can influence the rates of microbial DOM production, dissolution, and remineralization on a microspatial scale (Simon et al., 2002;Fukuda and Koike, 2004;Benner and Amon, 2015;Santschi, 2018).

Phytoplankton blooms and cell lysis events are significant sources of colloidal DOM (cDOM), where released labile colloids are available for enzymatic breakdown and bacterial uptake. Nascent organic colloids are also released into seawater from various biological sources as polymeric exudates and as cellular detritus comprised dominantly of proteins, polysaccharides, lipids and nucleic acids (Thornton, 2014). Within a dynamic microenvironment with changing environmental factors, colloidal organic particles present

102

readily available labile DOM for marine bacterial utilization, that are susceptible to extrinsic physical and chemical interactions. Individual colloidal particles can effectively behave as discrete packets of concentrated organic nutrients for a period before degradation, potentially functional as individual nanoscale hotspots. Influxes of viral-induced colloidal DOM can promote aggregation and influence organic carbon transport. The utilization of colloids by bacteria and heterotrophic flagellates can also support biodiversity and community shifts in bacterial populations (Tranvik et al., 1993;Yamada et al., 2018;Zhao et al., 2019).

Bacterial strategies targeting specific labile biopolymers can offer specific species competitive advantages within transient nutrient hotspots like microalgal blooms (Becker et al., 2017;Unfried et al., 2018). Marine heterotrophic bacteria can derive significant physiological benefit from such strategies and chemotactic motility to exploit increased collision encounters with organic colloidal particles within enriched microenvironments, such as phycospheres (Smriga et al., 2016;Seymour et al., 2017). Motile bacteria can dominate labile DOM consumption during episodic algal bloom release of organic matter, where interactions with organic colloids potentially offer some fraction of cells a competitive advantage (Smriga et al., 2016). Bacteria behavior can be modelled as patchy colloids where cell attachment onto bacterial surfaces is mediated by localized adhesive patches; such sites for binding and unbinding surfaces can be opportune sites of selective organic colloid attachment and aggregation on bacterial surfaces (Vissers et al., 2018). Understanding bacteria-particle interactions can offer insight into the mechanisms underlying bacterial utilization of colloidal organic particles and potential bacterial adaptive strategies that yield competitive advantage over other community members.

Ribosomes are ubiquitous cellular components that are released into seawater along with extracellular release of DOM and phytoplankton detritus. Bacterial ribosomes are molecular assemblies of peptides with ribonucleic acids that are the sites for mRNA transcript translation and protein synthesis (Ramakrishnan, 2002). They are comprised of 2 discrete subunits, a large 50S and a small 30S subunit, forming a 21 nm-sized 70S bacterial ribosome particle (Schuwirth et al., 2005). After their extracellular release, individual ribosome particles are ubiquitous point sources of labile DOM, presenting as potential discrete nanoscale influxes of organic carbon and nitrogen from bacterial scavenging. As such, ribosomes are ideal model organic colloidal particles for investigating the mechanisms and strategies in marine bacterial interactions with specific organic colloids. Extracellular production of ribosomes occurs across multiple taxa of marine bacteria due to viral lysis, and upon release, ribosomes are stable in seawater for sequencing and taxonomic profiling (Zhong et al., 2021). Paucity of quantitative data currently limits our understanding of the influence of bacterial on colloidal organic particles, their interaction and degradation rates.

Emerging methods in nanoscale imaging are expanding the capability for observing and understanding how marine microbes interact with organic colloids within their microenvironment (Taylor, 2019). Atomic force microscopy (AFM) is a high-resolution microscopy technique that measures the nanoscale topography of surfaces using the raster scanning of a sharpened probe tip under feedback control to maintain a constant physical force. Within microbial ecology, AFM imaging has been primarily used to study the sizes and shapes of various components of the marine microenvironments and their interactions with nanometer resolution. It has been applied for observing finer structures and taking

quantitative measurements of microbial biovolumes within natural assemblages (Nishino et al., 2004;Malfatti and Azam, 2009;Malfatti et al., 2010). Additional marine applications for AFM have been in the characterization of marine gels and diatom-derived extracellular polymers and the investigation of marine viruses collected from California coastal waters (Kuznetsov et al., 2010;Pletikapić et al., 2011;Radić et al., 2011;Kuznetsov et al., 2012). The high-resolution capability of AFM imaging has also been utilized for observing and characterizing organic colloids and biopolymers from natural waters (Santschi et al., 1998;Wilkinson et al., 1999). Expanding upon the finer details of individual components of marine microenvironments, AFM imaging has been used to observe morphological details in host-phage interactions for marine bacterium Roseobacter denitrificans OCh114 and for phytoplankton Phaeocystis globosa (Zhang et al., 2012;Sheik et al., 2013). Malfatti and Azam (2009) using AFM showed potential symbiotic interactions between heterotrophic marine bacteria and Synechococcus cells, which has implications in bacterial networks and associations within seawater (Malfatti and Azam, 2009). Seo et al. used AFM to observe marine bacterial capture of submicron particles and the relative frequency within natural bacterial populations, which has implications for the degradation of colloidal organic particles (Seo et al., 2007).

The capture of colloidal particles on bacterial surfaces is a potentially advantageous strategy in fluctuating spatiotemporal distributions of colloidal DOM for scavenging heterotrophic microbes. Localization of organic colloids upon bacterial surfaces suggests coupling between capture and uptake of cDOM. In the present study we used E. coli

ribosomes as model organic colloids to observe the surface attachment and fate of such particles in seawater microcosm experiments.

3.3 Materials and Methods

3.3.1 Bacterial growth response

Seawater was collected from the Ellen Browning Scripps Memorial Pier (San Diego, CA, US) for preparation of three experimental conditions: unprocessed whole seawater (WSW), 0.6-µm filtered seawater (0.6-µm filtrate) and filtered autoclaved seawater (FASW). WSW and 0.6-µm Filtrate were diluted 10x with FASW at the start of the experiment to achieve initial bacterial cell densities of 3.5×10^5 and 2.8×10^5 cells mL^{-1}, respectively. Marine bacterial isolates Alteromonas sp. (ALTSIO), Pseudoalteromonas sp. (Tw7), Pseudoalteromonas sp. (Tw2), Vibrio sp. (SWAT-3), and Vibrio cholerae strain 2740-80 were grown with shaking in Zobell 2216E medium overnight, diluted 1: 1000 in filtered autoclaved seawater (FASW), and acclimated for 48 h at 23°C. Cultures were then diluted into fresh FASW to an initial cell density of 5×10^4 mL^{-1} at the start of the experiment. Please see Table 3.S1 for phylogenetic classification and source of all isolates used in this study.

Three experimental conditions (WSW, 0.6-µm filtrate, and isolate cultures) for three treatments were setup for each of the three experimental conditions. Specific treatments used in each condition included the following: 0.3 or 3.3 µg E. coli ribosomes (New England BioLabs Cat# P0763S, Ipswich, MA USA) mL^{-1} culture (hereafter "R"); ribosome buffer (final concentration = 2 µM Hepes-KOH, pH 7.6; 1 µM Mg(OAc)2; 3 µM KCl; 0.7 µM

beta-mercaptoethanol) or no amendment. Experiments were conducted in triplicate, using culture volumes of 10 mL in 14 mL polycarbonate tubes, with rotary shaking, at 23°C.

Bacterial abundance for the five treatments was determined at 0 h and 24 h (n=120). Samples for bacterial abundance were fixed with formalin at a final concentration of 2% and frozen at -80°C. Upon thawing, samples were immediately placed on ice and stained 1x with SYBR Green I (Invitrogen, Molecular Probes Cat# S7563, Carlsbad, CA USA). Bacterial cells were enumerated with a BD Accuri C6 Plus flow cytometer (Ex. 488nm, Em. 533). Experimental treatments for WSW, 0.6-µm filtrate and ALTSIO cultures were sampled at 0 h and 24 h, and fixed and filtered on 0.22-µm polycarbonate filters (GTTP, Millipore). Filters were affixed to a glass slide with adhesive tabs for atomic force microscopy imaging.

3.3.2 Ribosome exposure experiments

AFM experiment was designed to expose select bacterial cultures to a continuous flow of media with suspended ribosomes to minimize the effect of potential colloid settling onto bacterial surfaces under otherwise relatively static conditions. Isolate cultures were prepared as follows. Alteromonas sp. ALTSIO, Pseudoalteromonas sp. TW7, and Flavobacterium sp. BBFL7 isolates were cultured in Zobell 2261E liquid medium. Overnight cell cultures were diluted tenfold into fresh Zobell medium and incubated for 6 hrs. 1 mL of culture was centrifuged at 3000 g for 5 minutes and resuspended with 0.02-µm syringe-filtered FASW (Whatman® Anotop®) to a final volume of 400 µL before application to AFM sample substrates. Substrates were prepared by securing freshly cleaved 12 mm mica discs onto clean glass slides using epoxy and treated with 1 mg mL^{-1} poly-

lysine solution to promote cell adhesion. 100 µL of the cell suspension was deposited onto mica and placed onto the AFM apparatus. The imaging fluid medium was circulated using syringe pumps (Harvard Apparatus) in withdrawal and infusion modes to continuously exchange fresh 0.02-µm Anodisc syringe-filtered FASW amended with ribosomes (conc. approx. 0.66 µg mL^{-1} (~1.8 × 10^{11} particles mL^{-1})) at a rate of 10 µL min^{-1}. After 1 hr, samples were fixed with formalin (20 µL of 37% formalin) for 15 minutes and rinsed with 1 mL of HPLC grade water 5 times. Samples were dried in a laminar flow hood and stored in plastic petri dish until imaged with AFM.

3.3.3 AFM imaging

AFM imaging was performed on a Dimension FastScan atomic force microscope (Bruker, Santa Barbara, CA USA) in PeakForce TappingTM Mode using ScanAsyst-Air probes (nominal spring constant: 0.4 N/m and tip radius: 5 nm, Bruker) for fixed and air-dried samples. Sample imaged under fluid conditions were imaged in 0.22-µm-filtered autoclaved seawater with ScanAsyst-Fluid probes (nominal spring constant: 0.7 N/m and tip radius: 20 nm, Bruker). Acquired AFM micrographs were processed and analyzed using Nanoscope Analysis (Bruker) and Gwyddion software (http://gwyddion.net).

3.4 Results and Discussion

3.4.1 Ribosomes as particle films on bacterial surfaces

As evidence of direct contact-dependent bacterial interactions with ribosome, fluorescently labelled ribosomes or ribosome fragments added at 5 × 10^9 to 5 × 10^{11} particles

mL^{-1} were found to cover surfaces of cultured Alteromonas sp. ALTSIO within 30 sec (Figure 3.S1A-B). Fluorescence micrographs showed varying levels of SYBR Green II-labelled ribosomes coverage on FM 4-64-labelled cells. Most cells presented significant coverage of fluorescence signal indicating ribosome interactions with bacteria surface. A subset of cells showed ribosome fluorescence localized on bacterial edges in addition to overall cell surface.

AFM imaging of ATLSIO and natural assemblages in 0.6-µm seawater filtrate amended with ribosomes showed bacteria surrounded or covered with films of particles (Figure 3.S1C-D). Particle features of individual ribosome associated with bacterial cells as contiguous films, forming a zone of enrichment. Particle films on and around cells vary in appearance for cells from 0.6-µm seawater filtrate. In comparison, ALTSIO cells amendment with ribosomes and AFM-imaged immediately showed particle films that cover regions extending up to 200 nm from the cell boundary.

Ribosome depletion was observed in atomic force micrographs of ALTSIO and 0.6-µm seawater filtrate cells deposited onto 0.22-µm polycarbonate filters immediately after ribosome amendment (< 5 min) and after 24 hr incubation (Figure 3.S2). The significant decrease of particles indicated the depletion of suspended ribosomes after incubation. For ALTSIO after 24 h the presence of particle films is completely diminished with little to no background ribosomes, likely due to bacterial degradation of ribosomes. In contrast, incubation of ribosomes with cells in 0.6-µm seawater filtrate for 24 h had more background ribosomes present, and devoid of any cell-associated particle films surrounding cells, suggesting a lower degree of ribosome utilization compared to ALTSIO cells. Near complete

depletion of background ribosomes, in combination with the observed increase in cell abundance for marine bacterial samples is consistent with utilization and degradation of ribosomes via physical interactions.

Cell-associated particle films were primarily observed as particle-enriched zones, effectively as a halo of colloidal ribosomes, with a higher local concentration of cDOM. The physical characterization of such enrichment zones can be challenging due to physical artefact during sample preparation, including forced deposition upon the filtration surface. Such manipulations flatten and obscure the origination 3-dimensional ultrastructure of the particle-enriched zone onto observation surface plane. This effect may present as particle accumulation around cell periphery of individual bacteria, which can be influenced by filtration artefacts due to calls covering filter pores. These observations support the hypothesis that bacteria can capture organic particles or develop a film-like layer of particles to be later utilized as a substrate repository. AFM micrographs of cells from whole seawater filtrate show observed cells with similar coverage and contiguous films of cell-associated ribosome particles (Figure 3.S1E). The surfaces of select cells were observed with patches of ribosome particles, suggesting intimate attachment and association between some bacterial cells and organic colloidal particles within a natural assemblage in cDOM-enriched marine microenvironments.

The addition of ribosome particles results in the coating of bacterial surfaces with a film of contiguous particles, effectively altering their surface properties and surface-mediated interactions with the marine microenvironment. One manifestation of the surface film is as a zone of enrichment, with particles densely populating the proximal areas around

cell edges, as observed in filtered samples. Such zones are suggestive of 3D structure to the particle film in a weakly bound association with the surface and susceptible to disruption from physical forces, such as from filtration or centrifugation. The formation of the surface particle film likely occurs through a quick process of particles populating the bacterial surface through rapid adsorption and attachment (Figure 3.S1). Variations in the adsorption process can influence bacterial sequestration of organic colloids and in turn influence bacterial behaviors in particle-enriched microenvironments. Bacterial utilization of various types of organic colloidal particles raises the possibility of potential bacterial adaptive strategies in selective transformation of particles and DOM distribution on a submicron scale in the marine microenvironment. Different bacterial species can have varying potential for interaction and particle degradation rates and exert influence on the bioavailability of colloidal DOM. Bacteria have access to colloids smaller than 200 nm due to diffusion and convective transport to the surface. Furthermore, they need to expend energy for larger colloids up to 2 µm to intercept particles through increased collision frequency of particles (Kepkay, 1994). In relation to these concentration-dependent processes, bacterial surface capture and retention of colloids is an effective strategy for bacteria to generate nanoscale hotspots of DOM. This results in small, localized regions with high effective concentrations of ribosomal particles. The mechanisms of particle attachment and utilization are not known, nor is the cause for heterogeneity within a neighborhood of cells. Further investigation is needed to determine mechanisms that may contribute to specific particle interaction rate for different bacterial species and the variability within a local population of cells. Additionally,

111

it remains to be determined how the age of colloidal DOM and potential refractory DOM molecules may influence the extent and rates of particle attachment to bacterial surfaces.

Our findings of films of organic colloidal particles on bacterial surfaces have significant implications in the ecophysiology of heterotrophic bacterioplankton, considering that cells can transport utilizable labile DOM on their surfaces. When exposed to the high colloidal concentration, bacterial cells are enrobed within a shroud of particles traveling with a nutrient hotspot, extending the residence time of ambient organic colloids. The surface capture of ribosomes is a quick process that occurs within seconds to minutes, suggesting that with sufficient concentration, the bacterial surface can become saturated, along with surface protein activities in particle breakdown and nutrient uptake. Brownian motion and convective diffusion of smaller colloids can consistently replenish surface particle films with organic colloids from the ambient microenvironment in elevated particle concentrations.

The apparent bacterial consumption of ribosome particles suggests general utilization of organic particles of similar size as a labile organic source of carbon and nitrogen for bacterial production. The breakdown of colloidal DOM can generate smaller colloidal particles and dissolved organic molecules that readily diffuse, which imposes a limitation on the advantage and utility of organic colloidal particle breakdown for individual bacteria. Any fragmented particles and organic molecules that remain suspended and unattached may be lost to bacteria due to the transience of the interaction. Bacterial surfaces can functionally generate nanoscale hotspots by forming contiguous films of particles due to attachment of ambient colloidal organic particles at elevated concentrations. This transformation of organic matter has implications for the residential times of nascent DOM

in the surface waters and its vertical transport in the water column. It is most likely that different bacterial taxa have varying levels of influence on organic colloids, where select members in a bacterial assemblage can drive greater levels of interactions and growth in response to influxes of organic colloidal particles. Further investigation is needed to quantify the variability of such utilization and the bacterial respiration and growth efficiency rates with respect to ambient concentrations of specific organic colloids, and the currently unknown factors that influence these rates.

The effect of being covered with ribosomal particles or associated with a contiguous particle film have implication for individual bacterial activity. The attached particles could effectively alter the properties of bacterial surfaces presented to the external environment and the biochemical activity of the surface proteins, enzymes, and transporters. The presence of cells covered with particle films or saturated with particles has interesting implications for a microbial community response to a sudden influx of colloidal organic particles. Select cells that form surface particle films can function as nutrient hotspots for neighboring bacteria, where indirect or direct contact with particle-coated cells can potentially result in the efficient breakdown and nutrient uptake for contacting cells. For example, coupled interaction between particle-coated cells and surface-enzyme expressing cells could be a potential mutually beneficial strategy within certain microbial consortia. Further work is needed to determine the properties of such surface particle films on bacterial surfaces and the influence of their variability on the interactions between bacterial species.

3.4.2 Surface attachment and capture of particles

Introducing colloids within circulating media and removing weakly-associated particles through fluid shear, we observed discrete patches or clusters of organic colloidal particles distributed on the bacterial surface. AFM cell surface imaging of isolates (Flavobacterium sp. BBFL7, Pseudoalteromonas sp. TW7, and Alteromonas sp. ALTSIO) in circulating FASW media with ribosome amendments show patches or clusters of particles as a common surface feature after exposure to ribosomes as extracellular organic colloids (Figure 3.1). Small individual patches or clusters of particles that are formed and retained upon few bacterial surfaces after an exposure period of approximately 60 mins to organic colloidal particles. Among the various cells, a few select cells were more populated with particulate features compared to many immediate neighboring cells that showed bare, particle-devoid surfaces or few individual particles. Cells within populations of the same isolated presented variable levels of particle attachment. Most cells within a population had significantly lower particle attachment or fewer intact particles retained upon the bacterial surface after interaction. AFM micrographs of select surface particle clusters and associated line section profiles observed in ALTSIO and TW7 cells showed observed particle clusters had varying physical dimensions and ranged between 40 – 200 nm in width and between 10 – 30 nm in height (Figure 3.2). After longer exposure of 4.5 h, the surface patches become more numerous and larger contiguous regions (Figure 3.S3). The aggregation of organic colloidal particles on bacterial surfaces is heterogeneous and becomes more unequal and extreme with a longer duration of colloidal particle exposure. More cells were observed with surface-associated particles, with more particle clusters observed in the interstitial spaces between individual cells. One notable observation is the expected increase of attached

114

particles with increased exposure time, which contributes to developing more prominent surface particle patches. Ribosomes stick onto bacterial surfaces, forming protruding features shown in 3D representations of surface particle clusters and patches on individual ALTSIO cells (Figure 3.S4). The frequency of particle attachment was variable for populations of cells within observed images. The formation of such prominent features may promote attachment of extracellular polymers or bacteria in potential biofilm formation, forming sites of physical intercellular interaction.

Figure 3.1: Particle clusters and patches on bacteria surfaces. AFM height images and respective SEM-simulated images of bacterial isolate surfaces during longer amendment with circulating ribosomes. *Flavobacterium* sp. BBFL7 **(A,D,G,J)**, *Alteromonas* sp. ALTSIO **(B,E,H,K)**, and *Pseudoalteromonas* sp. TW7 **(C,F,I,L)**. The images show prominent surface patches of organic particles (white arrows) on select cells after exposure to ribosomes for 1 h **(A-F)** and for 4.5 h **(G-L)**. Panel image scan sizes are 10 µm × 10 µm.
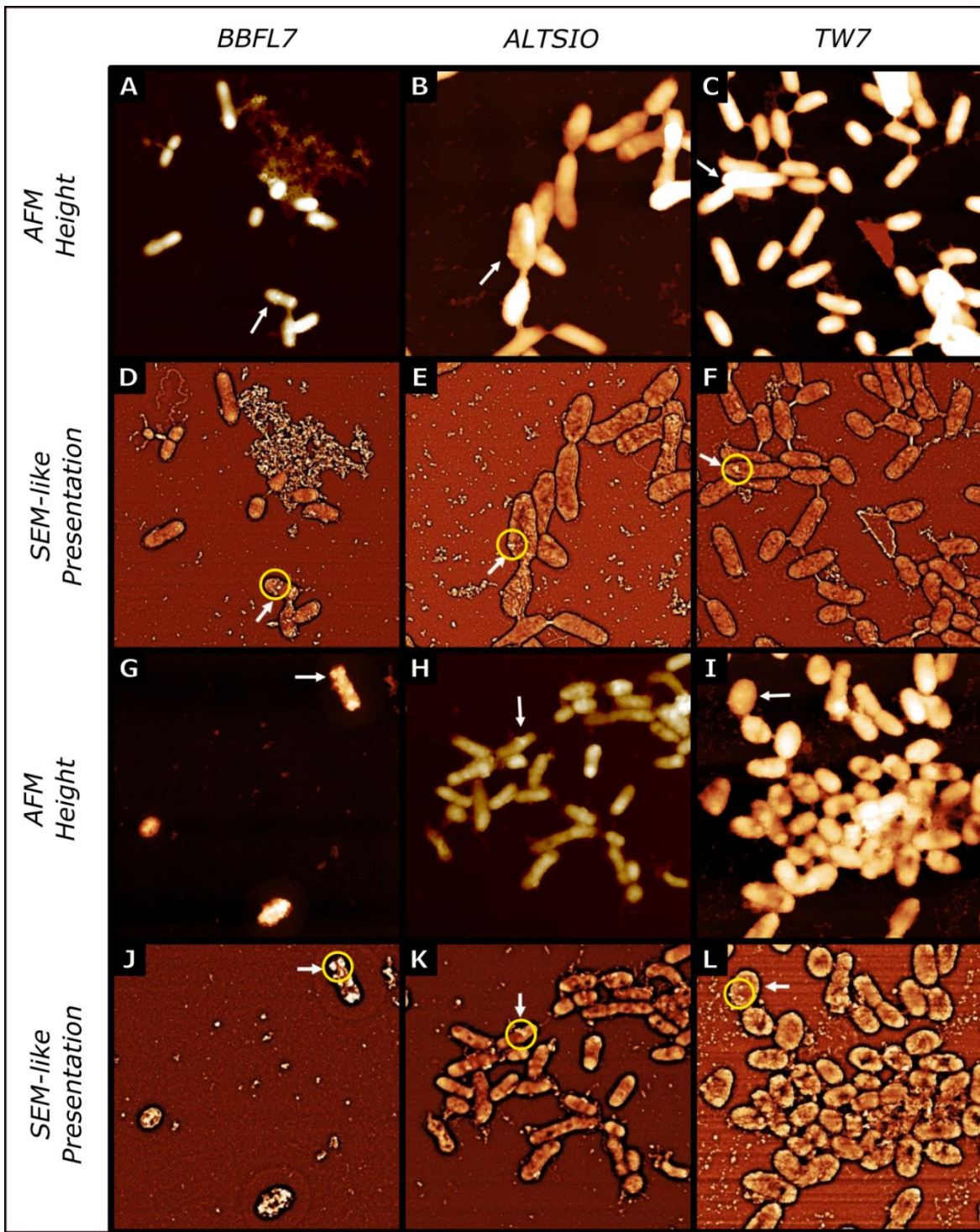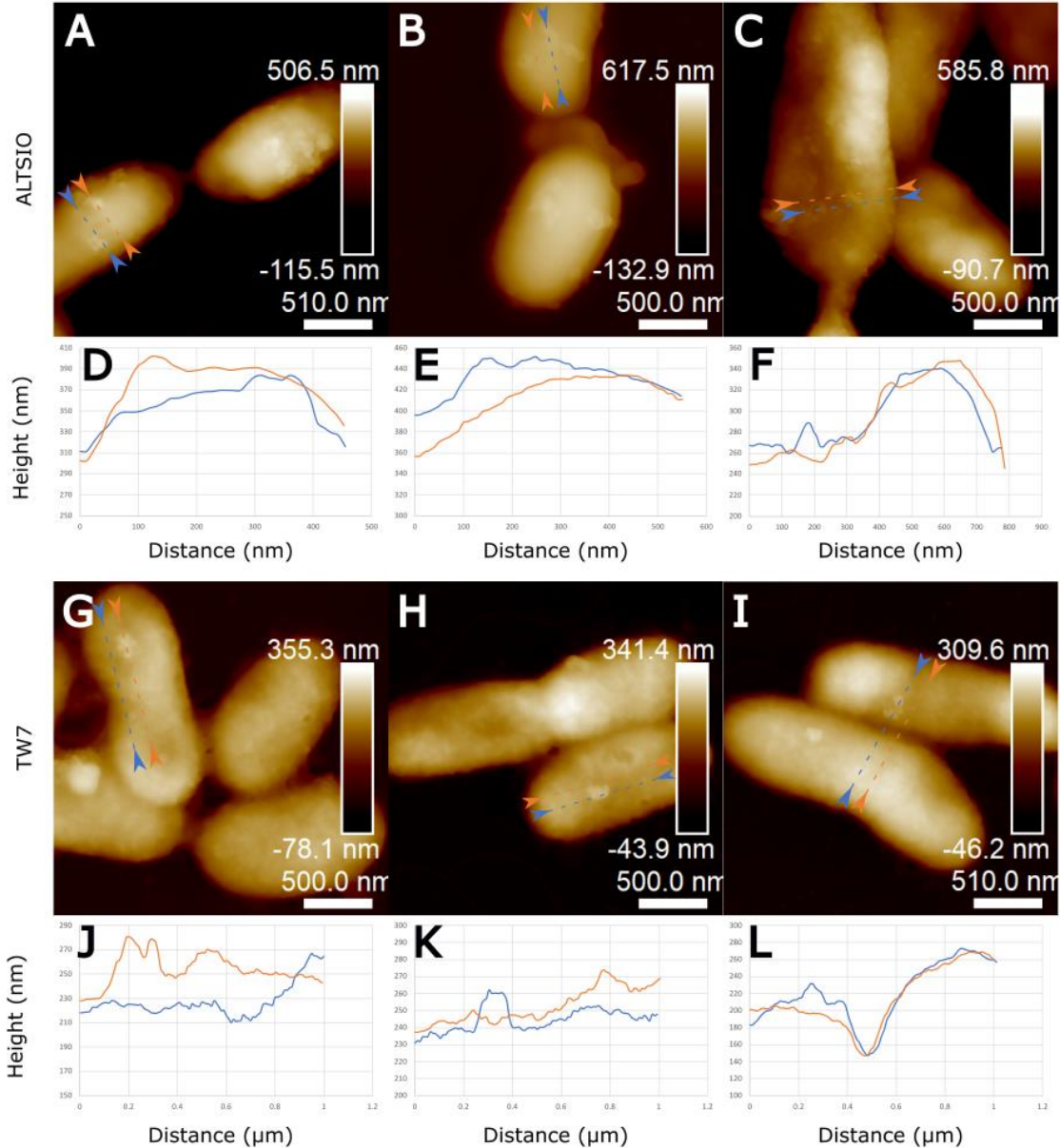
Figure 3.2: Surface profiles of individual ribosome particle clusters. AFM height images with demarcated line sections (blue and orange dashed lines and arrowheads) of surface-attached particle clusters of ribosomes on ALTSIO cells **(A-C)** and TW7 cells **(G-I)**. Respective surface profiles of paired line traces show the height dimensions of such features with reference feature-free profiles from proximate cell surface regions (**D-F**: ALTSIO and **J-L**: TW7); corresponding to respective line sections in AFM images. Most discrete surface-attached particle clusters are roughly 40–200 nm in width and 10–30 nm in height, corresponding to several multiples of ribosome particles. Image scale bars provided.

The observation of discrete surface clusters and patches in AFM imaging within circulating media, suggest intimate physical interaction of particles upon bacterial surfaces. Exposure of bacterial surfaces to elevated ribosomal particle concentrations in the ambient microenvironment leads to the development of discrete patches of particles distributed on the surface, as shown in Figure 3.1. Select cells appear to be preferentially disposed towards capturing or interacting with particles, even in a local neighborhood of cells. The retention of small individual patches or clusters of particles, formed upon few bacterial surfaces, after an exposure period of approximately 60 mins suggests the potential for intimate attachment to organic colloidal particles. With extended exposure time to ambient organic colloids, the proportion of cells with surface attached particles increases, and select cells present a disproportionately greater quantity of surface particle clusters. After longer exposure of 4.5 h, the surface patches become more numerous and contiguous as the bacterial surfaces become conditioned with attachment of organic colloids. The attachment of ambient particles onto preexisting patches can consequently contribute to the attachment of cells onto larger particle aggregates and other cells via surface patches (Vissers et al., 2018). We consider the differences in the development of particle films compared to surface particle patches likely due to differences in particle interaction frequency for suspended cells compared to surface-attached bacteria. Suspended cells are likely to have more frequent encounters with particles and develop substantial films which may obscure more intimately associated surface clusters or patches of particles. The particles patches can offer some insight into how various organic colloids interact with and condition bacterial surfaces. Significant variability was observed within cell populations of individual isolates, but

different marine bacterial species may potentially vary in their interaction with colloidal particles. The presented clustering of surface particles may be potentially influenced by physical properties that influence these interactions for an individual bacterium.

We consider the distribution of surface-attached particles on bacterial surfaces to be random, but more work is needed to consider the possibility of site-specific particle attachment. Possible developments of surface-attached particles include the successive attachment of particles to form nucleation sites for particle clusters or attachment sites for other bacteria. It is possible that organic colloids preferentially attached onto each other compared to bacterial surface, and the surface capture of particles can result in effective surface-localized aggregation of particles. For instance, given a bacterial cell expressing clusters of surface particles, other bacteria can potentially interact with the cell and attach onto the surface around the particle cluster, limiting the desorption and loss of particles, allowing both cells to benefit from degradation and nutrient uptake of the associated particles.

The presence of particle patches on the bacterial surfaces has potential implications in microbe–microbe interactions. Particle clusters on cell surfaces can become nucleation sites for aggregation and association with other labile colloidal DOM and potentially refractory DOM. These features can also become sites bacterial cell attachment to other surfaces, functioning as patchy sites of increased surface adherence (Vissers et al., 2018). Another possibility is that particle clusters can be surrounded by bacterial surface enzymes, resulting in the breaking down particles within an enclosed pocket. For instance, two bacterial cells attached together via particle clusters can result in both cells retaining organic

120

particles from the disruption of associated cells and fragmentation of particle clusters. The aggregation and distribution of organic colloidal particles through contact-dependent cell interactions could result in physical associations where some bacterial species or subpopulations can derive benefits from scavenging colloidal DOM from other cell surfaces. This potential mechanism is likely driven due to random encounters, and more investigative work is needed to determine if specific mechanisms exist to express such strategies to capitalize on elevated levels of ambient organic colloids.

3.4.3 Observed surface features relevant for bacterial-surface particle attachment

Surface-attached bacteria were observed with altered surface features (e.g., surface corrugations, surface pits) that can influence their interactions with organic colloidal particles like ribosome particles. Compared to discrete surface-attached particle clusters of ribosomes, some TW7 bacteria cell surfaces were observed to become corrugated with nanoscale patches of the surface raised in a semiregular pattern. AFM data shows that the corrugation patterns were similar among cells within an image field of 10 µm × 10 µm (Figure 3.3A-D). Line section surface profiles of select corrugation features indicate such features are approximately 20 nm in height and range between 50–100 nm in width (Figure 3.3E). The corrugation features contribute to rough surfaces with colloid size pocket regions on bacterial surfaces. In addition to surface corrugation, certain TW7 bacterial surfaces were observed with prominent membrane pit features. TW7 Bacterial cells were observed with pits on the surface ranging from 50–300 nm in width and 10–50 nm in depth, with variable surface pit sizes and depths, as shown with respective line traces shown in Figure 3.4A.

121

Surface pits were observed during live cell imaging of TW7 cells of an intact cell over a period of 92 minutes (Figure 3.4B). Data from consecutive horizontal line trace profiles across the cell are summarily plotted at 0-, 45- and 92-minute time points. The timelapse AFM showed a consistent expression and physical structure of the surface pit feature measuring approximately 50 nm deep and 300 nm wide throughout the duration of imaging. Observed surface pits in TW7 cells bear resemblance in size and structure to mouth-like pit structures observed in certain soil-isolated Sphingomonas bacteria (Hisano et al., 1995). Surface pits in Sphinogomonas A1 strain are 0.02 – 0.1 µm in diameter and part of the pleat-like surface structure involved in breakdown and uptake of intact alginate particles (Hashimoto et al., 2001).

Figure 3.3: Bacterial surface corrugation. AFM micrographs **(A,C)** and representative SEM-like presentations **(B,D)** of TW7 cells expressing surface corrugations. **(E)** Magnified images of cells with marked line section crossing the surface corrugation features with respective surface height profiles **(1-6)**. Image scale bars provided.
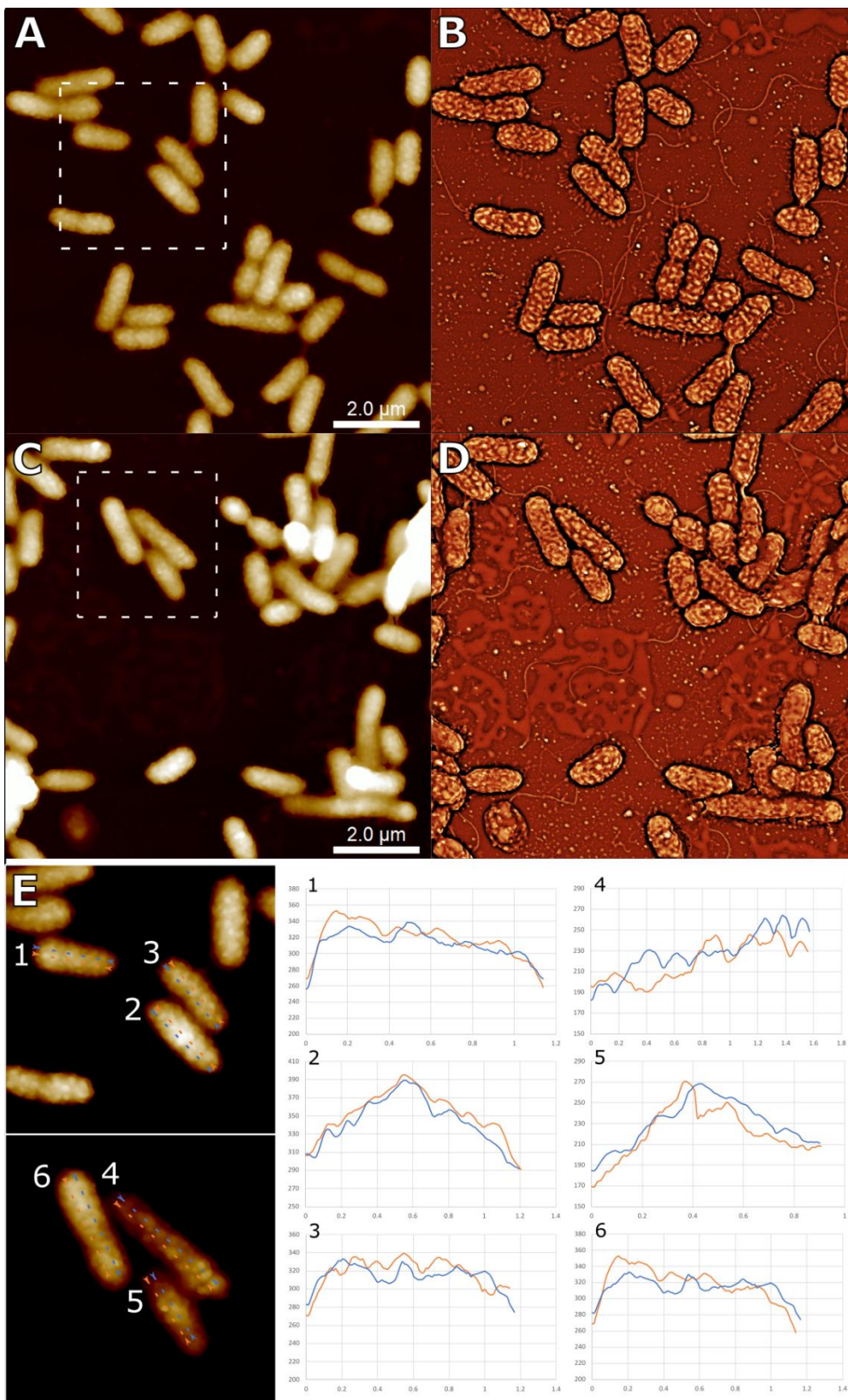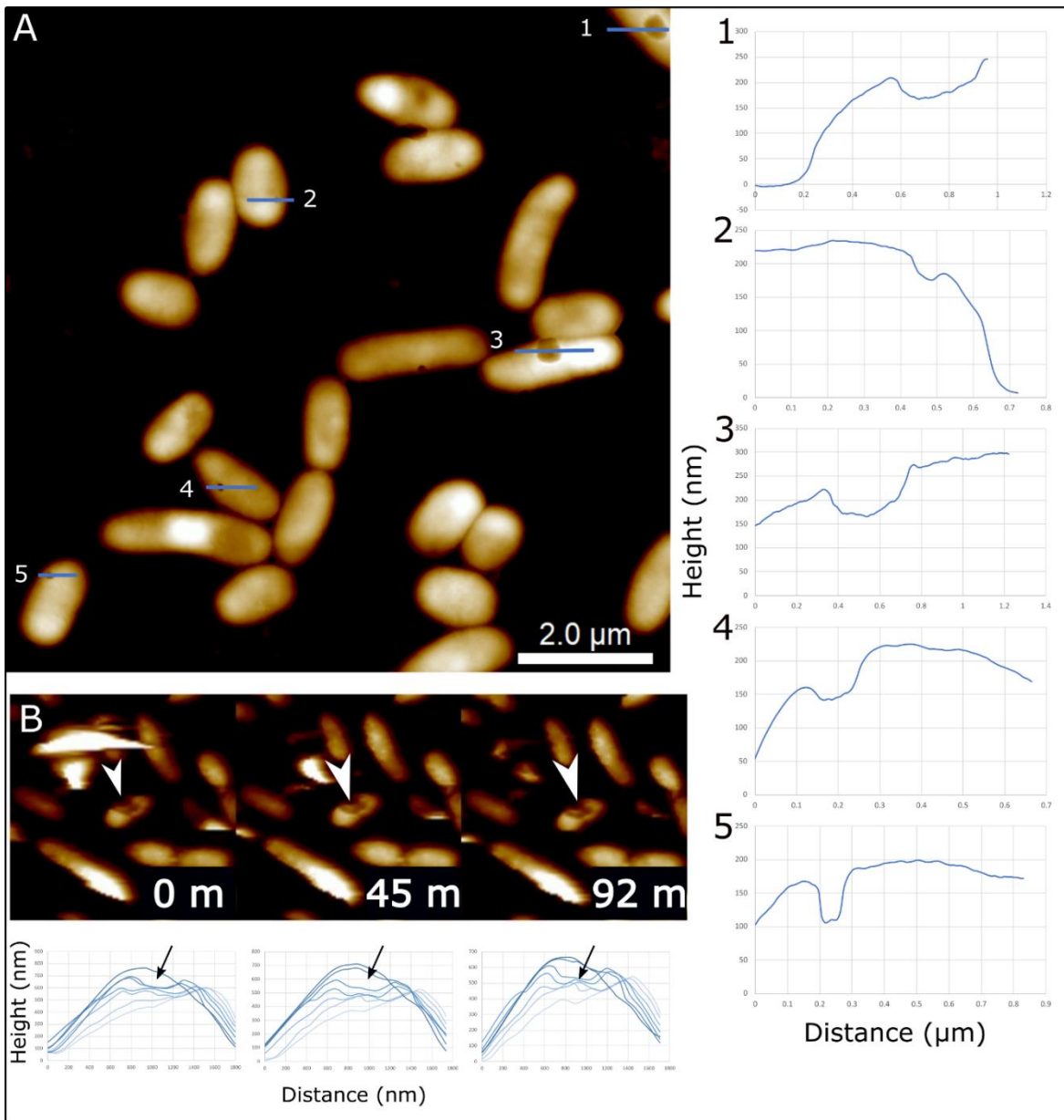
Figure 3.4: Surface pits form in live bacteria. (A) In TW7 cells, surface pits appear as depressions with variable cross-sectional profiles. Line section graphs **(1-5)** show the cross-sectional profiles of line segments labelled within the AFM image. **(B)** A surface pit (white arrow) was observed in fluid imaging of live TW7 cells over a period of 92 minutes, showing consistent pit dimensions and sizes, as shown with respective line traces. Image scan frames are shown at 0-, 45- and 92-minute time points with a scan area of 6.5 µm x 6.5 µm. Topographic data from consecutive horizontal line trace profiles across the cell are summarily plotted for each image, showing the height depression of the surface pit (black arrow).

Marine bacteria express potential adaptive surface features that have potential implications in modulating surface interactions with ambient organic colloidal particles. One observed adaption was the development of colloid-sized surface corrugations and raised protrusions modifying the bacterial surface. These raised features increase the surface area available for particle attachment, where select areas between features have increased contact area for particle attachment. Corrugation features are predicted to reduce surface energy barriers for colloidal and contact interactions, influencing the attachment rates of ambient particles onto bacterial surfaces (Kämäräinen et al., 2020). The variations in the potential particle contact area can form different areas for stronger and weaker attachment of organic particles on the bacterial surface. Such features may imply emergent changes in the packing organization of surface proteins and periplasmic compartment components. The observed corrugated features may result in the placement of organic colloidal particles within proximity of surface enzymes and relevant periplasmic proteins involved in hydrolysis, uptake, and translocation of nutrients. Alternatively, it may be possible that may develop from the depletion of surface accumulated organic matter, with residual organic matter resulting in corrugated features and increased surface roughness. The size similarities between the raised corrugation features and organic particles raises potential possibilities in their involvement in surface interactions with particles.

Bacterial surface pits were another type of observed adaptive bacterial surface features, where cells can form discrete membrane pockets and depressions for contained interaction sites with organic colloidal particles and DOM. Based on the breadth and depth of surface pits, such features have the potential to contain small aggregates of organic

colloidal particles with a contained space, with a potential artificially elevated local concentration of organic matter. Such features may have implications for the possibility of the degradation and direct uptake of organic colloids (Hisano et al., 1996). The expression of superchannels involved in the direct uptake of alginate have been observed previously, and such features may be involved in similar mechanisms (Hisano et al., 1995). One potential feature of surface pits is the possible formation compartmentalized enclosure around particles between interaction cells, where breakdown of nutrients if directly available to benefit the associated cells. The expression of surface pits has greater implications for bioremediation in bacteria-directed breakdown and uptake of particles and pollutants with a combination of surface pits and superchannel structures (Hashimoto et al., 2010).

The observations of the corrugated bacterial surface expression and pit formation were rare, less than < 1% of observed cells but these processes are likely to be generally overlooked among marine bacterial assemblages in the surface waters. These observations point towards potential evidence of bacterial strategies in exploiting surface interactions with ambient organic colloidal particles. The corrugation adaption of bacterial surfaces increases the available surface area for interaction, potentially creating preferential attachment sites for extracellular particles. This process can facilitate interaction with other cells and ambient biopolymers and indirectly influence interactions with extracellular particles and induce the utilization of ribosome particles and other organic colloids. Our observations from TW7 cells suggest surface pit formation can be strategy used in rare instances by bacteria. Some taxa of marine bacterial may potentially express surface pits more frequently compared to other cells in an assemblage. Such bacteria can potentially use surface pits to process intact

colloidal particles within a contained space, taking advantage of the confinement to generate a limited nutrient hotspot of organic matter localized around the cell. Further investigation is required to determine the conditions and mechanisms involved in the expression of these features and the consequential changes in the bacterial ecophysiology. Similarly, further research is needed to determine the mechanisms involved in surface pit expression and the variability among marine bacterial species. The presence of these adaptations has implications for variations in bacterial interactions and strategies of nutrient acquisition within marine microenvironments enriched with organic colloidal particles.

3.4.4 Growth on colloids – common among multiple isolates

The primary finding is the evidence of bacterial responses to the organic matter of colloidal ribosome particles through contact-dependent interactions. In growth response experiments, abundances significantly increased for all tested bacteria over a period of 18 hours when cultures were amended with ribosomes (3.3 $\mu g\ mL^{-1}$) in comparison to the non-amended controls, as summarized in Table 3.1. Natural bacterial assemblages in whole-seawater (WSW) and 0.6-µm-filtrate increased ~2-fold, while most of the isolate's (ALTSIO, Tw7, Tw2, and SWAT-3) abundances increased ~10-fold. V. cholerae abundance also substantially increased (~5-fold). Relative growth yields for different bacteria suggest that some isolates are better than others at incorporating ribosomal carbon into bacterial biomass. The increase in bacterial abundance in combination with the depletion of ribosome particles in ALTSIO and 0.6-µm-filtrate support the hypothesis that marine bacteria can readily degrade and utilize organic ribosomes in the ocean.

Table 3.1: **Marine bacterial growth response to 18 hr incubation with ribosome amendment**

Isolate	Ribosome	Buffer	Control
WSW	1.03E+07 ± 1.22E+06	2.75E+06 ± 5.30E+04	2.63E+06 ± 2.04E+05
0.6 μm Filtrate	5.12E+06 ± 8.70E+05	1.46E+06 ± 3.41E+04	1.33E+06 ± 1.32E+05
ALTSIO	2.58E+07 ± 2.08E+06	2.15E+06 ± 4.92E+04	2.52E+06 ± 9.69E+04
TW7	1.30E+07 ± 1.12E+05	1.13E+06 ± 2.51E+04	9.68E+05 ± 5.11E+04
TW2	1.83E+07 ± 2.66E+05	1.36E+06 ± 3.11E+04	1.00E+06 ± 2.08E+04
SWAT-3	4.82E+06 ± 7.04E+05	3.26E+05 ± 2.25E+04	1.13E+05 ± 5.77E+04
BBFL7	1.88E+06 ± 2.95E+06	2.09E+05 ± 1.57E+04	2.06E+05 ± 5.43E+04
V.C.	3.86E+06 ± 7.97E+05	6.52E+05 ± 1.49E+05	6.54E+05 ± 2.60E+05

Bacterial growth is observed for different marine isolates and assemblages at an amendment concentration of 3.3 µg mL^{-1} suggesting sufficient association, degradation, and utilization of ribosomes to support bacterial cell production that can involve direct contact and association. The addition of ribosome particles results in the coating of bacterial surfaces with a film of contiguous particles, effectively altering their surface properties and surface-mediated interactions with the marine microenvironment. Variations in the adsorption process can influence bacterial sequestration of organic colloids and in turn influence bacterial behaviors in particle-enriched microenvironments. Bacterial utilization of specific types of organic colloidal particles raises the possibility of potential bacterial adaptive strategies in transforming the particles and DOM distribution on a submicron scale in the marine microenvironment. Different bacterial species can have varying potential for interaction and particle degradation rates and exert influence on the bioavailability of colloidal DOM.

Apparent bacterial consumption for ribosome particles is indicative of the utility of other similarly-sized organic particles as a labile organic source of carbon and nitrogen for bacterial production. The breakdown of colloidal particles is an adaptive strategy with imposed limitations in the advantage and utility of organic colloids for bacterial utilization. Any fragmented particles and organic molecules that remain suspended and unattached may be lost to bacteria due to the transience of the interaction. Bacterial surfaces can function to generate nanoscale hotspots as contiguous films of particles form due to particle attachment at high ambient concentrations of colloidal organic particles. This transformation of organic matter has implications for the residential times of nascent DOM in the surface waters and

its vertical transport in the water column. From the observed utilization of amended ribosomes, it can be hypothesized that different isolates have different potential in processing them, where select members in a bacterial assemblage can derive a disproportionate advantage from influxes of organic colloidal particles. Further investigation is needed to quantify the variability of such utilization and the bacterial respiration and growth efficiency rates with respect to ambient concentrations of specific organic colloids, and the unknown factors that influence these rates.

Overall, the presence of extracellular colloids has many possibilities for influencing individual microbes. In elevated conditions of colloidal concentrations in local microenvironments, 3.3 µg mL^{-1} of ribosomes (~10^{12} ribosomes mL^{-1}), most marine bacteria in our study were responsive and utilized the colloidal DOM nutrient amendments to increase bacterial abundance. The initial immediate response is in the surface being covered with ribosomal particles, occasionally resulting in the formation of contiguous films, due to the high concentration of particles. This could effectively alter the properties of the surface presented to the external environment and the biochemical activity of the surface proteins, enzymes, and transporters. The presence of cells covered with particle films or saturated with particles has interesting implications for a microbial community response to a sudden influx of colloidal organic particles. Select cells that form surface particle films can function as nutrient hotspots for neighboring bacteria, where indirect or direct contact with particle-coated cells can potentially result in the efficient breakdown and nutrient uptake for contacting cells. Coupled interaction between particle-coated cells and surface-enzyme expressing cells could be a potential mutually beneficial strategy within certain microbial

consortia. Further work is needed to determine the properties of such surface particle films on bacterial surfaces and the influence of their variability on the interactions between bacterial species.

3.4.5 Ecological implications of bacterial particle capture

The ability for an individual heterotrophic bacterium to preferentially capture organic colloidal particle has ecological importance for its fate and survival within a bacterial community. Such bacteria can potentially become a transient nutrient hotspot by hosting discrete aggregates of labile organic colloids directly on their surface to their benefit or expense. The secure attachment of organic colloidal particles forms small clusters and patches of particles, which in excess can smother the surface proteins involved in organic matter degradation and nutrient uptake. A behavior that can develop nanoscale nutrient sources to influence bacterial physiology and behavior has the corresponding risk of inundating the surface with particles and blocking surface biological activity. Bacterial surface adaptions, such as surface corrugations and pits, can potentially modulate particle attachment for cells to take advantage of conditions of elevated organic particles. As potential intermediaries, organic particles can influence bacterial interactions within an assemblage as contact-dependent strategies for nutrient acquisition. A potential niche for particle-aggregating bacteria has the benefit of deriving physiological benefits from the enzymatic activity of neighboring bacteria. As such, directed bacterial surface interactions with organic colloidal particles can promote various bacterial associations and interactions with their microenvironment.

3.5 Conclusion

This study demonstrates that marine bacteria tested have the capacity for direct particle attachment onto their surfaces, as contiguous particle films and discrete nanoscale particle clusters and patches. Longer exposure to elevated ambient colloidal concentrations yields higher frequency and greater size of particle patches as more particles and smaller patches coalesce together. Select cells within bacterial population can promote cell interactions by taking advantage of particle clusters using adaptive features such as surface corrugations and surface pit formation. The presence of these particle patches has implications for the influence of colloidal fraction of DOM on microbe-microbe interactions and microbial community structuring. Furthermore, the discovery of surface pits in marine bacteria suggests the potential involvement of superchannel systems for the degradation and uptake of colloidal organic matter. The biological interactions with specific forms of colloidal organic matter can influence their residence time and lability of organic colloids. Further investigation is needed to determine the influence of various bacterial taxa on the interactions and cycling of colloidal organic matter. Understanding such behaviors can further the understanding of how marine bacterial communities can adapt and respond to discrete influxes of colloidal DOM into marine microenvironments from various phenomena such as in mass cell lysis events.

Chapter 3, in part, has been submitted for publication of the material as it may appear in Patel, N., Guillemette, R., and Azam, F. (2022). Bacterial surface interactions with organic

colloidal particles: nanoscale hotspots of organic matter in the oceanta. The dissertation author was the primary investigator and author of this paper.

3.6 Supplementary Data

Table 3.S1: Marine Isolates

Phylum	Class	Family	Genus	Species	Source
Gammaproteobacteria	Proteobacteria	Vibrionaceae	Vibrio	SWAT-3	Long and Azam, 2001
Gammaproteobacteria	Proteobacteria	Vibrionaceae	Vibrio	cholerae 2740-80	Goldberg and Murphy, 1983
Gammaproteobacteria	Proteobacteria	Pseudoalteromonadaceae	Pseudoalteromonas	Tw7	Bidle and Azam, 2001
Gammaproteobacteria	Proteobacteria	Pseudoalteromonadaceae	Pseudoalteromonas	Tw2	Bidle and Azam, 2001
Gammaproteobacteria	Proteobacteria	Alteromonadaceae	Alteromonas	ALTSIO	Pedler et al., 2014
Bacteroidetes	Flavobacteria	Flavobacteriaceae	Flavobacterium	BBFL7	Long and Azam, 2001

Figure 3.S1: Nonspecific binding of ribosomes to cells and particle films. Fluorescence images show bacterial cells (red: FM 4-64fx) variably covered with ribosome (green: SYBR Green II), when amended to a ribosome concentration of 5×10^9 particles mL^{-1} (before **(A)** and after **(B)** 60s ribosome amendment). AFM error mode images of cells from 0.6-µm-filtrate **(C)** and a marine isolate Alteromonas sp. ALTSIO cell **(D)** are associated with small films or clusters of ribosome particles (dashed regions). Cells were observed after ribosome amendment 3.3 µg mL^{-1} (= 8×10^{11} particles mL^{-1}). **(E)** AFM error mode image showing a cell from natural assemblage with the surface covered by large patches of particles (dashed regions) after amendment and exposure to ribosomes.
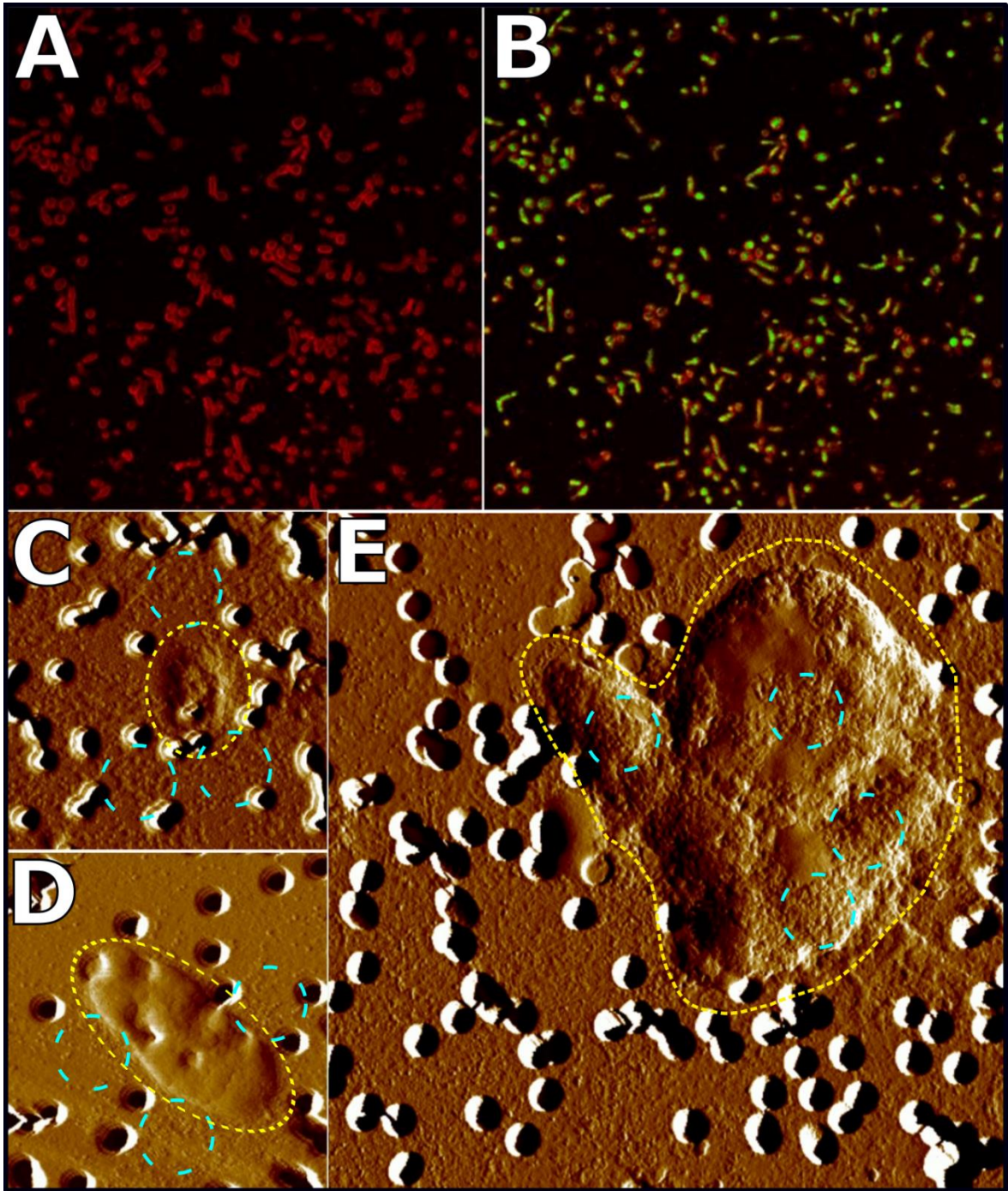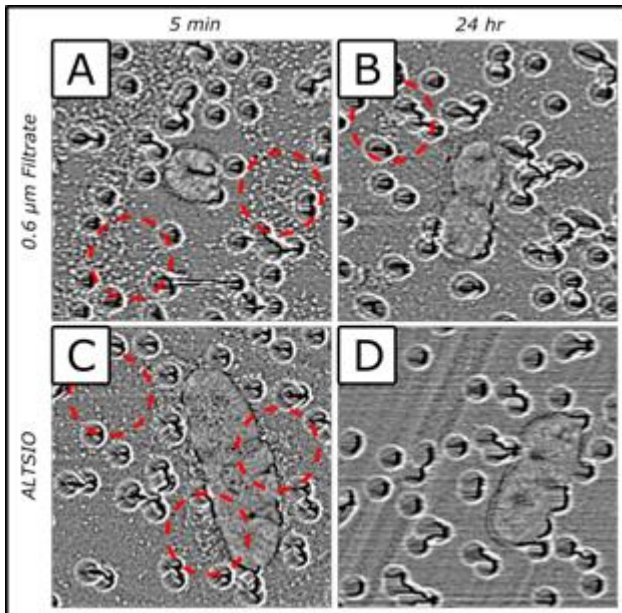
Figure 3.S2: Bacterial depletion of available ribosomes. AFM imaging study of bacterial depletion of added ribosomes. Ribosomes were amendment to bacterial isolate ALTSIO and 0.6 µm filtrate natural assemblages and incubated for 24h. Results show the depletion of ribosomal particles (red dashed regions) for 0.6-µm seawater filtrate cells **(A, B)** and Alteromonas sp. ALTSIO cells **(C, D)**. Mean curvature images processed from topographic data show fewer ribosome particles (white particle features) on the background 0.22-µm polycarbonate filter at 0 h, minutes after amendment, **(A, C)** and after 24 h incubation **(B, D)**.
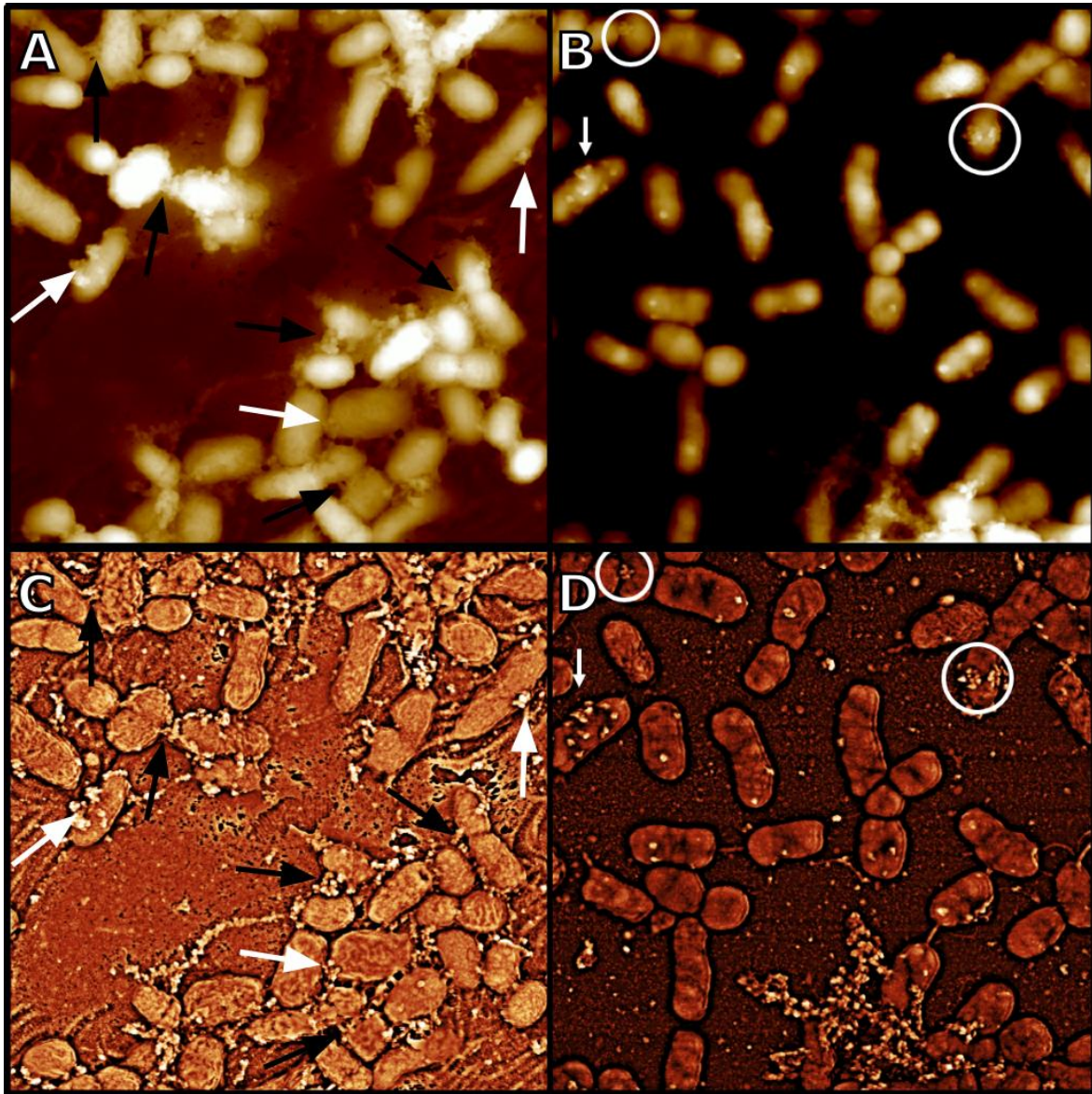
Figure 3.S3: Surface changes from attached ribosomes extended exposure. AFM **(A, B)** and respective SEM-like presentations **(C, D)** of Alteromonas sp. ALTSIO cells. Many cells have substantial surface patches of ribosomes after extended amendment times (4.5 h) to high concentrations. Example surface patches are indicated by white arrows and white circles. In certain regions, surface patches appear to coalesce into larger patches, towards forming a contiguous film of particles that covers a group of cells. Panel image scan sizes are 10 µm × 10 µm.
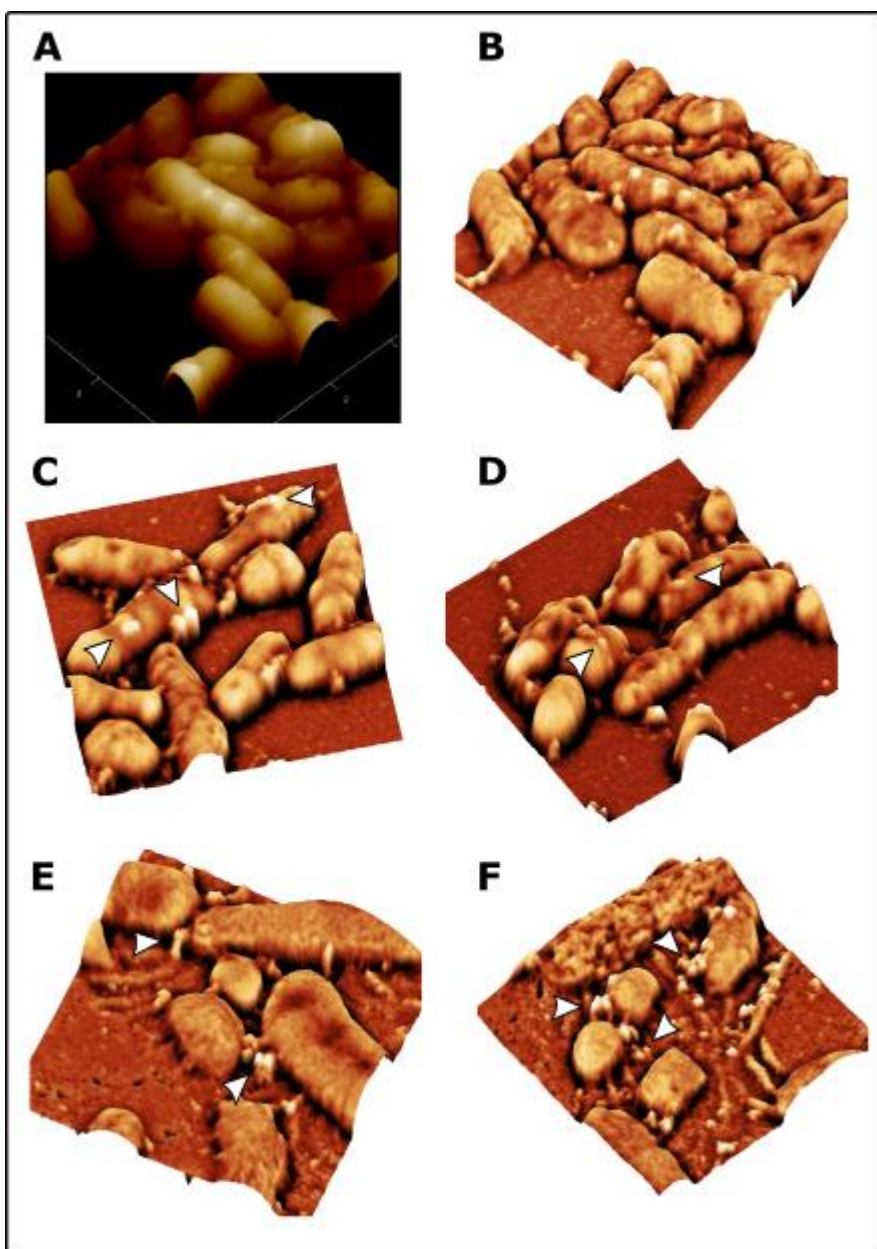
Figure 3.S4: 3D images of surface-attached particle clusters. 3D surface representations of AFM topographic data **(A)** and respective SEM simulated image **(B)** of an Alteromonas sp. ALTSIO cell with multiple surface particle clusters (white protruding features). **(C-F)** SEM-simulated images showing different regions and features of ribosome attachment on bacterial surfaces, where small groups of particles attach directly onto bacterial surfaces **(C,D)** or indirectly to cells **(E,F)**.

3.7 References

Amon, R.M., and Benner, R. (1994). Rapid cycling of high-molecular-weight dissolved organic matter in the ocean. *Nature* 369**,** 549-552.

Becker, S., Scheffel, A., Polz, M.F., and Hehemann, J.-H. (2017). Accurate quantification of laminarin in marine organic matter with enzymes from marine microbes. *Applied and environmental microbiology* 83.

Benner, R., and Amon, R.M. (2015). The size-reactivity continuum of major bioelements in the ocean. *Annual review of marine science* 7**,** 185-205.

Chin, W.-C., Orellana, M.V., and Verdugo, P. (1998). Spontaneous assembly of marine dissolved organic matter into polymer gels. *Nature* 391**,** 568.

Fukuda, H., and Koike, I. (2004). Microbial stimulation of the aggregation process between submicron-sized particles and suspended particles in coastal waters. *Aquatic microbial ecology* 37**,** 63-73.

Guo, L., and Santschi, P.H. (1997). Composition and cycling of colloids in marine environments. *Reviews of Geophysics* 35**,** 17-40.

Hara, S., and Koike, I. (2000). "Dynamics of organic marine aggregates: nanometer-colloids to marine snow," in *Dynamics and Characterization of Marine Organic Matter*. Springer), 277-298.

Hashimoto, W., Kawai, S., and Murata, K. (2010). Bacterial supersystem for alginate import/metabolism and its environmental and bioenergy applications. *Bioengineered bugs* 1**,** 97-109.

Hashimoto, W., Momma, K., Mishima, Y., Mikami, B., and Murata, K. (2001). Super-channel in bacteria: function and structure of a macromolecule import system mediated by a pit-dependent ABC transporter. *Bioscience, biotechnology, and biochemistry* 65**,** 1949-1956.

Hisano, T., Kimura, N., Hashimoto, W., and Murata, K. (1996). Pit structure on bacterial cell surface. *Biochemical and biophysical research communications* 220**,** 979-982.

Hisano, T., Yonemoto, Y., Yamashita, T., Fukuda, Y., Kimura, A., and Murata, K. (1995). Direct uptake of alginate molecules through a pit on the bacterial cell surface: a novel mechanism for the uptake of macromolecules. *Journal of fermentation and bioengineering* 79**,** 538-544.

Isao, K., Hara, S., Terauchi, K., and Kogure, K. (1990). Role of sub-micrometre particles in the ocean. *Nature* 345**,** 242.

Kämäräinen, T., Tardy, B.L., Nikkhah, S.J., Batys, P., Sammalkorpi, M., and Rojas, O.J. (2020). Effect of particle surface corrugation on colloidal interactions. *Journal of Colloid and Interface Science* 579**,** 794-804.

Kepkay, P.E. (1994). Particle aggregation and the biological reactivity of colloids. *Marine Ecology-Progress Series* 109**,** 293-293.

Klein, T.A., Ahmad, S., and Whitney, J.C. (2020). Contact-dependent interbacterial antagonism mediated by protein secretion machines. *Trends in microbiology* 28**,** 387-400.

Kuznetsov, Y.G., Chang, S.-C., Credaroli, A., Martiny, J., and Mcpherson, A. (2012). An atomic force microscopy investigation of cyanophage structure. *Micron* 43**,** 1336-1342.

Kuznetsov, Y.G., Martiny, J.B., and Mcpherson, A. (2010). Structural analysis of a Synechococcus myovirus S-CAM4 and infected cells by atomic force microscopy. *Journal of general virology* 91**,** 3095-3104.

Malfatti, F., and Azam, F. (2009). Atomic force microscopy reveals microscale networks and possible symbioses among pelagic marine bacteria. *Aquatic Microbial Ecology* 58**,** 1-14.

Malfatti, F., Samo, T.J., and Azam, F. (2010). High-resolution imaging of pelagic bacteria by atomic force microscopy and implications for carbon cycling. *The ISME journal* 4**,** 427-439.

Nagata, T., and Kirchman, D. (1996). Bacterial degradation of protein adsorbed to model submicron particles in seawater. *Marine Ecology Progress Series* 132**,** 241-248.

Nagata, T., and Koike, I. (1995). Marine colloids: Their roles in food webs and biogeochemical fluxes. *Biogeochemical processes and ocean flux in the western Pacific***,** 275-292.

Nishino, T., Ikemoto, E., and Kogure, K. (2004). Application of atomic force microscopy to observation of marine bacteria. *Journal of oceanography* 60**,** 219-225.

Pan, J., Fu, X., Wang, C., Song, N., Lv, X., and Xu, H. (2020). Adsorption and molecular weight fractionation of dissolved organic matters with different origins on colloidal surface. *Chemosphere* 261**,** 127774.

Passow, U. (2000). Formation of transparent exopolymer particles, TEP, from dissolved precursor material. *Marine Ecology Progress Series* 192**,** 1-11.

Pletikapić, G., Radić, T.M., Zimmermann, A.H., Svetličić, V., Pfannkuchen, M., Marić, D., Godrijan, J., and Žutić, V. (2011). AFM imaging of extracellular polymer release by marine diatom Cylindrotheca closterium (Ehrenberg) Reiman & JC Lewin. *Journal of molecular recognition* 24**,** 436-445.

Radić, T.M., Svetličić, V., Žutić, V., and Boulgaropoulos, B. (2011). Seawater at the nanoscale: marine gel imaged by atomic force microscopy. *Journal of Molecular Recognition* 24**,** 397-405.

Ramakrishnan, V. (2002). Ribosome structure and the mechanism of translation. *Cell* 108**,** 557-572.

Santschi, P.H. (2018). Marine colloids, agents of the self-cleansing capacity of aquatic systems: historical perspective and new discoveries. *Marine Chemistry* 207**,** 124-135.

Santschi, P.H., Balnois, E., Wilkinson, K.J., Zhang, J., Buffle, J., and Guo, L. (1998). Fibrillar polysaccharides in marine macromolecular organic matter as imaged by atomic force microscopy and transmission electron microscopy. *Limnology and Oceanography* 43**,** 896-908.

Schuster, S., Arrieta, J.M., and Herndl, G.J. (1998). Adsorption of dissolved free amino acids on colloidal DOM enhances colloidal DOM utilization but reduces amino acid uptake by orders of magnitude in marine bacterioplankton. *Marine Ecology Progress Series* 166**,** 99-108.

Schuwirth, B.S., Borovinskaya, M.A., Hau, C.W., Zhang, W., Vila-Sanjurjo, A., Holton, J.M., and Cate, J.H.D. (2005). Structures of the bacterial ribosome at 3.5 Å resolution. *Science* 310**,** 827-834.

Seo, Y., Ikemoto, E., Yoshida, A., and Kogure, K. (2007). Particle capture by marine bacteria. *Aquatic Microbial Ecology* 49**,** 243-253.

Seymour, J.R., Amin, S.A., Raina, J.-B., and Stocker, R. (2017). Zooming in on the phycosphere: the ecological interface for phytoplankton–bacteria relationships. *Nature microbiology* 2**,** 1-12.

Sheik, A., Brussaard, C., Lavik, G., Foster, R., Musat, N., Adam, B., and Kuypers, M. (2013). Viral infection of Phaeocystis globosa impedes release of chitinous star-like structures: quantification using single cell approaches. *Environmental microbiology* 15**,** 1441-1451.

Simon, M., Grossart, H.-P., Schweitzer, B., and Ploug, H. (2002). Microbial ecology of organic aggregates in aquatic ecosystems. *Aquatic microbial ecology* 28**,** 175-211.

Smriga, S., Fernandez, V.I., Mitchell, J.G., and Stocker, R. (2016). Chemotaxis toward phytoplankton drives organic matter partitioning among marine bacteria. *Proceedings of the National Academy of Sciences* 113**,** 1576-1581.

Taylor, G.T. (2019). Windows into microbial seascapes: Advances in nanoscale imaging and application to marine sciences. *Annual review of marine science* 11**,** 465-490.

Thornton, D.C. (2014). Dissolved organic matter (DOM) release by phytoplankton in the contemporary and future ocean. *European Journal of Phycology* 49**,** 20-46.

Tranvik, L.J., Sherr, E., and Sherr, B.F. (1993). Uptake and utilization of'colloidal DOM'by heterotrophic flagellates in seawater. *Marine Ecology Progress Series***,** 301-309.

Unfried, F., Becker, S., Robb, C.S., Hehemann, J.-H., Markert, S., Heiden, S.E., Hinzke, T., Becher, D., Reintjes, G., and Krüger, K. (2018). Adaptive mechanisms that provide competitive advantages to marine bacteroidetes during microalgal blooms. *The ISME journal* 12**,** 2894-2906.

Vissers, T., Brown, A.T., Koumakis, N., Dawson, A., Hermes, M., Schwarz-Linek, J., Schofield, A.B., French, J.M., Koutsos, V., and Arlt, J. (2018). Bacteria as living patchy colloids: Phenotypic heterogeneity in surface adhesion. *Science Advances* 4**,** eaao1170.

Wells, M.L., and Goldberg, E.D. (1991). Occurrence of small colloids in sea water. *Nature* 353**,** 342.

Wells, M.L., and Goldberg, E.D. (1993). Colloid aggregation in seawater. *Marine Chemistry* 41**,** 353-358.

Wilkinson, K.J., Balnois, E., Leppard, G.G., and Buffle, J. (1999). Characteristic features of the major components of freshwater colloidal organic matter revealed by transmission electron and atomic force microscopy. *Colloids and Surfaces A: Physicochemical and Engineering Aspects* 155**,** 287-310.

Yamada, Y., Tomaru, Y., Fukuda, H., and Nagata, T. (2018). Aggregate formation during the viral lysis of a marine diatom. *Frontiers in Marine Science* 5**,** 167.

Zhang, Y., Zhang, F., Yang, J., and Jiao, N. (2012). Host responses of a marine bacterium, Roseobacter denitrificans OCh114, to phage infection. *Archives of microbiology* 194**,** 323-330.

Zhao, Z., Gonsior, M., Schmitt-Kopplin, P., Zhan, Y., Zhang, R., Jiao, N., and Chen, F. (2019). Microbial transformation of virus-induced dissolved organic matter from picocyanobacteria: coupling of bacterial diversity and DOM chemodiversity. *The ISME journal* 13**,** 2551-2565.

Zhong, K.X., Wirth, J.F., Chan, A.M., and Suttle, C.A. (2021). Extracellular ribosomal RNA provides a window into taxon-specific microbial lysis. *bioRxiv*.

Chapter 4 AFM curvature radius analysis for detection and enumeration of surface-attached particles on marine bacteria

4.1 Abstract

Particle attachment of extracellular organic matter to marine bacterial surfaces is a significant process in the biogeochemical cycling of organic matter through the microbial loop. We applied curvature radius analysis to AFM image data to determine particulate features on marine bacterial surfaces. Curvature radius analysis transformation of bacterial cell topography to curvature measures describing the local curvature radius are useful in distinguishing sharp features of exogenous particle from the general bacterial surface, without time-consuming manual curation and independent of operator bias. We applied this approach in a time-lapse AFM investigation of marine bacteria *Alteromonas* sp. ALTSIO cells exposed to *E. coli* ribosomes in injected filtered autoclaved seawater media to observed particle attachment. Cells were initially imaged in a ribosome-free media for 90 minutes for reference images. After 90 minutes, imaging fluid media with added ribosomes (conc. of 8×10^{11} particles mL^{-1}) was introduced while scanning, with ribosome counts on cell surfaces correspondingly increasing over a period of 20–30 minutes. Cells presented an average increase of 6.0 ribosomes (range: 3.4–9.0) on their surfaces, with cells showing a marked response when imaged after ribosome exposure in circulating imaging medium. No marked response was observed for individual or averaged surface roughness of bacteria in response to ribosome exposure. Curvature radius analysis may be a useful approach for monitoring

bacterial surface response to particle attachment in quantitative comparisons of particle interactions with colloid particles.

4.2 Introduction

Aggregate marine bacterial activity is a predominant force influencing the biogeochemical cycling of carbon, wherein individual cells transform organic carbon in the ambient microenvironment through surface protein and enzyme expression and physical interactions. Individual marine bacteria exist in environments with nutrient availability constraints, where individual metabolite concentrations are low (ranging from picomolar to nanomolar levels), often presenting challenges in meeting physiological demand (Azam and Malfatti, 2007). Bacterial demand for organic matter is satisfied in part through directed degradation of larger particulate organic matter, where marine bacteria colonize particles and hydrolyze them into more readily utilizable nutrients (Nagata and Kirchman, 1996). On the other end of the size spectrum, small organic colloids outnumber bacteria 100-1000 times in abundance are a significantly large pool of concentrated packets of organic matter. Submicron-sized organic colloids, smaller than 120 nm in size, are present in the marine microenvironment at concentrations approximately 10^8–10^9 mL^{-1}, and replenished from biogenic sources, such as cell death and lysis events, and from the fragmentation or larger organic particles (Wells and Goldberg, 1991;1993;Nagata and Koike, 1995). Particularly, in phycospheres and detritospheres around phytoplankton cells and detritus, the concentration of organic colloidal particles is elevated in these enriched dissolved organic matter (DOM) zones and can stimulate bacterial activity and production (Smriga et al., 2016;Seymour et

al., 2017). Adaptive strategies in capturing and digesting organic colloids directly at the bacterial surface have significant implications for nanoscale nutrient hotspot formation and coupled uptake of nutrients derived from nutrient degradation (Simon et al., 2002;Fukuda and Koike, 2004).

Understanding the mechanisms and coupling of colloidal particle degradation and bacterial productivity can offer insight into how members of bacterial communities respond to discrete influxes of colloidal DOM. The bulk of previous research on bacterial degradation of organic particles has been performed on bacteria-sized particles or larger (greater than 1 μm), investigating cell colonization onto surfaces of large organic and marine snow particles and evolution of bacterial community composition (Tranvik et al., 1993;Yamada et al., 2018;Zhao et al., 2019). There is a paucity of information on the degradation and cycling of smaller nanoparticulate organic colloids, with smaller-sized particle attaching onto bacterial surfaces, including quantitative data for interaction rates between specific organic colloids and bacterial surfaces. Experimental data and observations are lacking for interactions of marine bacteria with submicron-sized environmental colloidal particles, including interactions with potentially ubiquitous organic colloids of proteins and other cellular components released from lysis events and biogenic sources. Different patterns in particle attachment and turnover rates for different organic colloids-bacterial combinations could offer insight into how specific marine bacterial isolates contribute to and exert influence upon the cycling of exogenous colloidal organic matter degradation and incorporation (Becker et al., 2017). The diversity of submicron-sized organic colloids presents a significant challenge for an individual bacterium in the handling of colloids of varying chemical

148

compositions in a dynamic microenvironment. One relatively unexplored area of investigation is in how attachment, accumulation, and breakdown rates of organic colloidal particles vary among bacterial species within assemblages under various conditions and influences from labile or refractory DOM reservoirs.

Diversity in the chemical composition raises many technical challenges in investigating the interactions between marine bacterial surfaces with submicron-sized environmental organic colloids. Conventional observation using fluorescence microscopy are not conducive to investigating interactions below 240 nm in spatial resolution, wherein such methods are limited in determining the spatial localization and size distribution of smaller cell-associated organic colloids. In addition, fluorescence-based methods require fluorescent stains and labels to target specific colloids, limiting studies to predetermined class of targeted organic colloids, which may fail to capture observations and dynamics of colloids enriched with refractory organic matter. Super-resolution fluorescence microscopy and electron microscopy techniques can potentially overcome resolution limitations but require significant considerations in sample preparation that may prevent live-cell imaging to study dynamic surface changes to exogenous colloid exposure. Sample preparation involving fixation or drying induce artefacts in observation of colloidal adsorption to surfaces. Atomic force microscopy (AFM) is a microscopy technique that can potentially overcome such limitations and image live bacterial surfaces in near in situ conditions with nanoscale resolution without necessitating the use of specific labeling of organic colloids. The operating principle in AFM involves an ultrasharp tip on the end of a microcantilever raster scanning across a sample surface, where physical forces between the scanning tip and

the sample surface are monitored by the cantilever deflection (Quate, 1994). A topographic image is produced from the height adjustments in maintaining a set contact force using feedback control for piezoactuated error correction. AFM capabilities of nanoscale imaging and force-sensitivity have been   applied for investigating the properties and dynamics of bacterial structures (Liu and Wang, 2010;Dufrêne et al., 2021). High-resolution imaging of bacterial cells has elucidated the dynamics and mechanical properties of the bacterial cell envelope in response to external stimuli (Viljoen et al., 2020). Dynamic real-time changes of bacterial surfaces in aqueous environments have been investigated in applications of high-speed AFM to characterize antimicrobial peptide responses in E. coli cells (Fantner et al., 2010). Marine bacteria have been observed to capture and retain submicron particles, where the surface can function as reservoir of nutrient resources within fluctuating microenvironments (Seo et al., 2007).

AFM visualization of the bacterial surface responses to exogeneous organic colloid exposure has the advantage of observing the dynamic changes with nanometer resolution, which can offer a unique, quantitative perspective to study bacterial behavior. Adsorbed particles on the bacterial surface extend from the local background regions in surface profiles, allowing for visualization of particles native to the surface, purely based upon physical interactions. The direct method of height-differential particle classification faces considerable limitations when attempting to determine individual particles on rough surfaces, where the local surface variation is comparable to or exceeds particle sizes over longer spatial scales (Klapetek et al., 2011). For example, adsorbed particles on bacterial surfaces can overlooked due to the background surface topography, partially undulations,

yielding limited results for image processing with height thresholding. Manual annotation of surface-attached particles can be a time-intensive process and is influenced by factors such as overabundant particle attachment and overcrowding, or misclassification due to operator bias. A curvature radius analysis approach can delineate particles from background cell surfaces by solely using topography data, independent of operator classification or manually curated data visualization (Mazeran et al., 2005). Surface curvature defined by the changes in slope of the local topography can be applied to quantitatively differentiate sharper particle-like features (high curvature) from flatter substrate regions (low curvature). The most common measures of surface curvature are mean curvature (A, units: m-1) and Gaussian curvature (G, units: m-2). Curvature radius, as a reciprocal measure, specifies the radius of the best fit sphere for the local surface region around a given point, and offers an intuitive comparison to an idealized spherical particle. In AFM topographic images, detected particles present as convex features on background surface with negative mean curvature (A < 0) and positive gaussian curvature (G > 0). Curvature analysis has applications in identifying individual adsorbed nanoparticles on cell surfaces from the reconstruction of the nanoparticle profile (Kim et al., 2007;Oikawa et al., 2007). Additionally, Gaussian curvature is incorporated in select automated AFM image analysis algorithms to designate boundaries for protein particle analysis (Marsh et al., 2018).

Curvature radius analysis was directly applied to AFM investigations of physical interactions between marine bacterial isolates and organic colloidal particles using E. coli ribosomes as model particles. We observed variability in the levels of particles detected on individual cells within a group of cells. After exposure to higher levels of suspended

ribosome particles, the number of detected particles increased from an initial steady-state level. We also observed that in live cells in a medium devoid of additional colloidal particles, cell surfaces are dynamic and particle-like feature may emerge and remain on the bacterial surface. Curvature radius analysis can be potentially generalized and integrated into automated data analysis workflows to quantify colloidal particle attachment on bacterial surfaces in limited applications.

4.3 Materials and Methods

4.3.1 AFM data collection

AFM images were collected in Peak Force TappingTM mode using a Dimension FastScan AFM (Bruker, Santa Barbara, US). Fixed samples of SWAT-3, TW7 and seawater assemblage cells were imaged in air using Scan-Asyst Air AFM tips (ksp: 0.4 N/m, Rnom: 2 nm). Briefly fixed cells were deposited onto polylysine-coated glass coverslips. Cells were rinsed with HPLC water and air-dried prior to imaging. Images were acquired at 512x512 or 1024x1024 pixel resolution at a scan rate of 2 Hz.

Live cell samples of Alteromonas sp. ALTSIO cells were imaged in 0.02 µm FASW using Scan-Asyst Fluid AFM tips (ksp: 0.7 N/m, Rnom: 20 nm). Overnight cultures of cells were diluted into fresh Zobell liquid media and grown to mid-exponential phase. 1 mL of cell culture was centrifuged at 3000 g for 10 minutes and washed twice with 1 mL of 0.2-µm filtered autoclaved seawater. 400 µL of the cell suspension was deposited onto a polylysine-coated mica surface. After 30 minutes, the fluid was exchanged for 0.02 µm syringe filtered autoclaved seawater medium. The imaging medium was circulated using two

syringe pumps (Harvard Apparatus) in withdrawal and infusion modes to continuously exchange fresh 0.02-µm Anodisc syringe-filtered FASW with and without amendment with *E. coli* ribosomes (conc. approx. 3.3 µg mL^{-1} (~8×10^{11} particles mL^{-1})) at a rate of 10 µL min^{-1}. Images were acquired in quantitative nanomechanical mapping mode at 256x1024 pixel resolution at a scan rate of 1 Hz.

4.3.2 Image data analysis workflow

Image analysis of time-lapse AFM datasets was processed using custom MATLAB scripts. Initial image preprocessing was performed on the raw data by applying line-flattening operations and gaussian low-pass filters. The frames from the image sequences were aligned by cross-correlating individual frames using a local feature from an arbitrary reference frame. Here we used one half of a cell in the middle of the image sequence as a reference feature to calculate the drift between successive frames and image alignment. Individual cells were demarcated using the average of the aligned images, after image smoothing and thresholding.

After image alignment, individual frames were smoothed with a gaussian filter and then were processed to calculate curvature maps to estimate the mean and gaussian curvature of the surface topography. Curvature analysis from the atomic force micrograph data was performed as previously reported (Mazeran et al., 2005). The mean and gaussian curvatures of the surface described by function $z = f(x, y)$ were estimated by using the following equations:

$$A = \frac{1}{2}\left(\frac{1}{R_1} + \frac{1}{R_2}\right) = \frac{z_x''\left(1 + z_y'^2\right) + z_y''(1 + z_x'^2) - 2z_y'z_x'z_{xy}''}{2H^3}$$

$$G = \frac{1}{R_1 R_2} = \frac{z_x'' z_y'' - z_{xy}'^2}{H^4}$$

where R1 and R2 are principal radii of curvature, and

$$H = \sqrt{1 + z_x'^2 + z_y'^2}$$

Individual particles on the microbial surface were identified by a curvature thresholding procedure as follows. The mean and gaussian curvature maps were individually scaled and normalized to curvatures corresponding to a radius of 100 nm. A continuous wavelet transformation using a Mexican hat wavelet was applied to the sum of the two scaled curvature maps with resolution scales corresponding to 1.5, 2.25, 3.38, 5.06, and 7.59 pixels, which correspond to 4.83, 7.25, 10.89, 16.31, and 24.46 nm, with the variances of the 2-D wavelet adjusted to compensate for the unequal sampling rates in the slow and fast scanning axes (pixel resolution: 3.22 nm (horizontal) and 12.89 (vertical). A threshold was applied through trial to the output of the wavelet transform to designate individual particle grains from convex curvature pixels.

Particle grains were filtered to exclude particles outside of the expected physical size range that do not correspond to individual ribosome particles. Predetermined thresholds corresponding to a radius of curvature of 24 nm and 40 nm were applied to peak curvature values in particle grains to monitor surface-attached particles over time. Cell regions were determined independently by manually demarcating cell boundaries to generate masks. The combination of thresholded particle grains and cell masks were used to enumerate the number of particles on individual cell regions and the fraction of projected cell area covered by attached particles.

4.4 Results and Discussion

4.4.1 Particle curvature detection on microbial surfaces

AFM observations of cells from natural marine assemblages show individual cells have variations in fine nanoscale features in surface topography, as shown in Figure 4.1. Surface features such as corrugations and ridge networks in general contribute to increased surface roughness on undulating cell surfaces. Sharp particle-like features on bacterial cells are observed with greater contrast and differentiation in data maps of mean and gaussian curvature in the entirety image compared to AFM height images, as shown in demarcated regions in Figure 4.1. The respective calculated surface curvature data maps enhance the contrast of topographic features approximately 10–20 nm in size, which correspond to mean curvature of -0.01 nm^{-1} or lower and Gaussian curvature of 10^{-4} nm^{-2} or greater. These minuscule features on the cell surfaces corresponding to individual clumped surface regions or attached particles are visualized with greater contrast from the surrounding cell-surface regions within larger image areas. Such features are obfuscated in height images due to data scaling to account for greater surface height variations at larger features over longer spatial scales.

Particle detection from thresholding curvature radius can be sufficiently achieved using mean curvature for visual inspection compared to Gaussian curvature, as observed in the contrast of particle features in the respective images. This approach offers an intuitive relation between the measured curvature of a surface feature to comparable spherical particle with equivalent curvature radius, characterizing the size and sharpness of features to a corresponding physical radius. Analysis of particle-attachment can be used to test hypothesis

regarding bacterial surface-particle interaction and distribution with various types of environmental colloidal particles. Curvature analysis has potential applications for investigating particle attachment to bacterial surfaces for biofouling, specific attachment, and particle capture for nutrient acquisition within natural assemblages (Hayden et al., 2012;Mei et al., 2013).
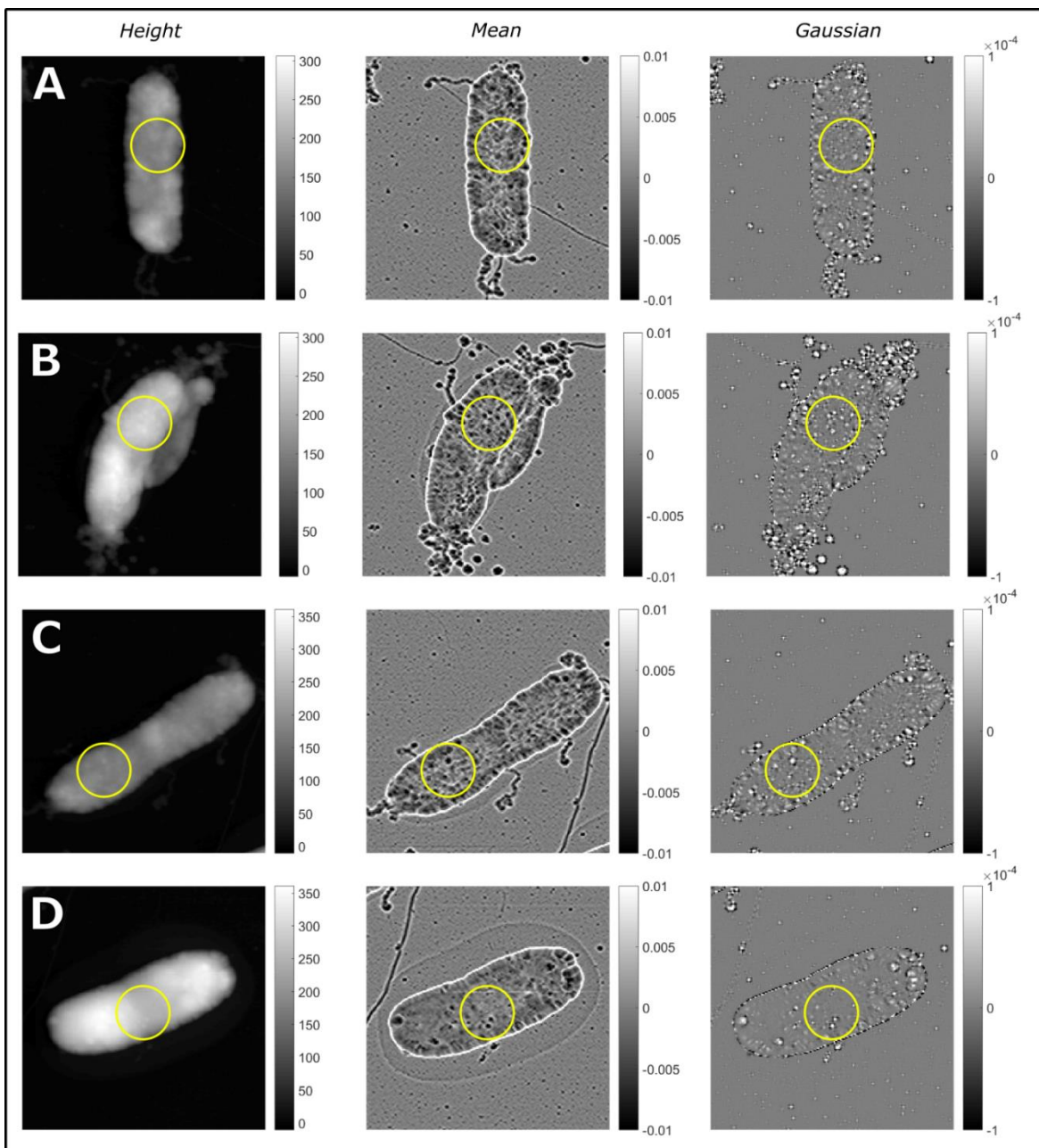
Figure 4.1: Curvature maps show particle-like features on marine bacterial surfaces. Atomic force micrograph height images (left column: **A-D**) of marine bacterial cells from natural seawater assemblage and respective mean curvature (center column) and gaussian curvature data maps (right column). Curvature maps show surface features on cell surfaces that correspond to attached particles and particle-sized structures (select features shown in yellow circled regions) (approximately 10-20 nm in size) that populate the surface with better contrast compared to height data. (Image scan sizes: 1.87×1.87 µm; units for curvature maps: nm^{-1} (mean) and nm^{-2} (Gaussian)).

4.4.2 Quantitative detection particles

Particle detection in AFM topographic images typically relies on relative height differences with a background substrate reference, which can pose significant challenges for analysis on rough surfaces (Klapetek et al., 2011). Individual particles are determined and characterized according to a minimum or Laplacian basis for an approximated background surface, often failing on bacterial surfaces. Automated analysis of particle features is desirable due to the time-consuming nature of manual classification and associated operator bias (Barrera et al., 2008). However, such analysis is hindered by non-deal background surfaces and surface data drift which are common in biological AFM imaging of live bacteria. Alternatively, a curvature radius-based approach offers an objective means for classification based on the physical similarity of features to ideal spherical particles using the local surface geometry. Curvature-reconstruction methods have been used for characterizing particles on cell surfaces and involve curve fitting high-fidelity particle profile data to determine particle curvature radius (Oikawa et al., 2007). These analyses require ultrasharp AFM probes that minimize tip convolution effects to discriminate particles based on their size (Kim et al., 2007). However, AFM image surveys of uncharacterized environmental samples of marine polymers, particles, and bacteria may fail to attain the requisite spatial resolution to employ these reconstruction methods. Furthermore, AFM tip fouling from various organic material may influence sample analysis. Alternatively, this application of curvature radius analysis can offer meaningful discrimination of surface-attached particles with less accuracy for qualified image analysis and comparisons. Surface profiles of exogenous particles are assumed to present greater

surface curvature compared to regions of bacterial surfaces and native embedded surface features. In regions with limited particle deposition, the differences in the magnitudes of average curvature radius distinctly separates individual particles from background regions. Generally, the surface curvature of bacterial cell surfaces is lower than that of organic colloidal particles, and correspondingly, the curvature radius is higher for bacteria.

There are limitations in differentiating individual exogenous particle attachment from finer surface features on bacterial surfaces from the formation of wrinkles, blebs, and clumped aggregates. Curvature radius-based particle detection can reveal the small deviations in surface height, presenting as changes in local surface curvature, as regions become flatter or form sharper protrusions and similar features. Such regional surface changes may arise from adsorption of high molecular weight DOM polymers for degradation and uptake (Reintjes et al., 2017). When applied to imaging marine bacteria in natural assemblages, individual bacterial cells present varying quantities of surface-attached particles, suggestive of intimate associations with colloidal particles that may influence cell physiology (Seo et al., 2007). Characterization of surface-attached particles in natural assemblages using image surveys may be limited due to the variability of attached particles. Dynamic changes in bacterial surfaces assessed from time-lapse AFM imaging may offer a more accurate measure of in situ rates of attachment and surface degradation of particles.

The primarily limitation of this approach is the collection of high-fidelity AFM data for the estimation of surface curvature and curvature radius. The analysis requires topographic data with high fidelity acquisition and high spatial resolution to adequately sample of particles of interest. Engineered substrates address limitations in biological AFM

imaging by involving reference features as fiducial markers to account for tip-fouling and resulting imaging artefacts and cell immobilization traps to resist tip-induced deformation and dislocation of surface-adherent bacteria (Fuentes-Perez et al., 2013;Peric et al., 2017). In addition to common limitations with biological AFM, curvature radius analysis is limited to regions with low surface concentrations, during initial particle adsorption where individual particles are distinguishable without blurring together into larger aggregate features.

Tip convolution during surface scanning has a broadening effect on detected particle features and attenuates the curvature of individual features, limiting the minimum measured curvature radius to tip radius (Winzer et al., 2012;Canet-Ferrer et al., 2014). The surface profile of sharper features, with curvature greater than the AFM tip, will be smoothed and broadened in the imaging, potentially obscuring the features within undulations of the background surface. Commercial AFM tips have radii ranging from 2–10 nm, which are suitable to detect submicron-sized marine organic colloids between 10–120 nm in size and investigate their physical interaction with bacterial surfaces.

One challenge in biological AFM imaging is the adsorption of organic material onto the AFM tip, which changes the tip morphology and effective tip radius and introduce artefacts in measured surface profiles (Allen et al., 1992). The size measurements of surface-attached particles and other similar features are influenced by the tip convolution effect, which may be challenging to compensate by deconvolution methods due to tip shape changes from biofouling. In the imaging of marine bacteria, weakly-attached organic matter can foul the AFM tip and introduce inaccuracies due to drift and tip-dragging between image scans,

which may be addressed using fiducial markers for tip profile and surface curvature references. Additionally, such reference features can compensate for intraframe variability due to transient tip contamination events, where near identical features present differences at various stages of an image scan. Bacteria supporting substrates may also prevent distortion of surface-attached particles by reducing the deformation of the background cell surface from tip-induced shear forces. Accounting for such limitations, curvature radius-based detection of particles can be readily integrated into automated image data processing and analysis workflows to determine constrained estimates of particle attachment.

The enumeration of surface-attached particles on bacterial surface provides a quantitative approach to characterize marine bacterial interactions with organic colloidal particles and attachment. An AFM-based approach is independent of labeling requirements for organic colloids and can enable the visualization of physical interactions of natural assemblages in near physiological conditions. Physical imaging characterizes the general physical interactions between marine colloids and bacterial surfaces, in determining initial rates of individual particle attachment to bacterial surfaces. This approach can be applied to visualize and investigate nanoscale interactions of heterotrophic bacteria scavenging extracellular organic colloid particles within enriched DOM hotspots.

4.4.3 Attenuated curvature of surface features

Curvature radius analysis of surface-attached particles and features is influenced by background topography attenuating the measured surface curvature. In AFM images of marine bacterial isolate Pseudoalteromonas sp. TW7 cells on a glass coverslip, as an

example, image data of a bacterial flagella deposited on cell shows measurably lower mean and Gaussian curvature for the flagellar section on the surface, as shown in Figure 4.2. AFM height and error images and calculated mean and Gaussian curvature maps are shown with respective line profiles of surface height, flagellar cross-sectional height, mean curvature, and radius of curvature, along the length of the bacterial flagella. The average cross-sectional heights of flagellar segments on the background glass substrate are approximately 10 nm, compared to the segment on top of the cell, which has an average approximate height of 5.8 nm. The average mean curvature of background flagellar segments is approximately -0.004 nm^{-1} compared to a curvature of -0.002 nm^{-1} for the flagellar segment on the bacterial surface, with corresponding radii of curvature are approximately 250 nm and 500 nm respectively.

A similar effect of attenuated curvature was observed in the AFM imaging of ribosomal particles deposited onto fixed, dried surfaces of marine bacterial isolate Vibrio sp. SWAT-3 cells, as shown in Figure 4.S2. The measured particle height and mean and Gaussian curvatures were influenced by image scan size and if they were present on the bacterial surface. Images of ribosomes particles deposited onto fixed cells were collected and analyzed for two scan sizes, 2.2 µm and 6.6 µm, and background and surface-attached ribosome particles were compared to reference ribosome AFM image collected at 2.0 µm scan size. The average heights of background ribosome particles were consistent and showed a decreased height for surface-associated ribosomes (2.2-µm image (background): 10.24 ± 0.07 nm (n=917); 2.2-µm image (surface-associated): 5.36 ± 0.37 nm (n=104); 6.6-µm image(background): 11.32 ± 0.04 nm (n=998); and 2.0-µm reference image: 11.47 ± 0.12

nm (n=351). The average mean curvature of background ribosome particles was decreased at a larger scan size consistent and for surface-associated ribosomes (2.2-µm image (background): -0.0675 ± 0.0004 nm^{-1}; 2.2-µm image (surface-associated): -0.0451 ± 0.0012 nm^{-1}; 6.6-µm image (background): -0.0021 ± 0.0001 nm^{-1}; and 2.0-µm reference image: -0.0714 ± 0.0010 nm^{-1}). The average Gaussian curvature of background ribosome particles was decreased at a larger scan size consistent and for surface-associated ribosomes (2.2-µm image (background): 4.43 ± 0.05 × 10^{-3} nm^{-2}; 2.2-µm image (surface-associated): 1.78 ± 0.09 × 10^{-3} nm^{-2}; 6.6-µm image (background): 3.92 ± 0.04 × 10^{-4} nm^{-2}; and 2.0-µm reference image: 5.00 ± 0.14 × 10^{-3} nm^{-2}). The measured peak curvature properties for ribosome particles decrease with increasing image scan size and decrease on cell surfaces. These influences can affect subsequent curvature radius analysis and thresholding parameters in feature detection.

Figure 4.2: Decreased peak curvature for features on cell surfaces. Marine bacteria *Pseudoalteromonas* sp. TW7 cells deposited upon a glass coverslip, with a bacterial flagellum deposited across a cell surface. (**A**: AFM height image, **B**: Error mode image, **E** Mean curvature map, **F**: Gaussian curvature map). Segments of the flagellum are designated by the red line **(A)** and the corresponding profiles for surface height **(C)**, cross-sectional height **(D)**, mean curvature **(G)** and radius of curvature **(H)** are shown. The flagellum segment on the microbial surface has diminished cross-sectional height and curvature, compared to counterpart segments on the background glass surface. (**(A,B,E,F)** Image scan sizes: 2.6 x 2.6 µm; units for images: **A**: nm, **B**: V, **E**: nm^{-1} and **F**: nm^{-2}).
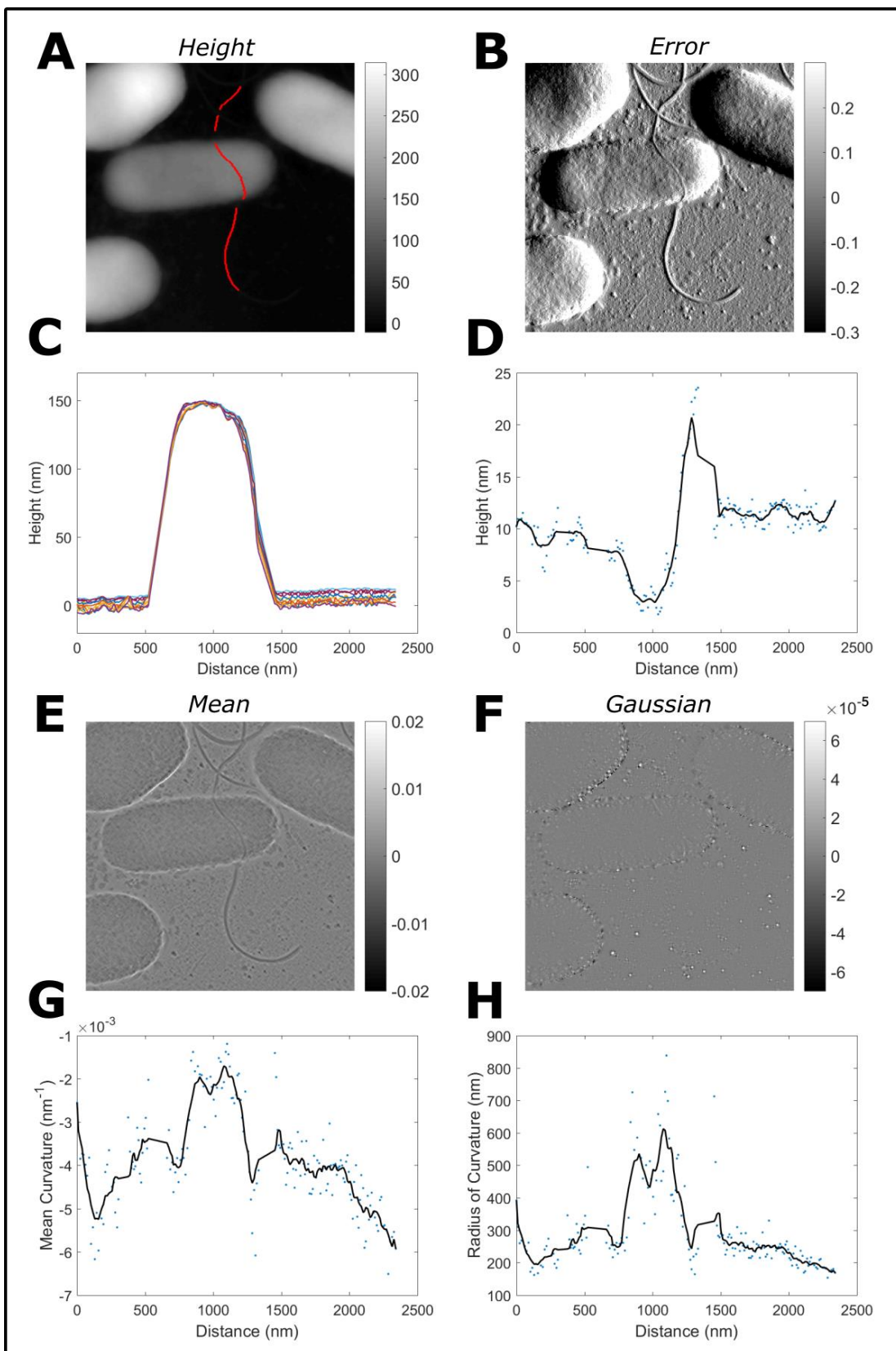
4.4.5 Curvature limitation on microbial surface

The example analyses of deposited ribosome particles and flagella on bacterial surfaces indicate a degree of complexity in the physical interactions between colloidal organic material and bacteria. The differences in measured size and curvature of particles on bacterial surfaces are likely due to suboptimal sampling frequency during AFM scanning, background deformation around the attached features, physical distortion of organic particles or a combination of these factors. The reduction in particle height and curvature may be influenced to a lesser degree by the surface forces distorting particle shape. Combined with the tip convolution of surface profile, these modifications to the measured particle topography limits the utility of curvature-thresholding detection and analysis of particles. The sampling frequency of the AFM is a key factor in surface reconstruction, and subsequent curvature measurements and appropriate thresholds for particle detection. As shown in the example, a 20-nm sized ribosome will not present the corresponding curvature beyond a certain image scale due to sampling resolution limitations and potential distorting effects on bacterial surfaces under certain experimental conditions. These observations suggest that curvature analysis has limited application in post-hoc analysis of topographic data and quantitative comparisons between independent AFM datasets regarding particle and feature detection on bacterial surfaces.

4.4.6 Time-lapse analysis of AFM datasets to enumerate particle attachment

A useful application of curvature-based thresholding is for the detection of exogenous particle features to monitor surface attachment of discrete organic colloidal

particles on the dynamic bacterial surfaces. The detection of sharp features on the bacterial surface is not severely restricted due to attenuated curvature and can incorporate surface feature detection from frame-to-frame changes. Curvature-based particle detection is ideally suited for time-lapse imaging and analysis of the bacterial surface responses to exposure to exogenous organic colloidal particles and its dynamics. In a time-lapse AFM experiment, marine bacteria Alteromonas sp. ALTSIO cells were exposed to an extracellular ribosome concentration of 8×10^{11} particles mL^{-1} in the ambient microenvironment. Imaging of live cells was performed in a 0.02-µm syringe-filtered autoclaved seawater medium initially showed a steady averaged level of surface attached particles. After approximately 90 minutes, the imaging medium was replaced with a seawater medium amended with E. coli ribosomes, the number of surface-attached particles increased after lag period in which particles were delivered to the vicinity of cell and increased steadily over a period of 20-30 minutes.

In image data, surface-attached ribosomes and particles were designated on bacteria from particle grains identified as convex surface features with a peak curvature radius threshold, as described in the methods section. Representative frames from AFM imagery are shown for ribosomes-exposed ALTSIO cells (Figure 4.S3) and a control cell (Figure 4.S4) with respective timestamps. The number of surface particles and cell-coverage fraction of projected cell surface area covered by particles from the time-lapse experiments are summarily plotted in Figure 4.3. Particle analysis with a curvature radius threshold of 24 nm shows a marked increase in surface-attached particles after ribosome amendment, with an average change of 6.0 attached ribosomes (range: 3.4–9.0). When a higher threshold of 40

nm was applied, the number of detected surface particles increases overall and an average change of 13.6 ribosomes was observed (range: 8.5–16.6). The individual cell response increased at a slower rate, with varying response, where relative changes appear independent to ribosome amendment. The average number of particles and cell-coverage fraction from consecutive frames before and after ribosome amendment is summarized for individual cells in Table 4.1 (n_{pre} = 15; n_{post} = 11). Compared to the control cell response with no ribosomes, cells exposed to ribosomes have increased quantities of surface attached particles after the addition of suspended ribosomes. 4 of the 6 cells show a marked increases in the quantity of surface particles over time and the remaining 2 show a slight increase.
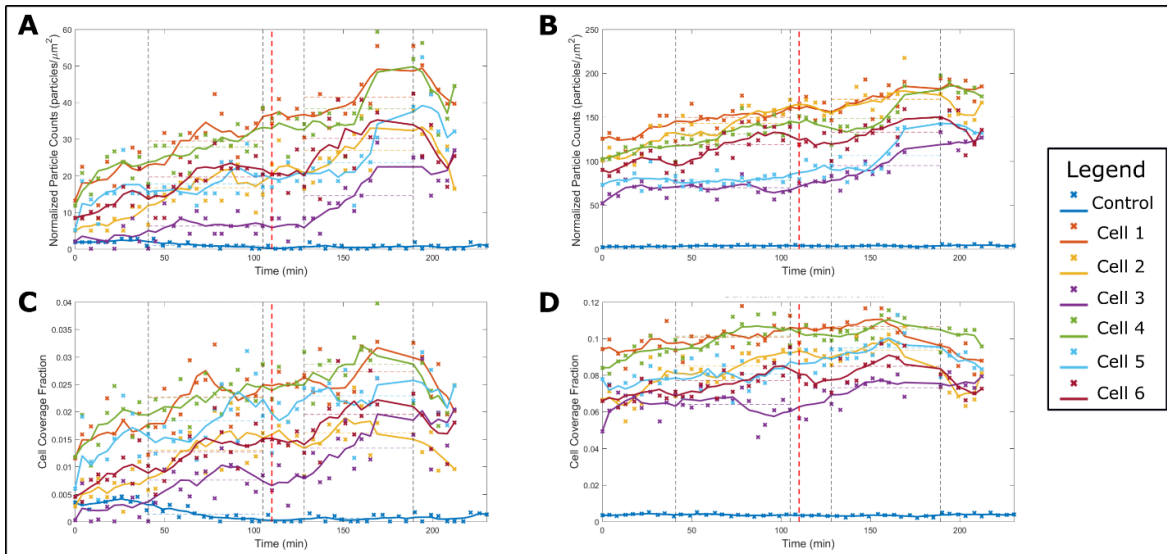
Figure 4.3: Particle counts and cell-coverage on bacteria increase after ribosome amendment in circulating imaging medium. Marine bacteria *Alteromonas* sp. ALTSIO cells were imaged in circulating 0.02-µm syringe-filtered FASW medium, with and without ribosome particles suspended in media (shown in Figures S3 and S4). Particle counts **(A,B)** and cell-coverage fraction **(C,D)** of projected bacterial surface covered by particles are shown in for two levels of curvature thresholding, corresponding to curvature radii of 24 nm **(A,C)** and 40 nm **(B,D)**. After ribosomes addition (vertical red line), cells have increasing number of particulate features. (Black vertical lines show time periods analyzed for comparison before and after ribosome amendment).

Table 4.1: Summary particle counts and cell-coverage fraction for individual cells before and after ribosome amendment

Particle counts

	24 nm threshold			40 nm threshold		
	Before	*After*	Δ	*Before*	*After*	Δ
Control	0.4 ± 0.6	0.7 ± 0.8	0.3	3.7 ± 0.8	4.3 ± 1.6	0.5
Cell 1	22.3 ± 6.0	31.4 ± 6.1	9.0	113.4 ± 9.5	129.7 ± 13.3	16.3
Cell 2	10.1 ± 3.8	16.4 ± 4.7	6.2	86.7 ± 11.8	103.2 ± 12.9	16.4
Cell 3	3.0 ± 1.6	7.0 ± 3.6	4.0	33.5 ± 3.7	45.7 ± 9.1	12.2
Cell 4	18.8 ± 3.6	25.8 ± 6.4	7.0	88.3 ± 10.0	100.1 ± 15.8	11.8
Cell 5	10.5 ± 2.6	13.9 ± 4.1	3.4	46.3 ± 3.5	62.8 ± 13.5	16.6
Cell 6	11.6 ± 3.2	17.8 ± 5.9	6.2	70.0 ± 10.4	78.5 ± 9.8	8.5

Cell-coverage fraction

	24 nm threshold			40 nm threshold		
	Before	*After*	Δ	*Before*	*After*	Δ
Control	3.3E-4 ± 5.4E-4	7.6E-4 ± 7.6E-4	4.3E-04	3.4E-3 ± 4.9E-4	3.8E-3 ± 9.0E-4	4.5E-04
Cell 1	2.3E-2 ± 5.6E-3	2.7E-2 ± 4.7E-3	4.5E-03	1.0E-1 ± 7.9E-3	1.1E-1 ± 6.2E-3	5.8E-03
Cell 2	1.3E-2 ± 5.2E-3	1.6E-2 ± 4.3E-3	3.2E-03	8.5E-2 ± 7.9E-3	9.4E-2 ± 9.3E-3	8.7E-03
Cell 3	7.6E-3 ± 3.8E-3	1.3E-2 ± 5.6E-3	5.8E-03	6.4E-2 ± 7.1E-3	7.3E-2 ± 6.1E-3	9.1E-03
Cell 4	2.3E-2 ± 3.7E-3	2.9E-2 ± 5.5E-3	6.1E-03	1.0E-1 ± 7.4E-3	1.1E-1 ± 7.2E-3	3.7E-03
Cell 5	1.8E-2 ± 5.6E-3	2.3E-2 ± 4.2E-3	4.5E-03	8.1E-2 ± 8.6E-3	9.5E-2 ± 8.6E-3	1.4E-02
Cell 6	1.3E-2 ± 4.0E-3	2.0E-2 ± 5.7E-3	6.9E-03	7.7E-2 ± 7.9E-3	8.5E-2 ± 8.3E-3	7.9E-03

($n_{pre} = 15$, $n_{post} = 11$)

In the control experiment without ribosomes, the nanoscale surface topography of the imaged cell was influenced by subtle erosion and deformation during the prolonged force imaging, resulting in emergence and slight movement of small particle-like features. There were few or no surface-attached particles when analyzed for features with curvature radius corresponding to ribosome particles. In comparison, the cells that were exposed to ribosomes presented particle-like features in the pre-exposure phase. The number of surface particles markedly increased after the imaging medium was changed to a medium supplemented with ribosome particles, after a time delay wherein all cells had a concerted increase in counted particles. Different cells had variable responses to enriched colloidal environments, where 4 of the 6 cells showed marked increases in surface particles numbers over time. In longer experiments, particle counts on bacterial surfaces are expected to increase over time due to greater levels of attachment. Greater particle attachment onto bacterial surface may have the potential to form contiguous films and structures of particles. Increased levels of attached particles lead to failure of particle detection from curvature radius as individual particles merge into larger aggregates.

The selection of detection threshold is critical in determining which surface features qualify as a surface particle. With a higher curvature threshold (lower curvature radius) for finer particle detection, there is an observable increase in particle quantities between the control period and the experimental ribosome exposure period. A 24 nm threshold for radius of curvature is more specific for ribosome particles whereas the 40 nm threshold is susceptible to including raised microbial surface features. At the 40 nm radius of curvature threshold, the fluctuating quantities of surface particles show no clear response to ribosome

171

amendments. The determination of an appropriate spatial scale is crucial for the accurate detection of a surface particle from the background bacterial surface. Similar considerations are needed for potential implementations of fiducial markers to adequately monitor reference features for volumetric analysis (Fuentes-Perez et al., 2013).

An alternate analysis of bacterial surface roughness shows no marked response to ribosome exposure as shown in Figure S5. The averaged cell surface roughness did not significantly change in response to extracellular ribosome exposure. Analysis of select regions on bacteria show varying changes over time, dependent on the analysis scale. On smaller scales, the measured surface roughness is more variable, and the monitored regions may fail to display indications of particle attachment. Surface roughness changes have been shown as a characteristic response to certain antibiotic treatments but may fail to show a response to discrete evets of surface remodeling (Fantner et al., 2010). Monitoring surface roughness as a parameter for particle attachment and bacterial-surface dynamics fails in part due to variations in bacterial surfaces due to distribution of cell material. The surface roughness of bacteria scales linearly with the scale of analysis and is reflected in the data, where larger areas present greater variability in surface roughness (Auerbach et al., 2000). Curvature radius analysis may be more useful in monitoring surface changes due to antimicrobial activity, such as in characterizing membrane disruption or cationic antimicrobial peptides attachment (Hayden et al., 2012). Such an approach can offer insight into localized surface response from compromised membrane structures and its development compared to a more generalized view of surface roughness development.

Applications of curvature radius analysis can potentially be used to investigate interactions between bacteria and organic colloidal particles and bacterial surfaces in near-physiological conditions, and in conditions of substrate limitation and amendment. Variability in the extent and rate of colloidal particle capture can be tested to determine which bacterial species are predisposed towards scavenging organic colloids. Modifications in the imaging media environment by introducing with substrate compounds and extracellular polymers can determine how stimulated biological changes can effect changes in bacterial behaviors for breakdown and uptake and responses to colloidal DOM exposure. Similarly, interactions can be assessed to determine which types of particles are more easily scavenged and cleared from ambient seawater. This method of analysis has potential applications for testing marine bacterial response to organic marine colloids of varying lability, ranging from protein particles (e.g., RuBisCO) to colloidal aggregates of refractory DOM. The measured number of attached particles and cell-coverage fraction may be useful in qualified comparisons for testing the influence of biological and biochemical factors on bacterial surface responses and particle attachment. This method can contribute towards insight of how bacteria modify of their microenvironment by processing and clearing ambient organic particles.

4.4.7 Limitations in time-lapse image analysis

The collection of topography data with high fidelity is a significant challenge and limitation in applying time-lapse AFM imaging for investigating cell surface-particle interactions. As a feature of raster scanning motion for image acquisition, increasing spatial

resolution comes at the expense of greater scanning time and lower temporal resolution to monitor dynamic processes. Higher spatial resolution requires more time to acquire data with greater sampling density, wherein the greater number of interactions with the cell surface exert more forces, and liable to deforming the biological surface and tip biofouling. With faster scan times, poorer feedback in AFM control can contribute greater inaccuracy in the measured surface profile. Furthermore, greater scan lines create more opportunities for lateral force & moments to disrupt bacterial adhesion sites and compromise secure cell attachment. Suboptimal force control during AFM imaging can results in excessive loading forces that can compress features and deform cell surfaces and result in tip fouling and induce tip artefacts. Tip artefacts can significantly compromise the accuracy of measured features due to tip broadening effect and limit the measured curvature of sharp features.

The challenges in collecting image data with high fidelity influence the image processing and surface curvature analysis for particle attachment. Image scan resolution imposes limitations on the maximum mean and Gaussian curvature measured due to the computation methods for calculating A and G. Imaging experiments are prone to mismatched curvature measurements for surveyed nanoscale features imaged at varying spatial scales, as observed above with ribosome data. This mismatch can contribute to challenges in corroborating independent datasets that apply curvature-based analysis. Furthermore, smoothing operations on topography and calculated curvature data can attenuate the influence of noise and improve feature contrast. When applied in excess, such operations can obscure potential particle features and blend multiple features together or with the background. A Gaussian blur operation was applied to mean and Gaussian curvature

maps to smooth image noise and generate particle feature masks. Wavelet transforms, using a Mexican hat wavelet, can offer an alternate approach in smoothing features at predetermined spatial scales, which can be used to compare processed images of different scan sizes (Maksumov et al., 2004;Sun et al., 2011). Image filtering and generating particle masks from curvature data, approximate the convex particle shape, where the maximum measured A and G values relate to approximated particle size.

The measured particle shape is fundamentally limited by the tip shape and sharpness in its influence in reconstructing the particle surface profile and the accuracy of its measured shape and curvature. An AFM tip ideal for imaging particles on bacterial surfaces will need to have a requisite sharpness to image small particles and avoid blunting and fouling of the tip from biological material, which compromise its utility due to introducing tip artefacts. Curvature radius analysis and thresholding for particle detection has limited utility for characterizing individual particles. This approach offers some utility in identifying particles and other convex surface features independent of manual analysis and reference heights. When integrated into automated data analysis workflows, curvature radius analysis can be useful in identifying dynamic regions for spatial analysis.

4.5 Conclusion

This work raises the potential for the application of curvature radius analysis an objective standardized AFM method for investigating particle interactions with bacterial surfaces. Future directions of this work primarily include standardized comparisons in quantifying particle attachment rates among various bacterial species and organic colloids.

Implementation of curvature radius analysis has inherent limitations due to properties of bacterial cells and particles that limit detection across varying spatial scales and background geometry. Despite such limitations, such analysis can be incorporated into time-lapse AFM image analysis to quantify particle attachment that may be involved in bacterial interactions with nanoengineered particles or microplastics. Furthermore, investigation into bacterial surface dynamics can yield insight into potential mechanisms involved in the surface attachment, dissolution, and breakdown of colloidal DOM. Further applications can be found in monitoring changes of bacterial surface topography in response to exposure to antibiotics and other antimicrobial compounds. Understanding how various bacteria can process or handle organic colloidal particles and yield insight into their influence on reshaping the marine microenvironment.

Chapter 4, in part, is currently being prepared for submission for publication of the material in Patel, N., Lal, R., and Azam, F. (2022). AFM curvature radius analysis for detection and enumeration of surface-attached particles on marine bacteria. The dissertation author was the primary investigator and author of this material.

4.6 Supplementary Data
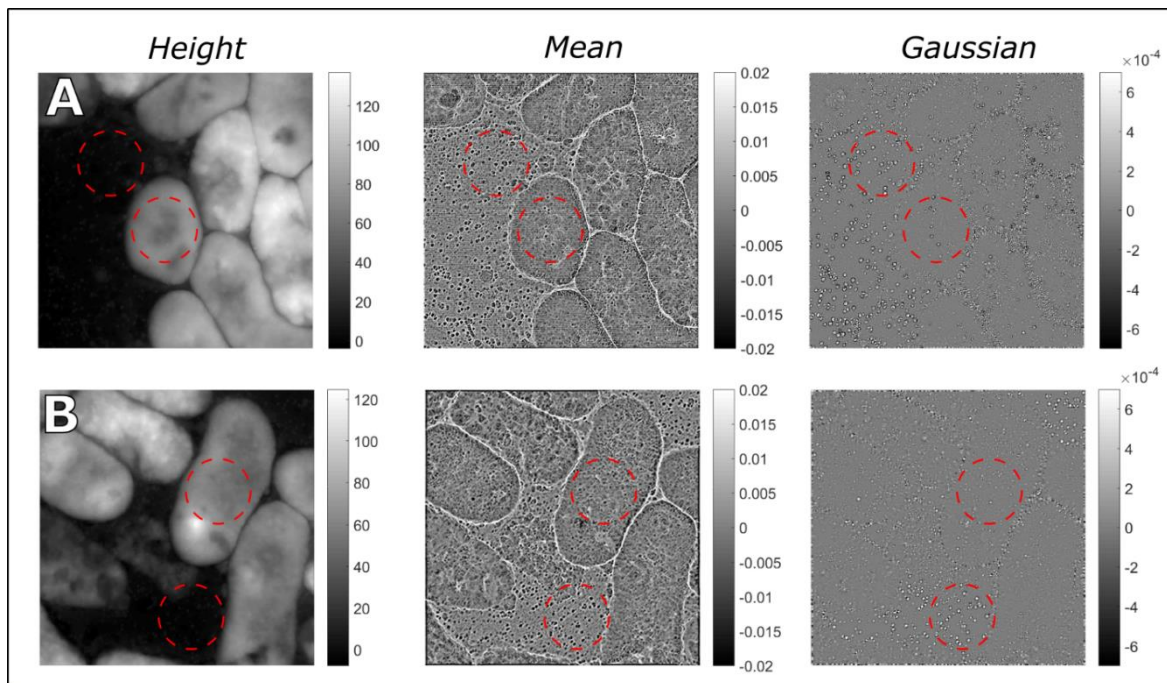
Figure 4.S1: Absorbed particles on bacterial surfaces are similar to particles on background substrate. AFM images **(A, B)** and respective mean and gaussian curvature data maps of diatom detritus particles deposited onto fixed *Vibrio* sp. SWAT-3 cells show uniform deposition of particles on background substrate and on cell surfaces to a lesser degree (red circled regions). (Image scan size: 3.3×3.3 µm; units for curvature maps: nm^{-1} (mean) and nm^{-2} (Gaussian)).
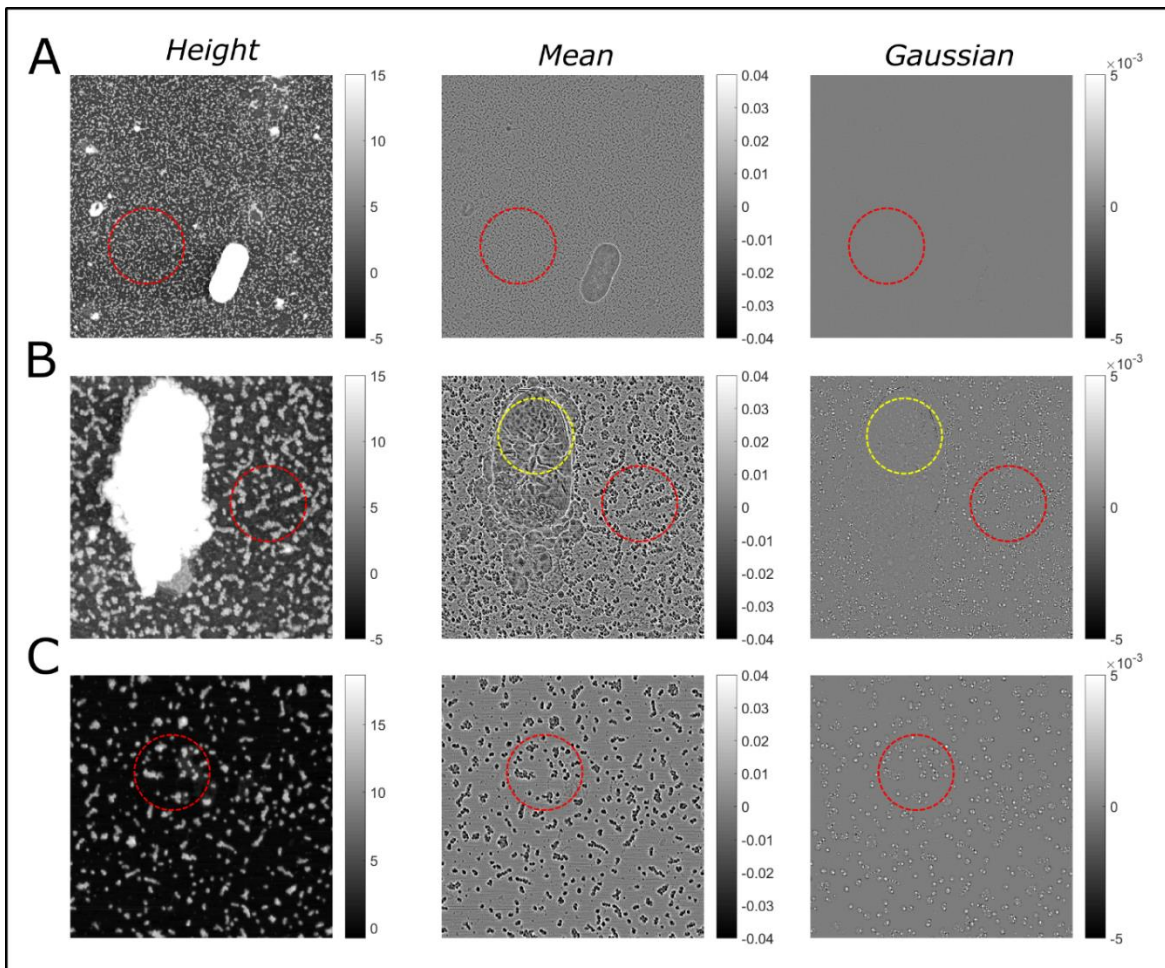
Figure 4.S2: Peak curvature of *E. coli* ribosomes is dependent on scan size and background. **(A-C)** SWAT-3 cells were imaged with subsequently deposited ribosome particles on mica surfaces at varying scan resolutions and shown with respective mean and Gaussian curvature maps (**A**: 6.64 x 6.64 µm (512 x 512 pixels), **B**: 2.2 x 2.2 µm (512 x 512 pixels), **C**: 2.0 x 2.0 µm (512 x 512 pixels). In larger scan sizes (A), curvature of ribosomes particles on the background substrate regions (red circled regions) are attenuated with though the particle heights are comparable to measurements at lower scan sizes. On cell surface regions (**B**, yellow circle), any ribosomes on deposited onto cells have attenuated mean and gaussian curvature values compared to the ribosomal particles in the nearby background regions. (Units for curvature maps: nm^{-1} (mean) and nm^{-2} (Gaussian)).

Figure 4.S3: AFM time-lapse images of marine bacterial cells exposed to circulating ribosomes. AFM image sequence (corresponding height and error mode) of marine bacterial isolate *Alteromonas* sp. ALTSIO cells in circulating FASW media. After approximately 90 minutes, bacterial cells were exposed to FASW media amended with ribosomes (8×10^{11} particles mL^{-1}). Cell topography data was analyzed (representative cell mask shown) for detected surface particles in each frame of the image sequence (representative particle mask shown). Analysis of labeled cells (1-6) is plotted in Figure 3 and summarized in Table 1. Select frames shown with timestamps from the acquired sequence of 44 images and total duration of 212 minutes. All images were collected at a scan size of 3.3×3.3 µm and scan resolution of 256×1024 pixels.
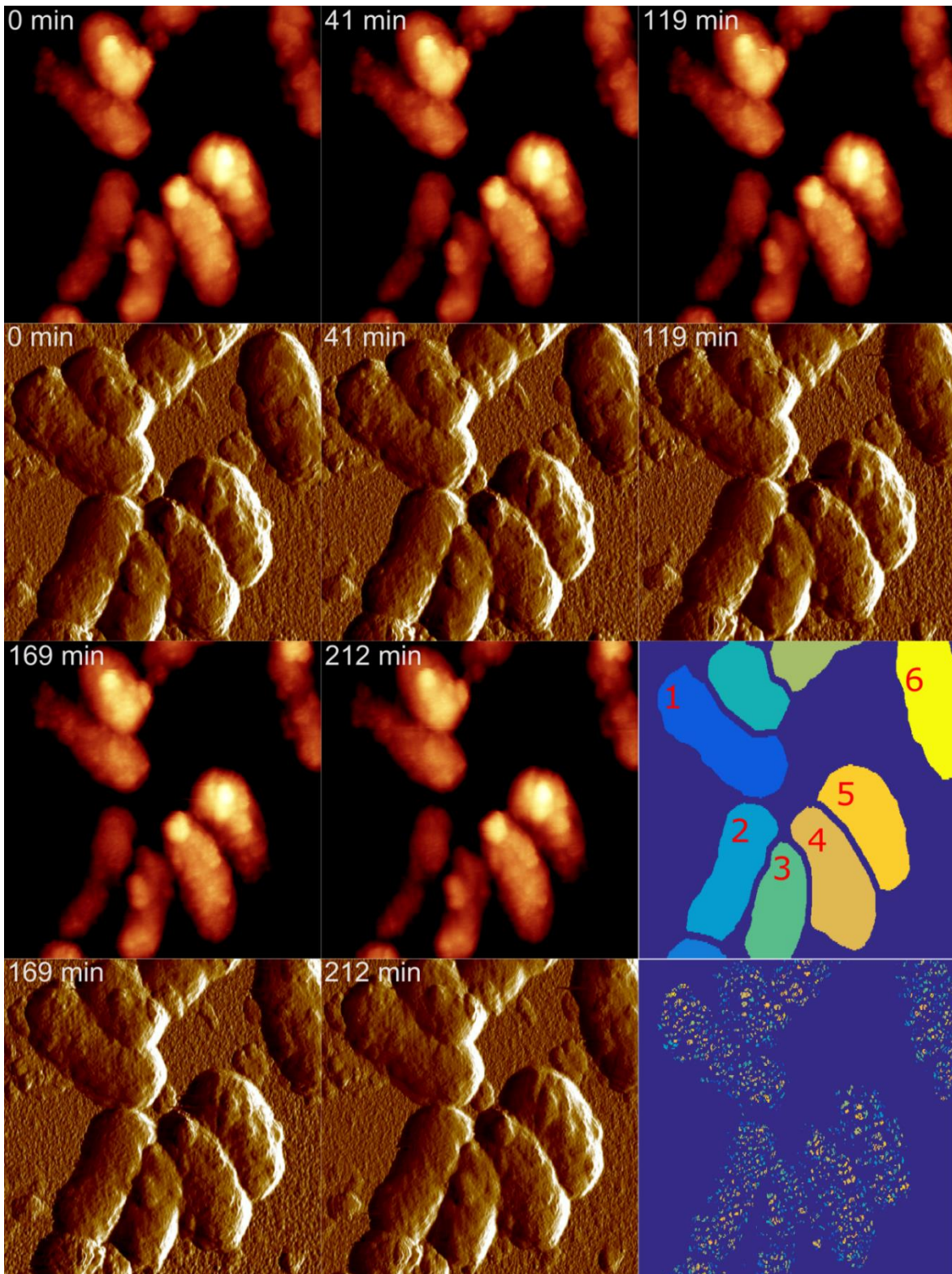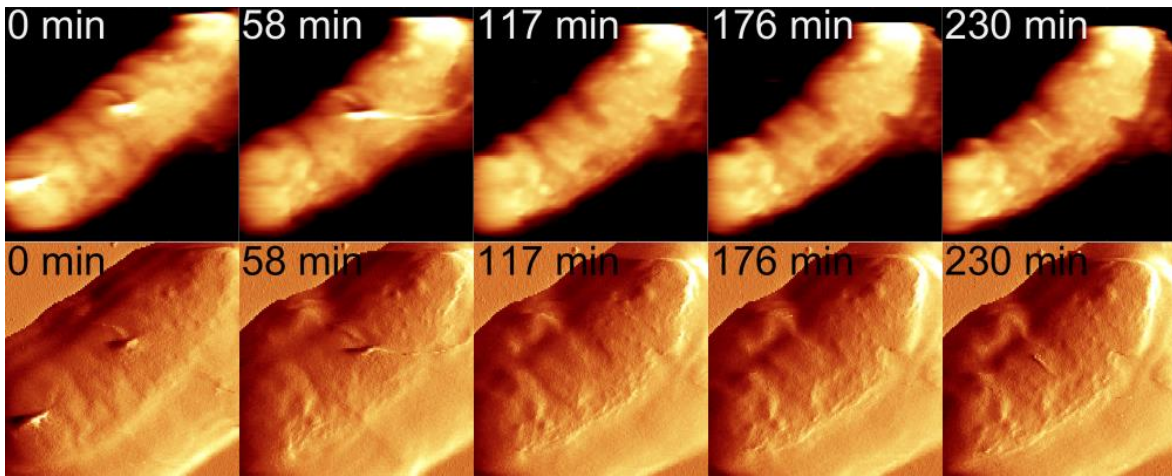
Figure 4.S4: AFM time-lapse images of marine bacterial cell surface changes in ribosome-free medium. AFM image sequence (corresponding height and error mode images) of an ALTSIO cell in circulating 0.02-µm syringe-filtered FASW medium. The bacterial cell has a dynamic surface layer with eroding region boundaries and emerging particulate features, presenting low to negligible levels of surface particles. Select frames shown with timestamps from a sequence of 52 images and total duration of 230 minutes. Image frames shown are cropped sections ($1.6 \times 1.6\,\mu\text{m}$) from original images collected at a scan size of 3×3 µm and scan resolution of 256×1024-pixels.
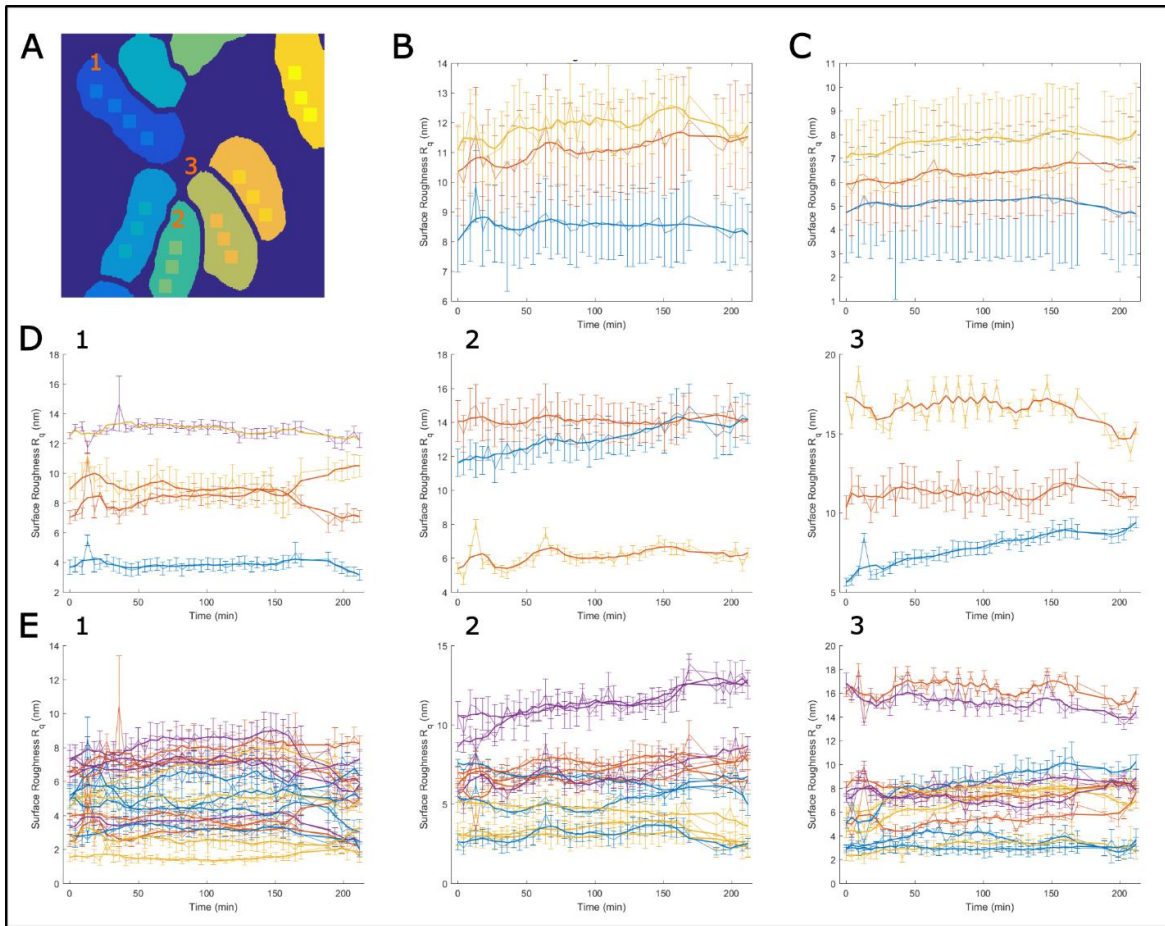
Figure 4.S5: Surface roughness analysis shows no bacterial response to ribosome amendment. Alternative analysis of bacterial surface changes due to particle attachment was performed by calculating surface roughness. **(A)** Calculations were performed in multiple 150×150 nm regions for cells (noted by square regions demarcated in cell mask image (scan size 3.3×3.3 µm). The regions were analyzed as a whole and as separate 75×75 nm quadrants. The average cell surface roughness for three different cells was analyzed and plotted for the 150 nm **(B)** and 75 nm **(C)** regions. The average roughness for individual cells does not show an apparent response to elevated ribosome particle conditions and no significant particle attachment after introducing ribosomes after the 90-minute timepoint. Surface roughness plots for individual 150 nm regions for cells are shown for marked cells **(1-3)** are shown for the entire region **(D)** and its quadrants **(E)**, showing varying types of surface roughness changes that do not show a marked change in response to particle attachment.

182

4.7 References

Allen, M.J., Hud, N.V., Balooch, M., Tench, R.J., Siekhaus, W.J., and Balhorn, R. (1992). Tip-radius-induced artifacts in AFM images of protamine-complexed DNA fibers. *Ultramicroscopy* 42**,** 1095-1100.

Auerbach, I.D., Sorensen, C., Hansma, H.G., and Holden, P.A. (2000). Physical morphology and surface properties of unsaturated Pseudomonas putida biofilms. *Journal of bacteriology* 182**,** 3809-3815.

Azam, F., and Malfatti, F. (2007). Microbial structuring of marine ecosystems. *Nature Reviews Microbiology* 5**,** 782.

Barrera, N.P., Ge, H., Henderson, R.M., Fitzgerald, W.J., and Edwardson, J.M. (2008). Automated analysis of the architecture of receptors, imaged by atomic force microscopy. *Micron* 39**,** 101-110.

Becker, S., Scheffel, A., Polz, M.F., and Hehemann, J.-H. (2017). Accurate quantification of laminarin in marine organic matter with enzymes from marine microbes. *Applied and environmental microbiology* 83.

Canet-Ferrer, J., Coronado, E., Forment-Aliaga, A., and Pinilla-Cienfuegos, E. (2014). Correction of the tip convolution effects in the imaging of nanostructures studied through scanning force microscopy. *Nanotechnology* 25**,** 395703.

Dufrêne, Y.F., Viljoen, A., Mignolet, J., and Mathelié-Guinlet, M. (2021). AFM in cellular and molecular microbiology. *Cellular Microbiology***,** e13324.

Fantner, G.E., Barbero, R.J., Gray, D.S., and Belcher, A.M. (2010). Kinetics of antimicrobial peptide activity measured on individual bacterial cells using high-speed atomic force microscopy. *Nature nanotechnology* 5**,** 280-285.

Fuentes-Perez, M.E., Dillingham, M.S., and Moreno-Herrero, F. (2013). AFM volumetric methods for the characterization of proteins and nucleic acids. *Methods* 60**,** 113-121.

Fukuda, H., and Koike, I. (2004). Microbial stimulation of the aggregation process between submicron-sized particles and suspended particles in coastal waters. *Aquatic microbial ecology* 37**,** 63-73.

Hayden, S.C., Zhao, G., Saha, K., Phillips, R.L., Li, X., Miranda, O.R., Rotello, V.M., El-Sayed, M.A., Schmidt-Krey, I., and Bunz, U.H. (2012). Aggregation and interaction of cationic nanoparticles on bacterial surfaces. *Journal of the American Chemical Society* 134**,** 6920-6923.

Kim, H., Oikawa, K., Watanabe, N., Shigeno, M., Shirakawabe, Y., and Yasuda, K. (2007). Identification of size differences of gold nanoparticles on cell surface by curvature reconstruction method using atomic force microscopy. *Japanese journal of applied physics* 46**,** L184.

Klapetek, P., Valtr, M., Nečas, D., Salyk, O., and Dzik, P. (2011). Atomic force microscopy analysis of nanoparticles in non-ideal conditions. *Nanoscale research letters* 6**,** 1-9.

Liu, S., and Wang, Y. (2010). Application of AFM in microbiology: a review. *Scanning* 32**,** 61-73.

Maksumov, A., Vidu, R., Palazoglu, A., and Stroeve, P. (2004). Enhanced feature analysis using wavelets for scanning probe microscopy images of surfaces. *Journal of colloid and interface science* 272**,** 365-377.

Marsh, B.P., Chada, N., Sanganna Gari, R.R., Sigdel, K.P., and King, G.M. (2018). The Hessian blob algorithm: Precise particle detection in atomic force microscopy imagery. *Scientific reports* 8**,** 1-12.

Mazeran, P.-E., Odoni, L., and Loubet, J.-L. (2005). Curvature radius analysis for scanning probe microscopy. *Surface science* 585**,** 25-37.

Mei, L., Lu, Z., Zhang, W., Wu, Z., Zhang, X., Wang, Y., Luo, Y., Li, C., and Jia, Y. (2013). Bioconjugated nanoparticles for attachment and penetration into pathogenic bacteria. *Biomaterials* 34**,** 10328-10337.

Nagata, T., and Kirchman, D. (1996). Bacterial degradation of protein adsorbed to model submicron particles in seawater. *Marine Ecology Progress Series* 132**,** 241-248.

Nagata, T., and Koike, I. (1995). Marine colloids: Their roles in food webs and biogeochemical fluxes. *Biogeochemical processes and ocean flux in the western Pacific***,** 275-292.

Oikawa, K., Kim, H., Watanabe, N., Shigeno, M., Shirakawabe, Y., and Yasuda, K. (2007). Measuring the sizes of nanospheres on a rough surface by using atomic force microscopy and a curvature–reconstruction method. *Ultramicroscopy* 107**,** 1061-1067.

Peric, O., Hannebelle, M., Adams, J.D., and Fantner, G.E. (2017). Microfluidic bacterial traps for simultaneous fluorescence and atomic force microscopy. *Nano Research* 10**,** 3896-3908.

Quate, C. (1994). The AFM as a tool for surface imaging. *Surface Science* 299**,** 980-995.

Reintjes, G., Arnosti, C., Fuchs, B.M., and Amann, R. (2017). An alternative polysaccharide uptake mechanism of marine bacteria. *The ISME journal* 11**,** 1640-1650.

Seo, Y., Ikemoto, E., Yoshida, A., and Kogure, K. (2007). Particle capture by marine bacteria. *Aquatic microbial ecology* 49**,** 243-253.

Seymour, J.R., Amin, S.A., Raina, J.-B., and Stocker, R. (2017). Zooming in on the phycosphere: the ecological interface for phytoplankton–bacteria relationships. *Nature microbiology* 2**,** 1-12.

Simon, M., Grossart, H.-P., Schweitzer, B., and Ploug, H. (2002). Microbial ecology of organic aggregates in aquatic ecosystems. *Aquatic microbial ecology* 28**,** 175-211.

Smriga, S., Fernandez, V.I., Mitchell, J.G., and Stocker, R. (2016). Chemotaxis toward phytoplankton drives organic matter partitioning among marine bacteria. *Proceedings of the National Academy of Sciences* 113**,** 1576-1581.

Sun, W., Romagnoli, J.A., Palazoglu, A., and Stroeve, P. (2011). Characterization of surface coats of bacterial spores with atomic force microscopy and wavelets. *Industrial & engineering chemistry research* 50**,** 2876-2882.

Tranvik, L.J., Sherr, E., and Sherr, B.F. (1993). Uptake and utilization of 'colloidal DOM' by heterotrophic flagellates in seawater. *Marine Ecology Progress Series***,** 301-309.

Viljoen, A., Foster, S.J., Fantner, G.E., Hobbs, J.K., and Dufrêne, Y.F. (2020). Scratching the surface: bacterial cell envelopes at the nanoscale. *MBio* 11**,** e03020-03019.

Wells, M.L., and Goldberg, E.D. (1991). Occurrence of small colloids in sea water. *Nature* 353**,** 342.

Wells, M.L., and Goldberg, E.D. (1993). Colloid aggregation in seawater. *Marine Chemistry* 41**,** 353-358.

Winzer, A., Kraft, C., Bhushan, S., Stepanenko, V., and Tessmer, I. (2012). Correcting for AFM tip induced topography convolutions in protein–DNA samples. *Ultramicroscopy* 121**,** 8-15.

Yamada, Y., Tomaru, Y., Fukuda, H., and Nagata, T. (2018). Aggregate formation during the viral lysis of a marine diatom. *Frontiers in Marine Science* 5**,** 167.

Zhao, Z., Gonsior, M., Schmitt-Kopplin, P., Zhan, Y., Zhang, R., Jiao, N., and Chen, F. (2019). Microbial transformation of virus-induced dissolved organic matter from picocyanobacteria: coupling of bacterial diversity and DOM chemodiversity. *The ISME journal* 13**,** 2551-2565.

Chapter 5 Conclusion

In the global ocean, aggregate marine microbial activity is a significant force in the biogeochemical cycling of carbon, transforming petagrams (10^{15} g) of carbon annually, as marine bacteria convert primary production exudates, particular organic matter, and labile dissolved organic matter into influx biomass for the marine food web. Macroscale influxes of organic matter generate discrete hotspots areas of elevated nutrient availability and increased aggregate bacterial activity. On smaller spatial scales, increasing sparsity creates a patchiness in the distribution of organic matter, influencing the available nutrients for marine bacteria uptake and breakdown. An individual bacterium is exposed to a diverse range of components in an ever-changing marine microenvironment. Typically, within a mL of seawater, there are 10^4 phytoplankton, 10^6 bacteria, 10^8 organic colloids, and 10^{12} metabolic species that populate the biologically and biochemically diverse surroundings at the single-cell level. Through individual interactions with the various components, an estimated 10^{29} marine bacteria in the global ocean contribute to the cycling of organic carbon by each cell individually processing few molecules and particles at a time.

Marine bacterial interactions with bacteria, viruses and other submicron organic colloidal particles likely occur universally with varying frequency in diverse microenvironments. These interactions can determine if a bacterium has adequate nutrient availability and can meet its physiological needs. Pelagic bacteria have been shown to be intimately associated with exopolymeric substances and viral particles in AFM observations. These close interactions and association imply a close coupling between bacterial cells and

extracellular organic matter in ambient seawater microenvironments. Additionally, marine bacteria have been observed to capture ambient colloidal particles on their surface, demonstrating a close physical association between particles and bacterial surfaces. The nature and diversity of such fundamental bacterial interactions has not been extensively studied. Little is known about any bacterial regulation of the generation and breakdown of colloidal DOM and potential tight-coupling for specific particle species. Furthermore, the degree of specificity is unknown in surface-particle interactions, including the kinetics and duration of particle attachment. Any potential dissolution and uptake of attached particles at the surface remains to be investigated. Further, the influence of chemical diversity and lability to colloidal organic matter introduces an additional degree of variability in how a marine bacterium interacts with ambient particles. The diverse responses of bacterial species define the interactions with colloidal organic matter and influences on the marine microenvironment from behaviors related to biological surface interactions, nutrient sequestration, and labile organic carbon drawdown.

In Chapter 2, from AFM micrographs, intimate physical interactions between bacteria were observed from bacterial nanotube structures connecting cells to form multicellular structures. Bacterial nanotubes can function as hollow physical linkages that form a contiguous biotic surface, potentially connecting interior cytoplasmic spaces across cells. These connections range between 200–600 nm in length and 50–160 nm in width in marine bacterial isolates. As membrane-derived tubular conduits, nanotubes have similar surface and nanomechanical properties as the connecting cell bodies, with some variations and differences in bulk mechanical properties, such as deformation and dissipation.

Nanotube structures were observed connecting bacterial cells in natural bacterial assemblages from enriched seawater. Extended interconnectivity between bacterial cells can be supported by bacterial nanotube, as multicellular structures of connected bacterial ensembles can interact with various forms of organic matter.

The architecture of an interconnection bacterial network has many significant implications in marine bacterial ecology. One area for future investigation is to explore prevalence of nanotube expression among marine microbial communities. Higher expression of bacterial nanotubes among specific species can have potential consequences that are yet to be explored, such as influencing shifts in microbial community composition. Another future direction is towards characterization of potential metabolite transport across nanotube structures. The expression of bacterial nanotubes could potentially allow for niche specialization among interconnected cells as an ecological advantage. The structures intimately connect bacterial cells without sacrificing available bacterial surface area for attachment. Such a physical arrangement of cell forms a multicellular biotic surface as a substrate for organic matter aggregation. Nanotube expression can be potential strategy for bacteria-stimulated formation of marine particles, due to enhanced adsorption of nanogels, biopolymers, organic colloids, and other labile dissolved organic matter. As an ecological adaptation, marine bacterial structures can support physical and biological interactions that exert increased bacterial influence over the attachment, cycling and degradation of colloidal organic matter.

In Chapter 3, bacterial surface interactions with organic colloids were investigated in a model system with marine bacterial isolates and *E. coli* ribosomes. Ribosome particles

were observed to form contiguous films of ribosome particles associated with bacterial surfaces. A film of particles implies a potential emergent structure of a fragile particle cloud around the bacterial surface, as an effective enriched zone of organic colloids carried by the cell. Under shear conditions, colloidal organic particles attach to the bacterial surface individually or as small aggregates, forming surface particle clusters on the bacterial surface. Individual particle clusters were observed to range from 40–200 nm in width. Individual and small colloids are labile on the surface and likely to aggregate into larger clusters or merge into contiguous surface patches. Extended exposure to colloidal particles results in larger surface clusters and patches on microbial surfaces, which can accrue between and become intermediary surfaces between individual microbial cells, holding cells together. Marine bacteria can express surface structures that can influence potential interactions with organic colloids likes ribosomes. Few cells were observed with surface corrugations that are approximately 50–100 nm in size, and 20 nm deep. Other bacteria were observed with hollow surface pits that ranged between 50–300 nm in width, and 10–50 nm in depth. A surface pit was observed in a live marine bacterium, which has significant implications for uptake and breakdown of whole particles of organic matter. Colloidal attachment to bacterial surfaces occurs as discrete cluster of a few individual particles that can develop into larger patches and films. As a dynamic substrate, bacterial surfaces can potential adapt with adjunctive expression of surface features, such as surface corrugation and surface pits, modulate the sequestration, breakdown, and uptake of colloidal particles.

Future work would involve investigation into the factors that influence cell-to-cell variability of particle-attachment processes. Determining the rate of surface particle clusters

formation and growth and their variability across bacterial species can identify which are predisposed towards scavenging colloids and particles. Additionally, it is undetermined whether clusters can be nucleation sites for other particles to attach onto and grown into films. For example, initial particle clusters of labile organic matter can be attachment sites for particles consisting of more refractory species of organic matter. As such, individual planktonic bacteria can be sites of aggregating colloidal particles and function as self-generating nanoscale hotspots of organic matter. The effective rate at which attached organic colloids form a nanoscale nutrient hotspot can potentially influence interactions among bacterial species as intermediary substrates. Another future direction is towards determining similar patterns exist for other types of colloidal particles interacting with marine bacterial surfaces. Particles comprising of HMW proteins, such as RuBisCO, are a potential model candidate and are ubiquitously released into the marine microenvironment, like ribosomes.

It is not understood how organic particles are processed once attached onto bacterial cells. It is undetermined what mechanisms may exist for the uptakes and degradation of surface-attached particles. One open question is whether such particles are dissolved or partially digested and released. A future direction of investigation involves elucidating mechanisms for the direct uptake of colloids. The influence of surface corrugation and surface pits on the membrane structure remains to be determined, and whether such features are associated with the reorganization of membrane proteins and periplasmic components. Reorganization of membranes components can potentially induce more effective localized nanoscale hotspots, wherein the attached colloids are near relevant membrane components of breakdown and uptake. These observed features suggest marine bacteria can derive

ecophysiological benefits from brief exposure to elevated colloidal DOM concentration in their ambient microenvironment.

In Chapter 4, a curvature radius-based method was applied for visualization of colloidal particle attachment and tracking on bacterial surfaces in AFM topographic images. Mean curvature data images, processed from surface height data, have an advantage compared to the original height images for visualizing sharp features on bacterial surfaces, independent of background surface height. In marine bacterial cell from natural bacterial assemblages, curvature data maps reveal bacterial cells with sharp features, corresponding to attached particle features. In AFM images with *E. coli* ribosomes and bacterial flagellum as reference features, the estimated curvature of ribosomes and flagellar segment features are observed with attenuated on bacterial surfaces, with peak curvature decreased by approximately two-fold. The same features have different mean curvature when situated on a flat substrate compared to on a bacterial cell, which imposes some limitation on curvature-thresholding detection. In a ribosome exposure experiment with marine bacterial isolate *Alteromonas sp.* ALTSIO, image data was processed using curvature radius analysis to quantify changes in particle attachment post exposure. For cells exposed to a ribosome concentration of 8×10^{11} particles mL^{-1}, cells presented an increase of 6.0 particles post exposure. No such change was observed without ribosome exposure. Alternative analysis of surface roughness shows no marked changes between pre- and post-exposure phases. Curvature radius analysis of cells exposed to ambient organic particles can quantify relative changes in particle attachment in qualified comparisons.

Future directions for investigation involve determining the quantitative relation between the increase in attached particles and ambient ribosome concentration. Such relationships can be used to establish the initial quantity and rate of particle attachment of cells. The kinetic relation for different bacterial species can provide insight for predicting bacterial responses to influxes of colloidal DOM into the marine microenvironment. Another direction in applying this analysis is towards determining surface particle degradation via AFM volumetric analysis. Furthermore, curvature radius analysis can be applied toward studying local surface effects and responses to antibiotics, such as the initiation and development of membrane disruption sites. Particularly, future applications include investigating the mechanisms in potential combinatorial treatments of antibiotics with other antimicrobial or phage therapies from direct empirical observations. The curvature radius analysis can offer a means to investigate surface responses and changes of individual marine bacterial cells from exposure to organic colloids.

The investigation of the bacterial-colloidal interactions is complex and complicated endeavor with limitations due to their spatial scale and diversity. In this interaction, bacteria primarily attach to particles at their surface, where the organic particles form the immediate ambient environment and a potential nutrient source. The expression of nanoscale surface features, such a surface corrugations and surface pits, can influence colloidal aggregates to form transient nanoscale nutrient hotspots localized at the bacterial surface. In addition to individual marine bacterial influence on organic colloids, multiple bacterial cells can be intimately connected via physical nanotubes structures. As interconnected bacterial consortia, groups of bacterial cells can interact with colloidal organic particles in different

emergent biological behaviors and interactions. The visualization of individual organic colloids interacting with bacterial surfaces can help quantity the frequency and lifespan of colloidal capture on bacterial surfaces. Visualization of bacterial surface-colloid interactions can provide helpful insight into the mechanisms of marine bacteria influencing organic particle aggregation and dissolution in the biogeochemical cycling of carbon in the global ocean.